We thank both reviewers and the editor for their constructive comments, which has greatly helped us to improve the paper. Below we include a point-by point response to the referee comments, and describe the corresponding changes we have made to the manuscript

Comments from reviewer #1

General Comments

A new dataset is presented and analysed to provide a global 3-D seasonally resolved dataset of dust properties with constrained size distribution, shape and refractive index properties. The dataset (DustCOMM) provides annual and seasonal mean 3-D dust size distributions, 3-D mass extinction efficiency at 550 nm wavelength and 2-D dust column mass loading. Since models are mostly unable to reproduce these properties in faith with measurements, this is a welcome and valuable step forwards in the dust field. The authors show that the DustCOMM results perform significantly better than global model simulations when evaluated against independent measurements. This is a notable achievement considering the challenges involved in representing global dust fields. The authors outline the benefits and potential future uses of the DustCOMM dataset to the community, which are likely to be substantial.

This paper covers a considerable amount of work and therefore methodology in order to deliver the final results in the DustCOMM dataset. Although the authors do a credible job of explaining the long and complicated methodology, in places it requires further explanation and clarity, potentially with re-ordering of some sections. The results impeccably described and presented. The description of measurements used requires some corrections and clarifications. Although the authors provide the datasets online, one of the links is broken. The article fits the scope of ACP and I recommend publication subject to the corrections detailed below.

We thank the reviewer for the constructive and helpful comments that helped us to further improve the paper. We address these comments below.

General Scientific Comments

1. Overall, it is not clear why there is a need for the AOD reanalyses in this study – i.e. column 3 in Figure 1. Given the volume size distribution, and an assumed dust density, it should be possible to calculate column mass loading directly from size distribution without the requirement for AODs, and without any uncertainty involved in the mass extinction efficiency (MEE) values. Currently this is not explained, and therefore the AOD reanalysis section (fig 1 column 3 and sections 2.3) seems superfluous. More details are given below.

   We thank the reviewer for this comment. We note that our dust size distributions are normalized such that the integral over the diameter range is unity, and with no information about the size-resolved volume of the particles. Therefore, the normalized

dust size distribution cannot be used directly with dust density to calculate the column dust loading. We have added the following sentence in section 2.3.3 (formerly section 2.3) to clarify this point: "Since our constraints on dust size distributions are normalized to unity, and also to ensure that our estimates of dust loading produce the same extinction as those from reanalysis dataset or satellite measurements, we use this approach to estimate the atmospheric dust loading…"

2. The authors do not include any dust properties in the longwave (LW) spectrum. The impact of the coarse particles on the radiative budget is one of the motivators of this study, and indeed highlighted in the discussions and conclusion as one of the benefits of the new dataset. The LW radiative effect makes up a large part of the total change in radiative effect due to a better representation of coarse particles (Kok et al., 2017). Thus the omission of LW dust properties here detracts slightly from the novelty of this work. There may be valid reasons for excluding the LW here, such as scope of material and lack of MEE observations in the LW spectrum. However, this should be discussed, since the total radiative impact of the constrained size distribution cannot be calculated without dust LW properties. Additionally, there may be some limitations in radiative studies which could be done with the DustCOMM data due to MEE being required spectrally (at least on some spectral resolution), rather than just at 550 nm as provided.

   The reviewer raises an excellent point here, as indeed a large portion of the uncertainty in dust radiative effects is due to uncertainty in LW interactions. That being said, we provide dust optical properties at the mid-visible wavelength (550 nm), rather than in the longwave spectrum, for several reasons. First, as the reviewer pointed out, measurements of dust mass extinction efficiency (MEE) in longwave are scarce and therefore it will be difficult to validate our constraints on dust MEE. Second, the estimation of dust mass loading in Eqn. 9 requires MEE value at 550 nm which is the same wavelength as the observational constraints on dust optical depth (e.g. Ridley et al., 2016). Third, the measurements of dust refractive index needed to constrain the single-particle extinction efficiency at the longwave spectrum are also scarce, potentially leading to large uncertainties in constraining the dust MEE. Despite these reasons, our future studies will focus on incorporating the available measurements of dust refraction index – such as those from Di Biagio et al. (2017, 2019) – to constrain the spectral dependence of dust optical properties for both longwave and shortwave spectra as part of DustCOMM dataset.

   To clarify these reasons for not including dust properties in the LW spectrum in this paper, we have included a paragraph in section 2.3.2. "We use this constrained globally-averaged $\widehat{Q}_{ext}$ to constrain $\hat{\epsilon}_\tau$ (Eqn. 8) for every location. We thus neglect any regional variation in $\widehat{Q}_{ext}$ because measurements of dust shapes and index of refraction are currently insufficient to constrain $\hat{\epsilon}_\tau$ on a regional basis. In addition, since measurements of dust refractive index needed to constrain $\hat{\epsilon}_\tau$ at other wavelengths are also scarce, we

limit our estimate here only to the 550 nm wavelength. We use 550 nm as the wavelength of choice because measurements to validate our estimate of $\hat{\epsilon}_\tau$ and the observational constraints to estimate the dust atmospheric loading are mostly available at mid-visible wavelength."

3. Section 2.1 (Constraining the 3-D atmospheric size distribution) is a crucial part of the paper, but difficult to follow. This section needs further explanation and clarity – see specific comments below.

   Thank you for pointing this out. Based on the specific comments by the reviewer, we have reordered both sections 2 and 3 to make it easier for the reader to understand. For example, in addition to other specific changes below, we now have the description of the model simulation and reanalysis datasets before the methodology that constrains the dust size distribution, mass extinction efficiency and the atmospheric loading.

Specific Comments

1. Links to datasets – the first asset link to the DustCOMM dataset v1 (https://doi.org/10.5281/zenodo.2620475) is broken.

   Thank you for pointing this out. The link has been fixed.

2. Abstract – l 17-21 – the use of model simulations should be mentioned here as this is a crucial part of the work.

   Thank you, that's a good point. We have re-written this part to reflect the use of global model simulations in constraining the dust size distribution. The new sentence now reads as:

   "This dataset leverages an ensemble of global model simulations with observational and experimental constraints on dust size distribution and shape to obtain more accurate constraints on three-dimensional (3-D) atmospheric dust properties than is possible from global model simulations alone."

3. It is not entirely clear what the benefits of model-constrained data presented here are over the data used in Kok et al. (2017). It would be useful to the reader to make this crystal clear, probably at the end of the introduction.

   We have included a sentence at the end of the introduction to clarify the difference between the Kok et al. (2017) results and the results in the study. We added the following to the last paragraph: "DustCOMM builds on the results from Kok et al. (2017), however, unlike the globally-averaged results obtained in Kok et al. (2017), our product constrains

the climatology of 3-D global atmospheric dust properties on seasonal and annual timescales".

4. All the way through the article, but particularly in the method, the authors should be absolutely clear which size distribution they are referring to - the Kok 2017 globally constrained size distribution, or the model-simulated size distribution(s) – when they state 'globally averaged size distribution,' or similar generalizations.

   Thank you for the comments. We have clarified this confusion where necessary.

5. Section 5.4 – would you expect DustCOMM to show improved inter-annual variability in dust loading compared to conventional models, if more than one year of data were constructed? Or would DustCOMM's ability in this context be limited by the underlying global models' limitations? This is another significant challenge for models, e.g. Evan et al. (2014).

   Thank you for the question. While we have not looked at this topic yet, we expect that the inter-annual variability in DustCOMM dust size distributions largely depends on the ensemble of model simulations used. However, the interannual variability of the dust mass loading will include not only the variability from the ensemble of model simulations but also from the observations used to constrain the dust aerosol optical depth and dust extinction. Although this study only present seasonal variability, DustCOMM inter-annual variability is expected to show some improvements when compared to individual model simulation.

6. Section 2.1 – p4 l21-35 – These lines cover methodology and results from Kok et al. (2017). While necessary and useful to repeat here, I suggest making it very clear that up to l 35 this is a repeat of method and size distribution from Kok et al. (2017).

   To improve clarity for this section, we have added an extra sentence before Eqn. 1, and re-write the paragraph following the same equation.

   "While details can be found in Kok et al. (2017), a summary of their globally-averaged size distribution is given here as:"

   "As reported in Kok et al. (2017), the constrained globally-averaged size distribution of emitted dust particles, $\left[\frac{d\tilde{V}_{emit}(D)}{dD}\right]_g$, is based on an analysis of different measurements of the emitted dust size distribution, while the size-resolved globally-averaged dust lifetime, $\left[\tilde{T}(D)\right]_g$, is based on an ensemble of global model simulations"

7. Section 2, p5, l1-17 – this section forms a crucial part of the method – the main correction/constraining of the model size distributions – yet it is difficult to follow. The authors should explain this section much more clearly and in detail, perhaps with additional figures in the supplement and/or outlining a specific example, to clearly illustrate how the PSDs are forced away from the model simulations. Some specific comments are given in the points below, but I suggest they review and rephrase these lines.

   We have re-written the paragraph before Eqn. 2 to better clarify the procedure. After Equation 2, we have also made additional clarifications to the sentences, including clearly explaining the dimensions x, y, and z. For this part, we added "…;x is the dimension for longitude, y is for latitude and z is for height."

8. It is not very clear at which point annual averages vs spatially varying size distributions are used from the simulations. E.g. p5 l5 – "annually-averaged, globally-averaged" size distributions are forced here – how/at which point are the spatially varying size distributions corrected? Better signposting of global averages vs spatial variations throughout the paper would be extremely useful in understanding the methodology.

   We made this distinction by specifying in each formula the independent variable of each parameter. For example, $\hat{f}_{k,i}(x, y, z, D_{k,i})$ in Eqn. 2 is a spatially-varying parameter defined for x-longitude, y-latitude and z-height, while the $\left[\bar{\bar{f}}_{k,i}(D_{k,i})\right]_g$ is the globally-averaged counterpart denoting that the parameter is averaged over all space (x-y-z). To make this clearer, we have explicitly defined the independent variable following its first use in Eqn. 2., adding "x is the dimension for longitude, y is for latitude and z is for height"

9. P5 l9-10 "to the global dust loading" – which global dust loading – simulated or from Kok 2017?

   The sentence has been re-written for clarity. It now reads "This correction factor (α) is defined by the ratio of the Kok et al. (2017) constraint on the fractional contribution of the particle bin to the simulated fractional contribution of the particle bin per unit global dust loading."

10. P5 l1-17 – the description of equation 2 is not clear enough. E.g. what is the numerator in the equation for alpha?

    The numerator is the fractional contribution of the Kok et al. 2017 globally-averaged size distribution defined between diameter $D_{k,i+}$ and $D_{k,i+}$. In addition to the description of α before Eqn. 2, we have added the following statement to improve the clarity after the

equation.: "the numerator, $\int_{D_{k,i-}}^{D_{k,i+}} \left[\frac{d\hat{V}(D)}{dD}\right]_g dD$, is the constraint obtained from Kok et al. (2017)"

11. P5 l16-17 – "where the discrete sum over each location and height equals unity, that is:..." – Why is the sum unity? Is this because the size distributions are normalized?

    Yes, that's indeed correct. This is a key point, so we have also rewritten this for clarity.

12. Fig S1 – Please include the Kok 2017 globally averaged constrained size distribution on each panel. This would enable the reader to see what the size distribution is being constrained by.

    That's a good idea. Since DustCOMM is forced to the Kok et al 2017 size distribution, both DustCOMM and Kok et al 2017 are the same and thus overlap in the Figure S1. Although not always visible, we have nonetheless included the Kok et al 2017 size distribution in Fig. S1 for completeness (see below).

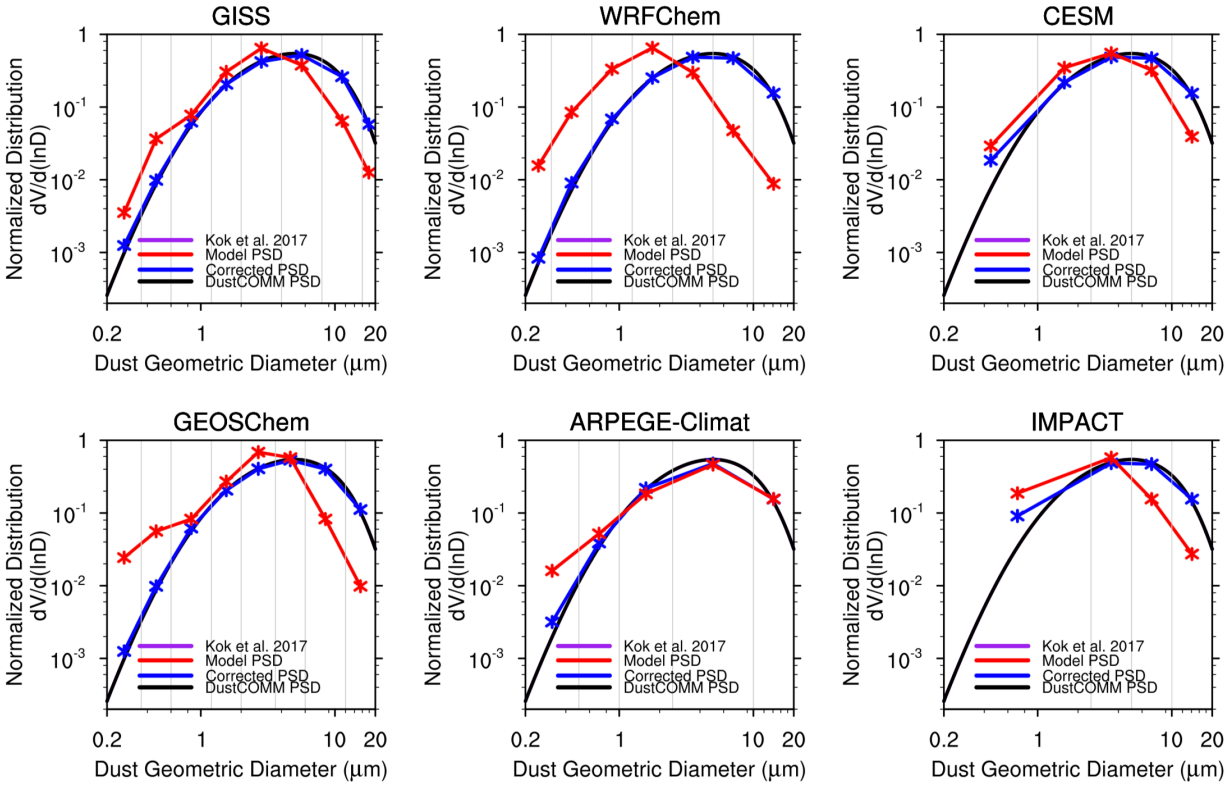

13. Figure S1 – please also include (either in this plot, or as a separate one), how the size distributions changed due to the re-binning/extension/curtailing, as described in Section 2.1.1.

We have included the figure below in the supplementary document

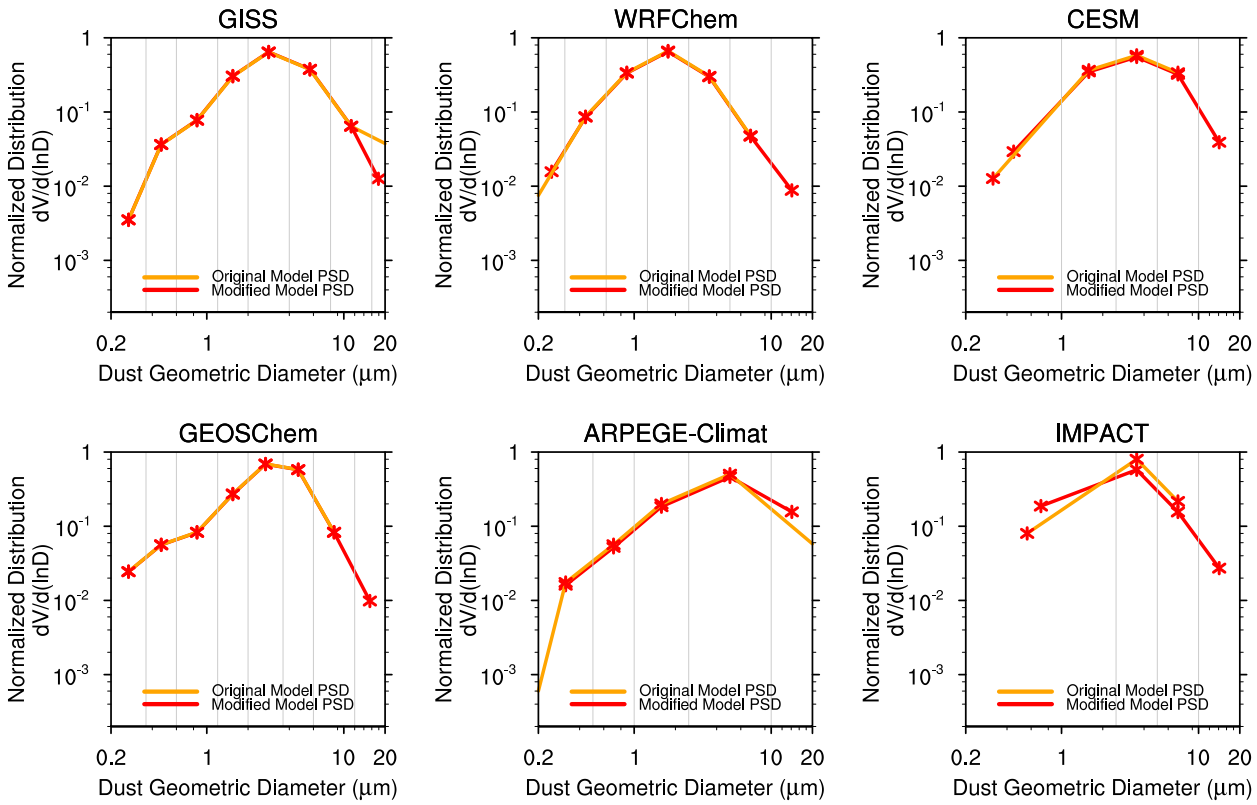

14. Section 2.1.1 – Is this diameter range correction performed after the size distribution correction (section 2.1)? Figure S1 suggests that first the diameter range correction is performed, and then the size distribution correction. But the ordering of the text (2.1 – size distribution correction, 2.1.1 – diameter range correction) suggests the opposite. Please clarify and order the text appropriately to follow the steps in the method.

This is indeed confusing. The order described in section 2.3.1 (formerly 2.1) does follow the steps taken in the methodology. That is, the dust mass fractions were corrected and then the size ranges were set to the common diameter limits. To make this clearer, we have added a statement that the dust mass fractions were re-normalized after the correction, such that the discrete sum still equals unity over each location. This statement at the end of section 2.1.1 reads: "After the dust mass fractions are corrected, they are re-normalized such that the discrete sum between D_{min} and D_{max} equals unity over each location and height."

For the 'uncorrected' model dust mass fractions, we highlight in section 2.1 (formerly 3.1) that, for consistency, they are also set to the same diameter limits between 0.2 and 20µm following the same procedure described in section 2.3.1.1 (formerly 2.1.1).

15. P6 l1-3 – Ryder et al. (2019) show that over the Sahara D>20µm contribute to at least 18% of SW extinction and 26% of LW extinction – these values are not negligible and represent aged Saharan dust.

    P6 l4, "dust particles with D>Dmax generally stay only for a short period in the atmosphere before they are deposited" – this is not the case in van der Does et al. (2018), as stated elsewhere in this manuscript.

    That's a good point – those two recent papers indicate that the community has greatly underestimated the effect of dust with D > 20 um. In this study, we need to limit the maximum diameter to 20 µm because results from Kok et al. 2017 used to constrain our dust size distribution is limited to this diameter. But to better acknowledge that particles greater than 20 µm might be important even farther from source regions (e.g. Ryder et al. (2019)), we have re-written this part of the paragraph:

    "Further, we set the upper diameter limit to $D_{max} = 20$ µm, because most global models generally do not incorporate dust particles beyond 20 µm and also because the observational constraints on the size distribution from Kok et al. (2017) is limited to this maximum diameter. Although advances in airborne observations in recent years have led to measurements of larger dust particles with $D > D_{max}$ in the atmosphere which has shown that the contribution of $D > 20$ µm to shortwave and longwave extinction are non-negligible (e.g. Ryder et al., 2013b, 2019; Weinzierl et al., 2009, 2017), there is still a scarcity of these measurements, such that an observational constraint on dust particles with $D > D_{max}$ would be very uncertain (e.g. Mahowald et al., 2014)."

16. P5 l1-6 – the authors should revisit the impact of particles d>dmax in the discussion (e.g. Section 5.4). For example, if better global constraints/observations on this size range became available, could such observations be incorporated into DustCOMM? \

    Yes, that's a good point. We have added the sentence below in section 4.4 (formerly 5.4) to clarify this point.

    "Given that dust particles with $D \geq 20$ µm can contribute substantially to dust extinction both in the shortwave and longwave spectrum (Ryder et al., 2019), future versions of DustCOMM could be extended to a diameter range beyond 20 µm as more measurements of dust size distribution with $D \geq 20$ µm become available."

17. P6 l30-32 – the authors essentially extend 4 models' size distributions towards a larger size range based on the other 2, which cover a wider diameter range. Does this implicitly assume that all the models behave the same way in terms of the coarse end of the size distribution? This seems unlikely. This should be discussed more, particularly since many of the results are most sensitive to the size changes above d=10 microns

No, our constraint does not implicitly assume that the models behave the same way. Since dry depositions in these models are controlled largely by gravitational settling, the rates of deposition of the dust particles are often different. Our constraints thus account for these differences by taking into account the differences in the spatial variability of the bin that overlaps between the two models. That is, in correcting for model simulation k in Equation 4a (for example), we account for the difference between the bins $[D_{k,N_k-}, D_{k,N_k+}]$ and $[D_{r,j_r-}, D_{r,j_r+}]$ in model r, which partially overlap with each other (Eqn. 4b). Although the correction factor $\beta_r(x, y, z)$ is expected to take into account the differences between model k and model r, we however still assume that the distribution largely follow the same form controlled by the rate of dust deposition in each model. We have added the sentence below to clarify this point.

"It should be noted that the correction of Eqn. 4 takes into account the potential difference in the dust deposition between models k and r, by considering the differences in the spatial variability of dust loading between similar bins of $[D_{k,N_k-}, D_{k,N_k+}]$ and $[D_{r,j_r-}, D_{r,j_r+}]$."

18. Equation 5 – please state how/if this equation is different to that from Kok et al. (2011), and if so why.

    Despite the similarity in Equation 5/6 and that from Kok 2011, an important difference is that Kok 2011 describes the size distributions at emission while Eqn. 5/6 describes the size distribution in the atmosphere. Because of that, our formulation in Eqn. 5/6 builds on the brittle fragmentation theory of Kok 2011, but adds analytical expressions of dust deposition and dust changes during transport. In addition, the generalizations of parameters in our equation also allow us to better fit different shapes of dust mass fractions over different locations, and thus able to place a better constraints on dust size distribution.

    To clarify this point, we have added the following section at the end of section 2.3.1.2 (formerly 2.1.2): "Finally, we note here that although our generalized theoretical function of Eqn. 6 builds on the brittle fragmentation theory of Kok 2011, it adds analytical expressions of dust deposition and dust changes during transport that allow us to better fit different shapes of dust size distribution over different locations."

19. Equation 5 & p8 l6 – why choose D_s for the geometric median diameter by volume? S subscript typically implies with respect to surface area. D_v would be more appropriate.

    Thank you for this comment. We have changed the subscript from s to v

20. P8 l20-27 – This seems a great generalization. It's not clear how b is applied to specific locations as implied.

The application of all the parameters in Equation 6, including the parameter b, was done by fitting the expression using Equation 7 for each location. As a result, values for b could be different from one location to the other, based on the shape of the corrected dust mass fraction from Eqn. 2. The distributions of these parameter, including parameter b, are included in supplementary Fig. S-2. To make this clearer, we have reworded the paragraph before Eqn. 7, and also added additional sentence to the paragraph after Eqn. 7.

"To determine the parameters in Eqn. 6 for each height, horizontal location, season, and model simulation, we fit the generalized size distribution of Eqn. 6 to the corresponding corrected dust size distribution from Eqn. 2 above. To do this, we minimize the chi-squared (χ^2_k) value for each height, location, and for each model k, such that:"

"The probabilty distribution of these parameters for all heights, horizontal locations, and model simulations of the annually-averaged dust size distribution is shown in the supplementary Fig. S-2"

21. Section 2.1.2 – What is the reason for choosing this method of fit (eqn 6) as opposed to fitting a series of lognormal modes, as is typically done for size distribution measurements? Presumably given the simulated size distributions have been corrected based on the same function, the fitting of the corrected size distribution is more naturally aligned with eqn 6?

    That's a good point. We use Eq. (6) because it includes some mechanistic understanding of what determines the functional form of dust size distributions. Furthermore, although lognormal modes are appropriate for several other aerosol species, dust size distributions generally do not follow lognormal distributions very well, in part because the emitted dust size distribution is distinctly lognormal, as detailed in Mahowald et al. (2014). We have added a sentence to clarify this point in the first paragraph of section 2.3.1.2: "Although fitting lognormal modes are appropriate for several other aerosol species, Mahowald et al., (2014) highlighted that dust size distributions are usually not lognormal and are thus better characterized by a generalized function based on mechanistic understanding of dust emission and deposition processes. "

22. P10, section 2.3, l26-30 – units for all quantities would be helpful. What do the authors mean by "mass-weighted" in "mass-weighted vertically-integrated 2-D mass extinction efficiency" and what are the units of epsilon_tau and epsilon_m?

    The units of each variable have now been included. And this phrase is indeed confusing as we meant "vertically-integrated 2-D mass extinction efficiency", thus the "mass-weighted" has been removed.

23. P10, section 2.3, l26-30 – I believe this calculation is the same as first used by Kaufman et al. (2005), which should be cited.

Good point. Kaufman et al. (2005) has now been cited.

24. P10 l31-32 – please list the reanalysis products (MERRA-2 etc) here to avoid confusion. Also see later comment about section ordering of 3.2. “Dataset” should be ‘datasets.’

    Thank you. This comment has been addressed in the paper.

25. P10 l32-p11 l2 – “This individual reanalysis dataset....” - I suggest removing this (and adding to section 3.2 if necessary). It is confusing here given that the AOD reanalyses have not yet been described.

    P11 l10 “the four data sets...” – this is also confusing given that the AOD datasets have not been properly introduced at this stage in the paper. See later comment about relocating section 3.2. Ordering and section 3 – I suggest the authors move sections 3.1 and 3.2 to before section 2. This would be easier to follow and understand. Section 3.3 should remain after section 2 since it follows on logically.

    This is a great idea to improve the paper’s clarity, thank you. As suggested by the reviewer, we have combined section 2 and 3 and reorder the subsections, such that the description of model simulations (section 2.1) and the reanalysis products (section 2.2) comes before the description of the DustCOMM products (section 2.3)..

26. P16 l35 – 2011-2015 is presumably limited by available years? Is there any impact of this difference in years used?

    Yes indeed, the dust AOD for JRAero is only available between 2011 and 2015. Although we did not analyze the impact of the difference in DAOD climatology between JRAero and the others, we expect that the relative difference will be smaller over the dust dominated region.

27. P17 l32 – and is also a 2-D diameter project of a 3-D shape, which may introduce bias (e.g. Chou et al., 2008).

    Thank you. We have reworded the relevant sentence of the 3rd paragraph of the section to better reflect this.

    “during the microscopy analysis, particle diameters are usually determined as the volume-equivalent geometric diameters based on 2-dimensional images (Chou et al., 2008). Because of the asphericity of dust aerosols, this could introduce some biases (e.g., Okada et al., 2001; Huang et al., in prep.).”

28. P17 l 36 “separate channels for different particle sizes” - this is not really relevant and could introduce confusion.

Thank you. This part of the sentence has been removed.

32. P17 l25-40 – there is a 4th category, which covers imaging probes, as used in the AER-D field campaign (section 4.18 of supplement) – which are beneficial since they do not suffer from uncertainties in converting scattered light to size as OPCs do.

    That's a good point. We have included two sentences to highlight this point. First sentence is added in the first paragraph stating: "Another category is the imaging probe whereby the particle image is detected by linear photodiode array providing a two-dimensional projection of the particle (Baumgardner et al., 2017; Ryder et al., 2018)."

    The other is added to second paragraph of section 2.4.1 stating: "Unlike the optical particle counters that require assumption regarding dust refractive index and shape to convert scattered light intensity to particle size, the imaging probes are not subject to these uncertainties (Baumgardner et al., 2017; Ryder et al., 2018)"

33. P18 l22-25 – OPCs have other sources of uncertainty – such as refractive index applied in the inversion of scattered light to size and the non-monotonic relationship between scattered light and particle size. These should also be mentioned.

    We have included a sentence to clarify these points.

    "In addition, optical particle counters also make assumptions about the refractive index to derive the dust size distribution, and are affected by the non-monotonic increase in the intensity of scattered light with particle size (Ryder et al., 2018; Weinzierl et al., 2011)."

34. P18 l11-25 and section 3.3.2 – in-cabin measurements are also subject to uncertainties and size-bias in sampling due to aircraft inlets. As such, the MEE values from studies in table 2 are likely biased high in some cases.

    Thank you for this comment. We have added a sentence in this paragraph to highlight this point. "For in-cabin measurements, studies have shown that the loss rate of coarse dust particles can be substantial due to the aircraft's instrument inlet, therefore leading to lower sampling rate and size bias (e.g. von der Weiden et al., 2009)."

35. P18 l14 – although the size distribution measured does not allow aerosol type to be distinguished, various chemical composition measurements made in parallel are now mostly a matter of routine during airborne campaigns. Individual studies often use these to infer size distributions or ranges dominated by different aerosol types.

    We thank the reviewer for this comments. While measurements of chemical composition helps to isolate dust from non-dust particles, there are still potential for mis-identification. We further address the discrepancy between measurements and our results in section 4.1

36. Section 3 – there is a huge variety of measurement data available, and I do not suggest the authors attempt to significantly widen their coverage. The authors should describe how and why the studies in Table 2 were selected. There also appears to be a geographical gap of sampling Arabian dust (Fig S1). Additionally, I suggest the studies of dust sampled during the AMMA airborne missions (Formenti et al., 2011) as being a very useful addition, since they provide summertime sampling in the Niger region, which is currently not covered by the studies in Table 2.

    We thank the reviewer for this comment. For the most part, the studies we selected for dust size distribution are those that reported actual measurements of coarse dust particles and not log-normal fit or parameterized distributions. The dust size distribution reported in Fig. 10 of Formenti et al. (2011) is a log-normal fit to measured data, such that we cannot use this data. We have included additional sentences in the second paragraph of section 2.4.1 that clarify how and why some of the studies in Table 2 are selected.

    "For the dust size distributions, our criteria for selection of studies are as follows: (1) the measured size range of the data should extend into the coarse dust (D > 5 um) size range; (2) the study should report the original in-situ measurements, instead of (lognormal) fits to the actual measurements; and (3) each study's measurements should be taken with commonly-used instrumentation in order to ensure some consistency with measurements taken by other studies. "

37. Table 2 – please indicate which studies relate to which numbers on the map on Figure S3.

    We now clarify this in the caption of Fig. S-3.

38. Section 3.3.2 and Supplement section 4 – The descriptions of data taken from each measurement campaign are too vague, and occasionally in error. Often it is not enough just to reference a paper as within the measurement papers observations are collected/averaged in different ways (time periods, meteorological regimes, altitudes, etc.) and it is not clear which are being used here. The authors should state specifically which data are taken from each paper, and what the values of MEE or MSE are, preferably listing them in a table in the supplement. Specific comments about data described in the supplement are given in the Supplement section.

    Thank you for the comment. We have made several additions to the supplementary section 4 to address this point. In addition, we also state in Table 2 where the data are taken from, by referencing the specific figure or table where applicable.

39. P18 l34-35 – Ryder et al. (2013b) SSA values fall well outside this SSA range. This is a fairly narrow SSA range selected. The authors should note that measured SSA is sensitive to the size range sampled in the observations, which is likely to exclude the coarse mode and often d>~2- 3 microns in many cases due to the effects of inlets. Only 3 studies are

cited, while there are a huge variety of studies in existence which have measured dust SSA.

We thank the reviewer for pointing this out. We have increased the uncertainty range to 0.03 and have also included citations to other studies.

40. P19 l9-11 – "These errors include errors due to the instrument measuring the extinction coefficient" – change to 'instrumental uncertainties.' "meteorological influence" – such as? "the assumption of internal or external mixing" – how is this important?

    For clarity, we have removed this sentence, and added "including instrument uncertainties" to the preceding sentence.

41. P20 l13-17 – Field campaigns additionally often sample a variety of cases which are representative of the within-season variability, and also often include uncertainties/ranges to cover the variability encountered.

    That is right. Thank you for pointing this out.

    We have added a sentence to highlight this point: "Furthermore, most of these measurements are campaign averages often over a variety of cases that could be representative of the season-averaged size distribution."

42. P21 l2-3 "(1) the ACE-2 campaign (June/July, 1997) off the west coast of Western Sahara and Morocco (Otto et al., 2007)" – would be better referred to as in the vicinity of the Canary islands. Same for caption of Figure 3.

    Thank you for pointing this out. We've corrected this accordingly.

43. P21 l6 "(2) the Fennec project (June 2011) between the Canary Islands and Mauritania/Mali (Ryder et al., 2013)" – If the authors refer to measurements between the Canary Islands and Morocco/Western Sahara (not Mauritania/Mali which are inland) the citation should be Ryder et al. (2013a – GRL) and the geographic references corrected. The same applies to the caption of Figure 3.

    Thank you for this comment. We realize the confusion and we have clarified it in the paper. Data from the two Ryder 2013 papers are used in our study. Here, we do in fact mean the Ryder et al. (2013 – GRL) which is represented in the paper as Ryder et al. (2013a). We have adjusted the text, the geographical reference and images accordingly. The representative location is now placed at 27.65N, 14.25W.

44. Figure 3 – what is the reason for the selection of altitude choice? It seems biased very high – presence of dust at z>6km is unlikely and concentrations will be very low at

5.5km – therefore the value of such high altitude comparisons is questionable. What is the reason for the selection of these 3 studies for Figure 3? The geographic spacing is very close, with all sampling JJA SAL dust. "ACE-2" in line 7 of the caption should read "AER-D."

Thanks for the correction. ACE-2 has been changed to AER-D.

We identify these 3 studies to show that DustCOMM performs better than model simulations for a range of heights. We recognize that dust concentrations are lower for $z>6$km, but we follow Fig. 1 of Ryder et al. (2013 – GRL) which shows that there are still some coarse dust particles at ~6km. To address this comment, we have added additional comments in Table 2, and a justification for the height selection in the supplementary document.

45. P22 l1 – 14% and 15% - in terms of which variable?

    This is in terms of the dust mass fraction – i.e. the fraction of dust per unit mass of dust loading. We have clarified this in the paper. The sentence now reads "On average, simulations in our model ensemble overestimate the dust mass fraction of the fine mode by ~14%, and underestimate that of the coarse mode by ~15%."

46. P23 l25 – and also Qinghai Province China?

    Yes, good point. We have added this to the text: "… and Qinghai Province, China (Li et al., 2000)"

47. P24 l17 – "weighted by the dust vertical distribution" – why is this necessary?

    We agree with the reviewer that "column-integrated dust MEE" explains our point in that sentence, and "weighted by the dust vertical distribution" is indeed not necessary. As a result, we have removed it.

48. P24 l31-32 – as stated earlier, it is not clear why the MEE and AODs need to be used to calculate the column mass loading, given that this is typical model output, and the size distributions are already available. It should be a direct step to calculate column mass loading from size distributions, given a dust density.

    See our response to similar comments above (General Scientific Comments #1)

49. Section 5.1 – are there any impacts of uncertainties in wet deposition on the size distribution biases?

Uncertainties in dust deposition broadly affect our estimates of dust size distribution, as we discuss in the fourth paragraph of the new section 4.1 (formerly 5.1).

50. P27 l30 – Fig 7a does not show MEE.

    Thank you. This is noted and has been corrected.

51. P27 l31 – there is no figure S7 in the supplement.

    Thank you. This is noted and has been corrected. We meant to say supplementary Fig. S-6

52. Section 5.4 – the implications of dust LW properties should be reflected on here, considering the points about the LW radiative impacts of dust being crucial to the total impact on the radiation balance described above.

    We thank the reviewer for this comment. We have now added a sentence in section 4.4 (formerly 5.4) that emphasizes the use of our dust size distribution for longwave radiative impacts. "With improved constraints on the dust size distribution and therefore the dust optical properties, DustCOMM could be used to determine the dust (shortwave and longwave) heating rates in the atmosphere more accurately than possible with current global model simulations. As a result, our constraints on dust size distribution could be used to better quantify radiative effects of dust, especially in the longwave spectrum which have remained very uncertain (Di Biagio et al., 2017; Dufresne et al., 2002; Kok et al., 2017; Song et al., 2018)"

53. P30 l20 – should 'indirect effects' be 'semi-direct effects'?

    Good point. We have included both indirect and semi-direct effects.

54. P30 l28 – some reference to the SW spectrum and 550 nm should be included, since refractive index and MEE are only considered at this wavelength.

    We have clarified that the DustCOMM mass extinction efficiency is at 550 nm. Since our constraints is taken from Kok et al. 2017, we have also included that reference in the sentence.

55. Section 5 – There is a general focus on in-situ observations for validation of DustCOMM. However, remote sensing observations are developing rapidly and it would be useful for the authors to consider whether lidar retrievals, for example, would be usable within the DustCOMM framework.

Remote sensing observations are certainly useful as we continue to develop DustCOMM. As we stated in section 4.4, we hope to incorporate more observational constraints within DustCOMM framework. For example, to constrain the vertical distribution of the atmospheric dust loading, lidar-based retrieval of dust extinction, such as from CALIPSO, will be very useful, and it is part of future work.

We have added a sentence in section 4.4 to further highlight this point. "For instance, a next step could be to include constraints on the dust vertical concentration profile over every location, in order to more accurately estimate dust deposition, and dust concentration at the surface and in 3D. For this, lidar-based retrieval of vertical dust extinction profiles from Cloud-Aerosol Lidar and Infrared Pathfinder Satellite Observations (CALIPSO) can be combined with the corresponding constraints on dust mass extinction efficiency from this study to obtain constraints on the dust vertical concentration profile."

56. P31 – l25-26 – the bias across the full size range should also be stated.

We have included an additional sentence to address this point.

"Because DustCOMM underestimates the measurements for $D \leq 0.5\mu m$, it shows a more negative bias (~50% more) over the full size range (between $D = 0.2 - 20\mu m$), although the error is markedly lower (~15 %), when compared to the ensemble of model simulations. Overall for $D \geq 0.5\mu m$, DustCOMM shows a bias against measured size distributions that is significantly less (about 46% less) than for an ensemble of global model simulations."

57. Are there any important dust altitude or seasonal changes in DustCOMM vs the models?

As Fig. 7 suggests, DustCOMM vertical profiles follow the form of the ensemble of global model simulations, but the fraction of dust mass in each bin is different from that of the model ensemble since the constraints adjust every location and height by the same factor. In addition, similar adjustment to the annually-average dust mass fraction between DustCOMM and model ensemble is also apparent at the seasonally-averaged timescale.

We have added a sentence in section 3.1.2.2 to clarify this: "Finally, similar changes in the spatial variability of the annually-averaged dust mass fraction are apparent in the seasonally-averaged values."

58. Discussion/Conclusion - It would be interesting if the authors could comment on bias of models vs measurements in previous studies (e.g. Hunneus et al., 2011; Evan et al., 2014), and similarities/improvements seen in those studies vs DustCOMM and the model simulations in this study.

Since models used in those studies (e.g. AeroCom in Hunneus et al., 2011) are similar to those used in our study here, they suffer from similar biases and shortcomings. That is the biases in dust properties are associated with biases in dust size distribution, it therefore suggest that better constraints on size distribution as done with DustCOMM should provide a better estimates of these dust properties. Here in section 4.4, we have added the sentences below to highlight this point.

"Furthermore, since recent studies associate much of the biases in dust properties, such as the dust aerosol optical depth, deposition fluxes and surface dust concentration, to model biases in dust size distribution (Evan et al., 2014; Huneeus et al., 2011), DustCOMM estimates can therefore serve as a better alternative. For example, DustCOMM's improved constraints on atmospheric dust loading and dust size distribution could contribute to better estimates of size-resolved dust concentration near the surface (e.g. Whicker et al., 2018). Over the ocean, such constraints on size-resolved dust concentration could potentially be used for constraints on dust deposition fluxes that are more accurate than possible from global model simulations."

59. AOD reanalyses – do the authors combine these into one single reanalysis dataset themselves? This is not really clear.

    Yes, they are combined into one single data and the details of this is given in the (new) section 2.2.

Technical Comments

1. P3 l12 – "The resulting product constrains the climatology of 3-D global atmospheric dust properties on seasonal and annual timescales" – change to "The resulting product constrains the climatology of 3-D global atmospheric dust properties and is provided on seasonal and annual timescales" – to avoid confusion that the authors are constraining the temporal variability of dust properties.

   Thanks for this comment. We have changed the sentence accordingly.

2. P3 l34-35 – "After correcting..." – unclear – do you mean you combine all models into one multi-model representation?

   Yes. We have added the word "multi-model" to make it clear

3. P6 l28 – "globally-averaged size distribution" – Kok 2017 or the simulated one? P7 l13 - "globally-averaged size distribution" – Kok 2017 or the simulated one?

We meant the Kok et al 2017 or the constrained globally-averaged dust size distribution here. We have changed them to “”constrained globally-averaged dust size distribution”. We have also clarified other places where globally-averaged size distribution are mentioned.

4. P9 l18 – typo – should be -10 to -4?

   Thank you. It is in fact between -10 and 4, but because we realize this can be confusing, we have changed this (and others) to be -10 to 4.

5. Eqn 8 – please provide units for epsilon_tau

   We have provided unit for this parameter, and others alike.

6. P10 l27 – “atmospheric “column” dust loading”?

   Yes. We have included “column”.

7. P14 l25 – change to “...of the in-situ emission measurements..”

   Thank you for the comment. The sentence now read “The dust MEE is influenced by the uncertainty in the constrained globally-averaged extinction efficiency, which in-turn is partially due to uncertainties in the in-situ emission measurements of index of refraction and dust particle shapes”

Supplement Comments

1. The supplement contains two Figure S1s. The second should be S3 (?).

   This is corrected. Thank you.

2. Section 3.1 – l7-8 – mention that it is the AOD which is assimilated.

   Yes. We have done that. The sentence now reads.

   “For the first time, meteorological and aerosol observations (which include bias-corrected **aerosol optical depth** from MODIS, AVHRR, MISR – over desserts, and ground-based AERONET instruments) are jointly assimilated into MERRA-2…”

3. Section 3.3 - “1.1ox1.1o” typo
   This has been corrected. Now written as $1.1^{o}x1.1^{o}$

4. Section 4 – To make this easier to navigate, relate each observational subheading to the numbers on fig S3 (map). Also include the campaign name in the heading for each section. Take care to state for each subheading whether the campaign was ground-based or airborne. Also explain the choice of altitude selection defined in table to where relevant. Please also be aware, and state where necessary, that although a large size range may have been measured, inlet-size effects may have prevented coarser particles from being measured for some campaigns.

   Thank you for the comment. We have included in each observational heading the campaign name as well as whether only PSD or MEE is taken or both. For cases where PSD are taken, we have also included sentences explaining the choice of our representative altitude.

5. Section 4 – a subsection on Kandler et al. (2009), as listed in table 2, is missing.

   Thank you for pointing this out. We have included a brief description of Kandler et al (2009).

6. Section 4.1 – please make the locations listed consistent with those listed in table 2.

   Thank you for the comments. We have corrected where discrepancies occur.

7. Section 4.7 – note that these size distributions were not corrected for refractive index. The FSSP was *not* used as it did not operate correctly. Instead the size distribution larger than d=3 microns was taken from a sunphotometer retrieval.

   Thank you for pointing this out. We have removed the mention of FSSP, and include a sentence mentioning that the they did not correct for refractive index.

   "The size distributions were not corrected for refractive index because they assumed that the refractive index of latex is approximately similar to that of dust."

8. Section 4.10 – Please note that these studies operated instruments behind significant pipework and suffered loss of the majority of coarse particles (e.g. Ryder et al., 2018, Table 1).

   Thank you for pointing this out. We have included a sentence in the section stating that: "Because of the aerosol inlet configuration on the aircraft, the measurement of coarse dust were particularly problematic."

9. Section 4.11 – Why is MEE only taken from DODO1 (winter time?). It appears that the MEE for DODO1 is taken from table 4 of Osborne et al. (2008), for the 'AM+CM' case (a value of 0.41). No coarse mode was measured during DODO1 (see McConnell et al., 2008).

The AM+CM DODO1 case in Osborne et al. (2008) was calculated using the coarse mode size distribution from DABEX since none was available from DODO1. This should be stated, or preferably the value from DODO2 used, where coarse mode was measured. Why is only z<1km used for the DODO2 size distributions?

Thank you for this helpful comment. We have clarified this point in the section.

10. Section 4.12 – is the campaign average size distribution used?

    These data are taken from their Fig. 8 which represent the composite size distribution for L02 on flight #060519a and L07 on flight #060604a. We have included an additional sentence in this section to clarify this point.

11. Section 4.13 – and also same aircraft as SAMUM1? SAMUM1 also used a high spectral resolution lidar.

    They used the Falcon aircraft, which was also used in SAMUM-1. We have added this information to the section.

12. Section 4.14 – 'used the same instrumentation...' – as which paper/campaign? Presumably the same as Kandler et al. (2009) which is missing? It is not clear which instruments the size distribution comes from – but probably because the 2009 section is missing.

    Thank you for pointing this out. Yes, the instrumentations are similar to that from SAMUM-1 (Kandler et al., 2009). This detail has been clarified in the section.

13. Section 4.15 – Data from Ryder et al. (2013a – GRL, Canary Islands) is also used in the paper (Figure 3) and should be described here. Please take care to specify whether Ryder et al. (2013a or 2013b) is being cited – both are given in the references as 2013. Comparisons of both can be found in Ryder et al. (2019). "For this study, mean distribution from PCASP and CDP were selected because they were the most credible based on the authors' analysis." – change to ..."based on the authors' analysis over the size range we use here." MEE is not given in Ryder et al. (2013b - ACP), presumably this is taken from Ryder et al. (2013a) (please state). Mean values in Ryder et al. (2013a) are 0.15 for fresh dust or 0.23 for aged dust – these appear much lower than the value plotted in Figure 8 (around 0.3).

    Thank you for these very helpful comments. We have re-written this section to include the descriptions of both Ryder et al. (2013a – GRL) and Ryder et al. (2013b – ACP). Indeed, data from both studies were used in this paper. For Ryder et al. (2013a), we obtained the dust size distributions as a function of heights, which were generously given to us by the first author. For Ryder et al. (2013b), we obtained the campaign averaged dust size

distribution already published. Appropriate geographical references have also been noted both in the supplementary document as well as in the main text and figures. For the MEE, we used the averaged values of 0.31+/-0.08 between the reported values for aged dust (0.23) and the SAL categories (0.39).

14. Section 4.16 “above the SAL” – I would expect a dust measurement to be taken ‘in’ the SAL – is this a typo?

    Thank you for pointing this out. It is indeed within the SAL layer. We have made the correction accordingly.

15. Section 4.18 – “The AER-D campaign uses similar instrument as the Fennec 2011 campaign. They use wing-mounted optical particle counters and shadow probes to measure dust sizes between 0.1 and 100 μm diameter.” – but additionally this AER-D used cloud imaging probes (CIP15 and 2DS) for size distributions at d>10 microns (which were used in Fennec but were not mentioned in Section 4.15 as the authors did not use the shadow probe data (d>18.5 microns) in this study).

    Thank you for the comments. We have included in this section that the imaging probes are also used.

Reply to reviewer #2

This study presents a new dataset, the Dust Constraints from joint Observational- Modelling-experiMental analysis (DustCOMM), which combines in-situ measurements, reanalysis products, and an ensemble of six global model simulations. Particularly, globally-averaged dust size distribution and extinction efficiency from observational and experimental data are used to constrain the DustCOMM products. The annual and seasonal mean products of 3-dimensional (3D) dust size distribution, 3D dust mass extinction efficiency, and 2D dust loading are provided for the time period from 2004 to 2008. It is found the dataset shows a better agreement with measurements than the six-model ensemble in terms of dust size distribution and mass extinction efficiency. This dataset may be used to constrain dust simulation in global models and to study dust impacts on the earth system. The paper is generally well written. The methodology to develop the datasets is thoroughly introduced and related uncertainties are also discussed in detail. I have a few comments would like the authors to address.

We thank the reviewer for the constructive and helpful comments that helped us to further improve the paper.

Major comments:

1. Here globally-averaged dust size distribution is used to obtain 3D dust size distribution. Is it possible to demonstrate that the regional differences in dust size distribution are small? Or have you considered using different dust size distribution for different regions, e.g., by applying regional averaged values to areas where individual measurements are available and the globally-averaged value to areas where measurements are not available? This might provide better spatial constraints on the dataset. Similarly, globally-averaged dust extinction efficiency at 550 nm is used. How large are the spatial differences? Is it possible to give a rough estimation based on available data?

   We thank the reviewer for this insightful comment. Assuming globally consistent size distributions and extinction efficiency is indeed one of the main assumptions in this paper.

   We used globally-averaged dust size distribution and dust extinction efficiency because the measurements to constrain these parameters on a regional basis across the different dust-source regions are currently insufficient. Since North African dust dominates most of the global dust emission and many of the measurements used to constrain the globally-averaged values are associated with the North African dust, constraining the regional dust properties with insufficient measurements will likely result in larger uncertainties than estimated in this study. Moreover, since our constraints are applied globally, regional differences in dust size distribution, for example, are assumed to follow the ensemble of the six model simulations.

To better clarify this point in the manuscript, we have added additional sentences to the first paragraph of section 4.3: "We used modelling constraints in DustCOMM where observational constraints were either not available or insufficient. For example, modelling constraints are used for the regional differences in dust size distribution and extinction efficiency because the measurements to constrain these parameters on a regional basis across the different dust-source regions are currently insufficient. To further reduce the uncertainty associated with using modelling constraints, we used an ensemble of six model simulations."

2. As discussed in the paper, dust aerosol optical depth from the reanalyses largely depends on the models' treatment of the dust cycle, and this adds uncertainties to the DustCOMM. I wonder if you considered using satellite products of dust optical depth, such as level 3 dust optical depth from the Cloud-Aerosol Lidar with Orthogonal Polarization (CALIOP).

   That's a good suggestion. Although our analysis includes both random and systematic errors in dust AOD by incorporating the satellite-based study of Ridley et al. 2016 with the ensemble of reanalysis datasets, we agree that the estimate of the dust AOD likely incurs additional uncertainties associated with model treatments of dust cycle. However, dust extinction retrieval from CALIOP also suffer from several uncertainties, such as weak signal-to-noise ratio during daytime versus nighttime retrievals (e.g. Kacenelenbogen et al., 2011; Winker et al., 2013) and erroneous assumption of aerosol extinction-to-backscatter ratio used in the extinction retrieval (e.g. Omar et al., 2009; Mamouri et al., 2013; Nisantzi et al., 2015). In addition, it is unclear how the limited spatial coverage of CALIOP AOD retrieval affects the climatological estimates. Nonetheless, our plan is that future versions of DustCOMM will incorporate extinction profiles from CALIOP in estimating the vertical distribution of dust concentration.

   We have added a sentence in section 4.4 to further highlight this point. "For instance, a next step could be to include constraints on the dust vertical concentration profile over every location, in order to more accurately estimate dust deposition, and dust concentration at the surface and in 3D. For this, lidar-based retrieval of vertical dust extinction profiles from Cloud-Aerosol Lidar and Infrared Pathfinder Satellite Observations (CALIPSO) can be combined with the corresponding constraints on dust mass extinction efficiency from this study to obtain constraints on dust vertical concentration profile."

3. Sections 4-5 show that the new dataset has a better agreement with in-situ measurements than the multi-model mean. I think it is better to add some discussion to emphasize why this dataset is a good complement to the currently available observational data, especially individual measurements. For instance, the global coverage and vertical distribution of the

dust size distribution and mass extinction efficiency of the dataset make it easier to be adapted to global models to constrain simulations or to study global dust impacts.

We discuss these possible uses of DustCOMM in section 4.4 (formerly section 5.4). There we discuss how DustCOMM can be used to constrain dust impacts in models, and how it can also serve as alternative to global model simulations.

Minor comments:

1. Lines 21-23, page 2, this can be a bit misleading since both small are large dust particles absorb and scatter shortwave and longwave radiation.

   Yes, the result of the combined absorption and scattering (i.e. extinction) is cooling for fine dust and warming for coarse dust. For clarity, we now specify that "fine dust **predominantly** cools the climate system by extinguishing shortwave (SW) radiation …"

2. Line 6, page 3, "To address this problem", not sure the dataset would be able to address the "numerous important biases". You may want to point out a few detailed problems.

   Thank you for the comment. Our dataset does address the problem showing significant improvement over model simulation, although it does not completely eliminate the biases. We have re-written this part as: "To address the problem of size and shape biases in models"

3. You may want to add the horizontal and vertical resolutions of the DustCOMM product at someplace in Section 2.

   Thank you. We have added a sentence in section 2.3 stating "We estimate all DustCOMM products at 2.5^{o} X 2.0^{o} horizontal grid with 35 levels that is up to 100 hPa."

4. Line 17, page 11, what time period does the "climatology" refer to?
   The climatology is between 2004 and 2008. We have added this to the sentence

5. Section 3.1, are all the model results interpolated to the same horizontal and vertical grids? And what's the resolution?

   Yes. We stated in the last paragraph of section 2.1 (formerly 3.1) that "…we interpolated seasonal and annual climatologies of these dust properties to a common resolution of approximately 2.5^{o} by 2.0^{o} spatial resolution, with 35 levels from the surface to 100 hPa"

6. Line 35, page 16, why the JRAero in a different time period is used? It's not available from 2004 to 2008?
   Yes. JRAero is only available between 2011-2015.

7. Line 16, page 21, do you refer to Fig. 4 instead of Fig. S4?
   Thanks for the comment. We have deleted the statement in parenthesis because it is no longer available in the supplementary document.

8. Line 16-18, page 21, can you please add some discussion about why the DustCOMM has a larger bias than model ensemble for D ≤ 0.5 μm?

   Thank you for the comment. We discussed this in section 4.1 (formerly 5.1). First, we highlighted that "DustCOMM's underestimation of dust with $D \leq 0.5\mu m$ may be caused by the contamination of the measured size distributions by other aerosol species for $D \leq 0.5\mu m$." Second, we discussed that "the constraint on the globally-averaged dust size distribution could also underestimate the contribution from dust with $D \leq 0.5\mu m$."

9. Line 19-24, page 23, "...regardless of the season and location", except Sde Boker, Israel.

   Although the statement is true overall, we have removed this part of the sentence.

10. Table 1, please remove "deg" in column four, since you already added a degree symbol there.
    Thank you. We have done just that.

11. Figs. 2-3, can you please add latitude, longitude, and location of the measurements on the top of each plot? Or you may number the measurements listed in Table 2 and then simply list the corresponding numbers in the figure.

    Thank you for the comment. We have instead added the names of the campaign listed in Table 2 on each plot.

12. Fig. 5, is it possible to add a globally averaged PSD and its PDF to the plot?
    Since DustCOMM globally-averaged values are forced to the globally-averaged values from Kok et al. 2017, the globally-averaged PSD the reviewer requested is also represented by the black lines.

13. Fig. 6, why is dust mass fraction for D= 0.2-2.5 μm high over the ITCZ? Is this consistent with observations?

Because dust concentration is usually low over the ITCZ region, they are dominated by the fine particles.

14. Fig. 7, it would be more interesting to show individual model results (as in Fig. 5) instead of multi-model results.

    Thank you for the comment. We have included the individual model results in Figure 7.

15. Fig. 8, why do some blue dots have a light blue outline?

    Those are cases with different measurement type as explained in section 2.4 (formerly 3.3). To avoid confusion, we have removed this from the figure.

References

Baumgardner, D., Abel, S. J., Axisa, D., Cotton, R., Crosier, J., Field, P., Gurganus, C., Heymsfield, A., Korolev, A., Krämer, M., Lawson, P., McFarquhar, G., Ulanowski, Z. and Um, J.: Cloud Ice Properties: In Situ Measurement Challenges, Meteorol. Monogr., 58, 9.1-9.23, doi:10.1175/AMSMONOGRAPHS-D-16-0011.1, 2017.

Di Biagio, C., Formenti, P., Balkanski, Y., Caponi, L., Cazaunau, M., Pangui, E., Journet, E., Nowak, S., Caquineau, S., Andreae, M. O., Kandler, K., Saeed, T., Piketh, S., Seibert, D., Williams, E. and Doussin, J.-F.: Global scale variability of the mineral dust long-wave refractive index: a new dataset of in situ measurements for climate modeling and remote sensing, Atmos. Chem. Phys., 17(3), 1901–1929, doi:10.5194/acp-17-1901-2017, 2017.

Di Biagio, C., Formenti, P., Balkanski, Y., Caponi, L., Cazaunau, M., Pangui, E., Journet, E., Nowak, S., Andreae, M. O., Kandler, K., Saeed, T., Piketh, S., Seibert, D., Williams, E. and Doussin, J.-F.: Complex refractive indices and single scattering albedo of global dust aerosols in the shortwave spectrum and relationship to iron content and size, Atmos. Chem. Phys. Discuss., 1–42, doi:10.5194/acp-2019-145, 2019.

Chou, C., Formenti, P., Maille, M., Ausset, P., Helas, G., Harrison, M. and Osborne, S.: Size distribution, shape, and composition of mineral dust aerosols collected during the African Monsoon Multidisciplinary Analysis Special Observation Period 0: Dust and Biomass-Burning Experiment field campaign in Niger, January 2006, J. Geophys. Res., 113(D23), D00C10, doi:10.1029/2008JD009897, 2008.

Dufresne, J.-L., Gautier, C., Ricchiazzi, P. and Fouquart, Y.: Longwave Scattering Effects of Mineral Aerosols, J. Atmos. Sci., 59(12), 1959–1966, doi:10.1175/1520-0469(2002)059<1959:LSEOMA>2.0.CO;2, 2002.

Evan, A. T., Flamant, C., Fiedler, S. and Doherty, O.: An analysis of aeolian dust in climate models, Geophys. Res. Lett., 41(16), 5996–6001, doi:10.1002/2014GL060545, 2014.

Huneeus, N., Schulz, M., Balkanski, Y., Griesfeller, J., Prospero, J., Kinne, S., Bauer, S., Boucher, O., Chin, M., Dentener, F., Diehl, T., Easter, R., Fillmore, D., Ghan, S., Ginoux, P., Grini, a., Horowitz, L., Koch, D., Krol, M. C., Landing, W., Liu, X., Mahowald, N., Miller, R., Morcrette, J. J., Myhre, G., Penner, J., Perlwitz, J., Stier, P., Takemura, T. and Zender, C. S.: Global dust model intercomparison in AeroCom phase i, Atmos. Chem. Phys., 11(15), 7781–7816, doi:10.5194/acp-11-7781-2011, 2011.

Kacenelenbogen, M., Vaughan, M. A., Redemann, J., Hoff, R. M., Rogers, R. R., Ferrare, R. A., Russell, P. B., Hostetler, C. A., Hair, J. W. and Holben, B. N.: An accuracy assessment of the CALIOP/CALIPSO version 2/version 3 daytime aerosol extinction product based on a detailed multi-sensor, multi-platform case study, Atmos. Chem. Phys., 11(8), 3981–4000, doi:10.5194/acp-11-3981-2011, 2011.

Kandler, K., SchüTZ, L., Deutscher, C., Ebert, M., Hofmann, H., JäCKEL, S., Jaenicke, R., Knippertz, P., Lieke, K., Massling, A., Petzold, A., Schladitz, A., Weinzierl, B., Wiedensohler, A., Zorn, S. and Weinbruch1, S.: Size distribution, mass concentration, chemical and mineralogical composition and derived optical parameters of the boundary layer aerosol at Tinfou, Morocco, during SAMUM 2006, Tellus B Chem. Phys. Meteorol., 61(1), 32–50,

doi:10.1111/j.1600-0889.2008.00385.x, 2009.
Kok, J. F., Ridley, D. A., Zhou, Q., Miller, R. L., Zhao, C., Heald, C. L., Ward, D. S., Albani, S. and Haustein, K.: Smaller desert dust cooling effect estimated from analysis of dust size and abundance, Nat. Geosci., 10(4), 274–278, doi:10.1038/ngeo2912, 2017.
Li, S.-M., Tang, J., Xue, H. and Toom-Sauntry, D.: Size distribution and estimated optical properties of carbonate, water soluble organic carbon, and sulfate in aerosols at a remote high altitude site in western China, Geophys. Res. Lett., 27(8), 1107–1110, doi:10.1029/1999GL010929, 2000.
Mahowald, N., Albani, S., Kok, J. F., Engelstaeder, S., Scanza, R., Ward, D. S. and Flanner, M. G.: The size distribution of desert dust aerosols and its impact on the Earth system, Aeolian Res., 15, 53–71 [online] Available from: http://www.sciencedirect.com/science/article/pii/S1875963713000736 (Accessed 15 December 2017), 2014.
Mamouri, R. E., Ansmann, A., Nisantzi, A., Kokkalis, P., Schwarz, A. and Hadjimitsis, D.: Low Arabian dust extinction-to-backscatter ratio, Geophys. Res. Lett., 40(17), 4762–4766, doi:10.1002/grl.50898, 2013.
Nisantzi, A., Mamouri, R. E., Ansmann, A., Schuster, G. L. and Hadjimitsis, D. G.: Middle East versus Saharan dust extinction-to-backscatter ratios, Atmos. Chem. Phys., 15(12), 7071–7084, doi:10.5194/acp-15-7071-2015, 2015.
Omar, A. H., Winker, D. M., Kittaka, C., Vaughan, M. A., Liu, Z., Hu, Y., Trepte, C. R., Rogers, R. R., Ferrare, R. a., Lee, K. P., Kuehn, R. E. and Hostetler, C. A.: The CALIPSO automated aerosol classification and lidar ratio selection algorithm, J. Atmos. Ocean. Technol., 26(10), 1994–2014, doi:10.1175/2009JTECHA1231.1, 2009.
Ridley, D. A., Heald, C. L., Kok, J. F. and Zhao, C.: An observationally-constrained estimate of global dust aerosol optical depth, Atmos. Chem. Phys. Discuss., 16(23), 1–31, doi:10.5194/acp-2016-385, 2016.
Ryder, C. L., Highwood, E. J., Rosenberg, P. D., Trembath, J., Brooke, J. K., Bart, M., Dean, A., Crosier, J., Dorsey, J., Brindley, H., Banks, J., Marsham, J. H., McQuaid, J. B., Sodemann, H. and Washington, R.: Optical properties of Saharan dust aerosol and contribution from the coarse mode as measured during the Fennec 2011 aircraft campaign, Atmos. Chem. Phys., 13(1), 303–325, doi:10.5194/acp-13-303-2013, 2013.
Ryder, C. L., Marenco, F., Brooke, J. K., Estelles, V., Cotton, R., Formenti, P., McQuaid, J. B., Price, H. C., Liu, D., Ausset, P., Rosenberg, P., Taylor, J. W., Choularton, T., Bower, K., Coe, H., Gallagher, M., Crosier, J., Lloyd, G., Highwood, E. J. and Murray, B. J.: Coarse mode mineral dust size distributions, composition and optical properties from AER-D aircraft measurements over the Tropical Eastern Atlantic, Atmos. Chem. Phys. Discuss., 1–49, doi:10.5194/acp-2018-739, 2018.
Ryder, C. L., Highwood, E. J., Walser, A., Seibert, P., Philipp, A. and Weinzierl, B.: Coarse and Giant Particles are Ubiquitous in Saharan Dust Export Regions and are Radiatively Significant over the Sahara, Atmos. Chem. Phys. Discuss., 1–36, doi:10.5194/acp-2019-421, 2019.
Song, Q., Zhang, Z., Yu, H., Kato, S., Yang, P., Colarco, P., Remer, L. A. and Ryder, C. L.: Net radiative effects of dust in the tropical North Atlantic based on integrated satellite observations

and in situ measurements, Atmos. Chem. Phys., 18(15), 11303–11322, doi:10.5194/acp-18-11303-2018, 2018.
von der Weiden, S.-L., Drewnick, F. and Borrmann, S.: Particle Loss Calculator – a new software tool for the assessment of the performance of aerosol inlet systems, Atmos. Meas. Tech., 2(2), 479–494, doi:10.5194/amt-2-479-2009, 2009.
Weinzierl, B., Petzold, A., Esselborn, M., Wirth, M., Rasp, K., Kandler, K., SchüTZ, L., Koepke, P. and Fiebig, M.: Airborne measurements of dust layer properties, particle size distribution and mixing state of Saharan dust during SAMUM 2006, Tellus B Chem. Phys. Meteorol., 61(1), 96–117, doi:10.1111/j.1600-0889.2008.00392.x, 2009.
Weinzierl, B., Sauer, D., Esselborn, M., Petzold, A., Veira, A., Rose, M., Mund, S., Wirth, M., Ansmann, A., Tesche, M., Gross, S. and Freudenthaler, V.: Microphysical and optical properties of dust and tropical biomass burning aerosol layers in the Cape Verde region—an overview of the airborne in situ and lidar measurements during SAMUM-2, Tellus B Chem. Phys. Meteorol., 63(4), 589–618, doi:10.1111/j.1600-0889.2011.00566.x, 2011.
Weinzierl, B., Ansmann, A., Prospero, J. M., Althausen, D., Benker, N., Chouza, F., Dollner, M., Farrell, D., Fomba, W. K., Freudenthaler, V., Gasteiger, J., Groß, S., Haarig, M., Heinold, B., Kandler, K., Kristensen, T. B., Mayol-Bracero, O. L., Müller, T., Reitebuch, O., Sauer, D., Schäfler, A., Schepanski, K., Spanu, A., Tegen, I., Toledano, C., Walser, A., Weinzierl, B., Ansmann, A., Prospero, J. M., Althausen, D., Benker, N., Chouza, F., Dollner, M., Farrell, D., Fomba, W. K., Freudenthaler, V., Gasteiger, J., Groß, S., Haarig, M., Heinold, B., Kandler, K., Kristensen, T. B., Mayol-Bracero, O. L., Müller, T., Reitebuch, O., Sauer, D., Schäfler, A., Schepanski, K., Spanu, A., Tegen, I., Toledano, C. and Walser, A.: The Saharan Aerosol Long-Range Transport and Aerosol–Cloud-Interaction Experiment: Overview and Selected Highlights, Bull. Am. Meteorol. Soc., 98(7), 1427–1451, doi:10.1175/BAMS-D-15-00142.1, 2017.
Whicker, C., Adebiyi, A. and Kok, J. F.: Improved Model Estimates of Desert Dust Aerosol Surface Concentration, Am. Geophys. Union, Fall Meet. 2018, Abstr. #A21I-2799 [online] Available from: http://adsabs.harvard.edu/abs/2018AGUFM.A21I2799W (Accessed 19 May 2019), 2018.
Winker, D. M., Tackett, J. L., Getzewich, B. J., Liu, Z., Vaughan, M. A. and Rogers, R. R.: The global 3-D distribution of tropospheric aerosols as characterized by CALIOP, Atmos. Chem. Phys., 13(6), 3345–3361, doi:10.5194/acp-13-3345-2013, 2013.

Dust Constraints from joint Observational-Modelling-experiMental analysis (DustCOMM): Comparison with measurements and model simulations

Adeyemi A. Adebiyi[1], Jasper F. Kok[1], Yang Wang[1], Akinori Ito[2], David A. Ridley[3], Pierre Nabat[4], Chun Zhao[5]

[1]Department of Atmospheric and Oceanic Sciences, University of California Los Angeles, CA, USA
[2]Yokohama Institute for Earth Sciences, JAMSTEC, Yokohama, Kanagawa, 236-0001, Japan
[3]Monitoring & Laboratory Division, California Air Resources Board, Sacramento, CA, USA
[4]Centre National de Recherches Météorologiques, Université de Toulouse, Météo-France, CNRS, Toulouse, France
[5]School of Earth and Space Sciences, University of Science and Technology of China, Hefei, Anhui 230026, China.

Correspondence to: Adeyemi A. Adebiyi (aadebiyi@ucla.edu)

Abstract. Mineral dust is the most abundant aerosol specie by mass in the atmosphere, and it impacts global climate, biogeochemistry, and human health. Understanding these varied impacts on the Earth system requires accurate knowledge of dust abundance, size, and optical properties, and how they vary in space and time. However, current global models show substantial biases against measurements of these dust properties. For instance, recent studies suggest that atmospheric dust is substantially coarser and more aspherical than accounted for in models, leading to persistent biases in modelled impacts of dust on the Earth system. Here, we facilitate more accurate constraints on dust impacts by developing a new dataset: Dust Constraints from joint Observational-Modelling-experiMental analysis (DustCOMM). This dataset combines an ensemble of global model simulations with observational and experimental constraints on dust size distribution and shape to obtain more accurate constraints on three-dimensional (3-D) atmospheric dust properties than is possible from global model simulations alone. Specifically, we present annual and seasonal climatologies of the 3-D dust size distribution, 3-D dust mass extinction efficiency at 550 nm, and two-dimensional atmospheric dust loading. Comparisons with independent measurements taken over several locations, heights, and seasons show that DustCOMM estimates consistently outperform conventional global model simulations. In particular, DustCOMM achieves a substantial reduction in the bias relative to measured dust size distributions in the 0.5-20 μm diameter range. Furthermore, DustCOMM reproduces measurements of dust mass extinction efficiency to almost within the experimental uncertainties, whereas global models generally overestimate the mass extinction efficiency. DustCOMM thus provides more accurate constraints on 3-D dust properties, and as such, can be used to improve global models or serve as an alternative to global model simulations in constraining dust impacts on the Earth system.

1. Introduction

Even though mineral dust accounts for a substantial fraction of the total mass of aerosol particles in the atmosphere and produces important impacts on the Earth system, global models are unable to accurately reproduce dust abundance, size, and optical properties (Kinne et al., 2006; Huneeus et al., 2011). Model difficulties in reproducing these atmospheric dust properties are largely associated with their inability to accurately simulate important dust

processes, such as dust emission, transport, and deposition (e.g. Ginoux et al., 2001; Shao, 2001; Zender et al., 2003; Huneeus et al., 2011; Kok et al., 2017). Dust aerosols are emitted from source regions such as the Sahara, the Middle-East, and Asian deserts, and are deposited after they are transported for thousands of kilometres (Duce et al., 1980; Prospero et al., 1981; Weinzierl et al., 2017). Their abundance and long-range transport allow them to play a significant role in the processes that impact global climate (Boucher et al., 2013), biogeochemistry (e.g. Mahowald et al., 2008, 2009; Ito et al., 2019), and human health (e.g. Giannadaki et al., 2014). Specifically, dust affects global climate directly by influencing the amount of radiation that can reach or leave the atmosphere and the surface (Haywood et al., 2003; Kok et al., 2017), or indirectly by changing the amount, reflectivity and lifetime of clouds (e.g. Lohmann & Diehl, 2006; Doherty & Evan, 2014; Amiri-Farahani et al., 2017). In addition, dust also impacts global biogeochemistry through deposition of iron and phosphorous-rich micro-nutrients (Mahowald et al., 2008; 2009; Ito et al., 2019), both of which are linked to the ability of ocean and land ecosystems to absorb atmospheric carbon dioxide (e.g. Watson et al., 2000; Blain et al., 2007). Finally, dust particles are easily inhaled by humans, with smaller dust particles penetrating deep into the lungs and leading to cardiopulmonary disease, lung cancer, and eventually death (e.g. Giannadaki et al., 2014). Therefore, obtaining accurate constraints on the many impacts of dust on the Earth system requires accurate knowledge of the sizes, abundance, and optical properties of atmospheric dust particles (Mahowald et al., 2014).

Uncertainties in dust aerosol properties directly translate into uncertainties in estimating their impact on the Earth system, such as dust radiative impacts (e.g. Huneeus et al., 2011; Zhao et al., 2013; Albani et al., 2014). Several studies have associated a large part of these uncertainties to the uncertainty in simulating the dust size distributions (e.g. Huneeus et al., 2011; Kok, 2011; Evan et al., 2014). Specifically, global models simulate too much fine-mode dust ($\sim D \leq 2.5\ \mu m$) and too little coarse-mode dust ($\sim D \geq 5\ \mu m$), both at emission and during transport in the atmosphere (e.g. Kok 2011; Kok et al., 2017). This bias is particularly problematic because fine dust predominantly cools the climate system by extinguishing shortwave (SW) radiation, whereas coarse dust warms it by also extinguishing longwave (LW) radiation (e.g. Tegen & Lacis, 1996; Dufresne et al., 2002). Whereas previous modelling studies affected by the size bias found that the combined (SW+LW) effect of dust is to cool the climate system (e.g. Tegen & Lacis, 1996; Tegen et al., 1996; Colarco et al., 2014), it is unclear whether the dust LW warming effect may overcome the dust SW cooling effect when the underestimation of coarse-mode particles is corrected (Kok et al., 2017). Since the dust radiative effect is sensitive to the representation of size distribution in global models, constraining the dust size distribution, and how it varies spatially, is thus important.

In addition to the sensitivity of dust size distribution, dust radiative effects are also sensitive to the shape of dust particles (e.g. Kalashnikova & Sokolik, 2004). Global models generally assume that dust particles are spherical (Ginoux et al., 2001; Miller et al., 2006; Huneeus et al., 2011), even though observations suggest that they are highly non-spherical (Okada et al., 2001; Potenza et al., 2016). This idealization in the representation of dust shape in global models is used to simplify model physics (e.g. Miller et al., 2006) and the calculation of their optical properties, but recent studies show that neglecting the asphericity of dust in models causes an underestimation of about 30% of dust aerosol optical depth (AOD) or extinction produced per unit mass of dust (Potenza et al., 2016; Kok et al., 2017). This is largely caused by the greater surface-to-volume ratio of non-spherical particles, compared to that of equal-volume

spherical particles (e.g. Kalashnikova & Sokolik, 2002, 2004). The assumption of spherical dust in climate models is also problematic because the resulting underestimation of dust AOD largely masks the positive bias associated with the fine dust particles in models, which results in an overestimation of dust AOD and extinction at remote regions when the dust emissions are scaled to match the observation of AOD near the source regions (e.g. Kok et al., 2017). Hence, to properly constrain dust impacts on radiation, observational constraints must be applied to both the dust size distribution and dust shape.

Global model simulations of the global dust cycle are thus subject to numerous important biases, which have obscured a detailed understanding of the impacts of dust on the Earth system. To address the problem of size and shape biases in model simulation of dust properties, we propose a methodology to more accurately obtain 3-D dust properties than is possible from global model simulations alone. Specifically, we propose a new product called the Dust Constraints from joint Observational-Modelling-experiMental analysis (DustCOMM), which combines an ensemble of global model simulations with observational and experimental constraints on dust size distribution and shape. DustCOMM builds on the results from Kok et al. (2017), however, unlike the globally-averaged results obtained in Kok et al. (2017), our product constrains the climatology of 3-D global atmospheric dust properties and it is provided on seasonal and annual timescales. Below, section 2 describes the details of the methodology, as well as the data used. In section 3, we present the constrained spatial distribution of the dust size distribution, mass extinction efficiency and the atmospheric dust loading, which we evaluate using independent *in-situ* measurements of dust size distributions and mass extinction efficiencies. Section 4 discusses some discrepancies between DustCOMM and measurements, the impact of dust asphericity on the DustCOMM product, and the possible use of DustCOMM to improve estimates of dust impacts in the global model simulations. Section 5 summarizes the paper. Finally, we note that all the DustCOMM dust aerosol properties (dark shaded boxes in Fig. 1) presented in this study are publicly available (Adebiyi et al., 2019a).

2. Data and Methodology

We describe here all the steps we took to obtain the DustCOMM products. First, we use three sets of input datasets to create the DustCOMM products (Fig. 1): (1) the constrained globally-averaged data from Kok et al., (2017); (2) six model simulations of size-resolved dust mass concentrations, from which we estimate the modelled dust size distribution; and (3) reanalysis datasets of the dust aerosol optical depth. We focus here only on describing the model simulations (section 2.1) and the reanalysis products (section 2.2), as details of the *in-situ* measurements used to constrain the globally-averaged datasets are described in Kok et al., (2017). Second, we describe the framework used to obtain DustCOMM dust size distribution, mass extinction efficiency, and atmospheric dust loading (section 2.3). Finally, we describe the independent measurements we use to evaluate DustCOMM dust size distribution and the dust mass extinction efficiency in section 2.4.

2.1 Model Simulations

We use model outputs of dust aerosol properties from six leading atmospheric global models, namely: the Goddard Institute for Space Studies (GISS) ModelE atmospheric general circulation model (Miller et al., 2006); the Weather Research and Forecasting model coupled with Chemistry updated by the University of Science and Technology of China (USTC) suitable for quasi-global simulation (WRF-Chem; Zhao et al., 2010, 2013; Hu et al., 2016); the Community Earth System Model (CESM; Hurrell et al., 2013); the Goddard Earth Observing System coupled with Chemistry (GEOS-Chem; See Kok et al., 2017); the ARPEGE-Climat model from the Centre National de Recherches Météorologiques Earth system model (Michou et al., 2015); and the Integrated Massively Parallel Atmospheric Chemical Transport (IMPACT; Ito & Kok, 2017 and references therein) model. We use the different simulations from global climate and chemical transport models between 2004-2008 (except for WRF-Chem and IMPACT which are 2007-2016 and 2004 respectively) to capture the general model uncertainties that are associated with the dust emission, transport, and deposition processes. The GISS, CESM and GEOS-Chem model simulations are described in Kok et al. (2017) and the references therein (see section 5 of their supplementary document). Here, we supplement these simulations with three additional simulations from the WRF-Chem, ARPEGE-Climat and IMPACT models. The WRF-Chem model simulation represents an updated USTC version of the one used in Kok et al. (2017). Further details of these three additional model simulations are thus given in the supplementary document.

We obtain the spatially-varying dust size distribution from each of the six model simulations, which we use to define the spatial variability of the DustCOMM dust size distribution (see Section 2.3.1). Specifically, the spatial variability of DustCOMM dust size distribution follows the ensemble of the six model simulations. We summarize the particle bin ranges, time periods, spatial resolutions, as well as the meteorology used for each model simulation of the dust size distribution in Table 1. All the models use discrete bins that represent the dust particles up to about 10 μm, except for the GISS, ARPEGE-Climat, and IMPACT models, which extend beyond the 10μm diameter limit. Four of the models – WRF-Chem, CESM, ARPEGE-Climat, and IMPACT – have a lower diameter limit smaller than 0.2μm. For consistency, we set the lower diameter limits for all the model simulations to the common diameter of 0.2μm, and correct the upper diameter limit to 20μm, following the procedures we describe later in section 2.3.1.1. In addition, since the time periods are different for the available model dataset (Table 1), we focus on annual and seasonal climatologies, which we obtain here from the monthly means of the model outputs.

In order to test our hypothesis that integrating experimental and observational constraints on dust size and shape distributions can constrain 3-D dust properties more accurately than possible from model simulations alone, we obtain a model ensemble of 3-D dust size distribution and mass extinction efficiency and 2-D dust column loading. To do so, we interpolated seasonal and annual climatologies of these dust properties to a common resolution of approximately 2.5° by 2.0° spatial resolution, with 35 levels from the surface to 100 hPa. In addition, we correct each modelled dust size distribution to a common particle bin spacing between 0.2-20μm by assuming a power-law distribution between nearby model particle bins. After putting all the model simulations on the same footing in this manner, we thus represent the ensemble of the model dust size distribution with the mean, standard deviation and range (minimum-maximum value), as a function of particle sizes, horizontal locations, heights, and seasons. Where necessary, the 95% confidence interval of the model ensemble is estimated as 1.96 times the standard error (e.g. Altman & Bland, 2005). We also perform a similar aggregation and interpolation procedure on the modelled dust

aerosol optical depth and column-integrated atmospheric dust loading, which are used to calculate the column-integrated dust mass extinction efficiency (MEE) for each model and thus for the model ensemble.

2.2 Reanalysis Dust Aerosol Optical Depth

We obtain the dust aerosol optical depth from four reanalysis products to constrain the atmospheric dust loading for DustCOMM (see section 2.3.3). These four reanalysis products are: the Modern-Era Retrospective analysis for Research and Applications, Version 2 (MERRA-2; Gelaro et al., 2017); the Navy Aerosol Analysis and Prediction System (NAAPS; Lynch et al., 2016); the Japanese Reanalysis for Aerosol (JRAero; Yumimoto et al., 2017); and the Copernicus Atmosphere Monitoring Service (CAMS) interim Reanalysis (CAMSiRA; Flemming et al., 2017). While the description of each reanalysis product can be found in the supplementary documents, we give a general overview in this section.

A key advantage of these reanalysis products is that they assimilate data from several observing systems, and thus provide a complete spatial and temporal coverage of atmospheric composition that captures its variabilities and trends (Buchard et al., 2017). Most of these four reanalysis products assimilate similar satellite and ground-based observations of AOD, which includes data from at least one or all of the following observing systems: the *Terra* and *Aqua* satellites of MODerate resolution Imaging SpectroRadiometer (MODIS), the Advanced Very High Resolution Radiometer (AVHRR), the Multi-angle Imaging SpectroRadiometer (MISR), as well as ground-based observation of AOD from several Aerosol Robotic Network (AERONET) stations (Lynch et al., 2016; Flemming et al., 2017; Gelaro et al., 2017; Yumimoto et al., 2017). In addition, some reanalysis products also assimilate other aerosol constituents and reactive gases, like carbon monoxide and ozone observations from the Measurements Of Pollution In The Troposphere (MOPITT) instrument on the Terra Satellite, Solar Backscatter Ultraviolet (SBUV/2) instruments (from various National Oceanic and Atmospheric Administration (NOAA) platforms), and Microwave Limb Sounder (MLS) ozone profiles (e.g. Flemming et al., 2017). These observations are mostly bias-corrected before they are assimilated through radiatively-coupled aerosol models, and used to constrain the different species that constitute the aerosol particles in the atmosphere.

Although the total AOD is constrained, errors in each reanalysis model's treatment of emission, transport, and deposition of mineral dust introduce uncertainties. Dust emission and deposition in the assimilation procedure are either modelled or sometimes constrained by observations. For example, the dust emission for NAAPS is constrained by using a regional source tuning that is, in turn, constrained by space-based and ground-based AOD observations (Lynch et al., 2016). Other reanalysis products use dust emissions that are parameterized and model-dependent (e.g. Yumimoto et al., 2017). In general, wet deposition is partially constrained by the assimilated global satellite-based precipitation information, such as from the NOAA Climate Prediction Center MORPHing technique data (CMORPH). Dry deposition is still mostly model dependent, but may also be adjusted based on assimilated AOD. For all the reanalysis products, aerosol transport in the atmosphere is constrained by the assimilation of several meteorological observations of winds and temperature. Hence, in order to constrain the dust AOD, the assimilation procedure takes advantage of the best features in both the observations and model simulations.

Similar to our treatment of the model simulations described in section 2.1 above, we use annual and seasonal climatologies of dust AOD obtained from monthly averages of the reanalysis products. We use the reanalysis dust AOD from 2004-2008 for each reanalysis product except for JRAero, for which we use 2011-2015. In order to combine the different reanalysis dust AOD products, we interpolate each product to approximately 2.5° by 2.0° spatial resolution and estimate the ensemble mean and standard error over each location (see section 2.3.3).

2.3 Constraining DustCOMM Products

Our aim is to create a new product – DustCOMM – that constrains the spatial variability of three major properties of atmospheric dust which determine many of its impacts on the Earth system, namely (1) the atmospheric dust size distribution, (2) the dust mass extinction efficiency, and (3) the column-integrated atmospheric dust loading. We do so by combining observational, experimental and theoretical constraints on dust properties and abundance with global model simulations of the size-resolved spatially-varying dust concentration (Fig. 1). After we present a general overview of the methodology here, we describe the details of the methodology and the calculation of the associated uncertainty estimates in the following sub-sections.

We obtain the first constrained product in our dust climatology, the dust size distribution, by bias correcting the six global model simulations (see section 2.3.1; left panel of Fig. 1). Specifically, we bias correct these model simulations using the constraint on the globally-averaged dust size distribution from Kok et al. (2017), which was obtained from measurements of the emitted dust size distribution and model simulations of the globally-averaged dust lifetime. Model simulations of the size-resolved dust lifetimes were used because this cannot be readily constrained with observations or measurements. Similarly, we use the constraints on the globally-averaged size distribution from Kok et al. (2017) to correct modelled size distributions because dust size distribution measurements are insufficient to constrain the dust size distribution for every location. After correcting the model simulations of the dust size distribution, we combine them into a single multi-model constraint on the 3-D dust size distribution. To do this, we estimate the sub-bin distributions by fitting the dust size distribution after the bias correction with a generalized analytical function based on brittle fragmentation theory (Kok, 2011). We then use the resulting distributions from the multiple models to obtain a constraint on the atmospheric dust size distribution, for each horizontal location and height level.

We use these constrained size distributions to obtain our second product, namely the size-integrated 3-D dust mass extinction efficiency (section 2.3.2; middle panel in Fig. 1). Specifically, we combine the constrained 3-D dust size distribution with the constraint on the size-resolved globally-averaged single-particle dust extinction efficiency at 550 nm obtained from Kok et al. (2017). This size-resolved single-particle dust extinction efficiency leverages measurements of dust index of refraction and also accounts for the non-spherical shape of dust particles. As we did for the size distribution, we use the globally-averaged dust extinction efficiency here because measurements of dust shapes and index of refraction are currently insufficient to constrain this for every location. As with the size distribution, we also constrain the mass extinction efficiency over each horizontal location and height level.

We obtain our third product – the column-integrated atmospheric dust loading – by combining the constraint on dust mass extinction efficiency with dust aerosol optical depth from multiple reanalysis products (section 2.3.3; right panel in Fig. 1). Using four state-of-the-art reanalysis products (see section 2.2), we calculate the ensemble average of dust aerosol optical depth, accounting for systematic and random errors. We propagate the errors in the dust mass extinction efficiency and dust aerosol optical depth to obtain the mean and the uncertainty of the column-integrated atmospheric dust loading over each horizontal location.

We estimate all DustCOMM products at a horizontal resolution of 2.5° X 1.9° with 35 levels that is up to 100 hPa.

2.3.1 Constraining the 3-D atmospheric dust size distribution.

We constrain the spatially-varying atmospheric dust size distributions by combining constraints on the globally-averaged dust size distribution with an ensemble of simulations of the 3-D spatial variability of the dust size distribution (Fig. 1). We obtain the globally-averaged atmospheric size distribution, $\left[\frac{d\hat{V}(D)}{dD}\right]_g$, from Kok et al. (2017; see their Fig. 2a), which was obtained by combining constraints on the size distribution of emitted dust particles with simulations of the size-resolved dust lifetime. While details can be found in Kok et al. (2017), a summary of their globally-averaged size distribution is given here as:

$$\left[\frac{d\hat{V}(D)}{dD}\right]_g = \left[\frac{d\hat{V}_{\text{emit}}(D)}{dD}\right]_g \cdot \left[\frac{\tilde{T}(D)}{\bar{\tilde{T}}}\right]_g \quad (1)$$

where the long-square parentheses $[\ \ ]_g$ indicate quantities that are globally averaged, quantities with $\hat{}$ accents are partially constrained by observations, and quantities with $\tilde{}$ accents are obtained from model simulations. As reported in Kok et al. (2017; hereafter referred to as K17), the constrained globally-averaged size distribution of emitted dust particles, $\left[\frac{d\hat{V}_{\text{emit}}(D)}{dD}\right]_g$, is based on an analysis of different measurements of the emitted dust size distribution, while the size-resolved globally-averaged dust lifetime, $[\tilde{T}(D)]_g$, is based on an ensemble of global model simulations; $\left[\bar{\tilde{T}}\right]_g$ is the mass-weighted mean of $[\tilde{T}(D)]_g$. The constrained K17 globally-averaged size distribution is normalized such that $\int_0^{D_{\max}} \left[\frac{d\hat{V}(D)}{dD}\right]_g dD = 1$. Where $D_{\max}$ represents the maximum geometric diameter above which the contribution to extinction is negligible ($D_{\max} = 20\mu m$, see section 2.3.1.1).

We use this constrained K17 globally-averaged atmospheric dust size distribution (Eqn. 1) to bias-correct our spatially-varying model simulations of the annually-averaged dust size distribution. This is necessary because models generally under-estimate coarse dust particles, largely because they assume too much fine dust in the emitted dust size distribution (Kok, 2011). We thus force the annually-averaged, globally-averaged dust size distribution of each simulation in our ensemble to match the K17 constraint on the globally-averaged size distribution (see supplement Fig. S-1). Specifically, we first calculate the factor needed to correct each particle bin of a model's simulated 3-D size distribution. This correction factor (α) is estimated as the ratio of the K17 constraint on the fractional contribution of

the particle bin to the simulated fractional contribution of the particle bin per unit global dust loading. For location and height, we thus multiply the simulated dust size distribution with the correction factor, such that:

$$\hat{f}_{k,i}(x,y,z,D_{k,i}) = \tilde{f}_{k,i}(x,y,z,D_{k,i}) \cdot \alpha_{k,i} \quad (2)$$

$$where \quad \alpha_{k,i} = \frac{\int_{D_{k,i-}}^{D_{k,i+}} \left[\frac{d\hat{V}(D)}{dD}\right]_g dD}{\left[\bar{\tilde{f}}_{k,i}(D_{k,i})\right]_g}$$

The annually-averaged 3-D distribution of the dust size distribution for each particle bin i simulated by model k is $\tilde{f}_{k,i}(x,y,z,D_{k,i})$, and the corresponding simulated globally-averaged dust mass fraction is $\left[\bar{\tilde{f}}_{k,i}(D_{k,i})\right]_g$; x is the dimension for longitude, y is for latitude and z is for height. Further, the numerator, $\int_{D_{k,i-}}^{D_{k,i+}} \left[\frac{d\hat{V}(D)}{dD}\right]_g dD$, is the constraint obtained from Kok et al. (2017), while $D_{k,i-}$ and $D_{k,i+}$ respectively denote the lower and upper geometric diameter limits of particle bin i of model k, and $i = 1, 2, \ldots, N_k$ with N_k as the total number of dust particle bins for a given model simulation k. From Eqn. 2, we derive the resulting corrected spatially-varying dust size distribution, $\hat{f}_{k,i}(x,y,z,D_{k,i})$ that is normalized such that the discrete sum over each location and height equals unity, that is: $\sum_{i=1_k}^{N_k} \hat{f}_{k,i}(x,y,z,D_{k,i}) = 1$.

Each model simulation in the ensemble has a particle size range and spacing that differs from other models (see Table 1 and section 2.1 for details). In order to combine the corrected size distributions from the different models into a single estimate, and to quantify the uncertainty across the different models, each corrected size distribution must be in a consistent size range and spacing with other models. We therefore process the corrected size distributions over a given location as follows: (1) we correct and scale each model's lower and upper diameter limits to the common diameter range of 0.2 – 20 μm (see section 2.3.1.1); and (2) we estimate the sub-bin distribution for each model's bias-corrected size distribution by fitting a generalized analytical function, extending the Kok et al, (2017) theoretical expression of dust size distribution to the 3-D dataset (see section 2.3.1.2).

2.3.1.1 Correcting model simulations to a common diameter range

For all simulations in the model ensemble, we set the lower and upper diameter limits to common limits defined by $D_{\min} = 0.2\ \mu m$ and $D_{\max} = 20\ \mu m$, respectively. The lower diameter limit ($D_{\min}$) is based on the lowest common diameter included in all the model simulations used in our analysis (Table 1). In addition, possible contaminations by other aerosol species are significantly more likely below $0.2\ \mu m$ in measurements of dust aerosol particles (e.g. Dubovik et al., 2000). For these reasons, we set the lower diameter limit to $D_{\min} = 0.2 \mu m$, consistent with previous studies (e.g. Mahowald et al., 2014, Kok et al., 2017). Further, we set the upper diameter limit to $D_{\max} = 20\ \mu m$, because most global models generally do not incorporate dust particles beyond 20 μm and also because the observational constraints on the size distribution from Kok et al. (2017) is limited to this maximum diameter. Although advances in airborne observations in recent years have led to measurements of larger dust particles with $D > D_{max}$ in the atmosphere which has shown that the contribution of $D > 20\ \mu m$ to shortwave and longwave extinctions are

non-negligible (e.g. Ryder et al., 2013b, 2019; Weinzierl et al., 2009, 2017), there is still a scarcity of these measurements, such that an observational constraint on dust particles with $D > D_{max}$ would be very uncertain (e.g. Mahowald et al., 2014).

To correct each model simulation to the common diameter range of $[D_{\min}, D_{\max}]$, we first create a new particle bin for the lower and/or upper diameter limit, and then we use the K17 constraints on the globally-averaged size distribution (Eqn. 1) to estimate the equivalent fraction of dust mass in that bin. This dust mass fraction is estimated in a way that is consistent with the size distribution obtained earlier from Eqn. 2. Specifically, for simulations with a lower diameter limit ($D_{k,1_k-}$) less than $D_{\min}$, we estimate the equivalent dust mass fraction for the bin between $D_{\min}$ and $D_{k,1_k+}$ (where $D_{k,1_k+}$ is the upper diameter limit of bin 1; such that $D_{k,1_k+} > D_{\min}$) by scaling the mass in the nearest bin with a factor that depends on the globally-averaged size distribution. For instance, the first particle bin of the CESM model (Table 1) has a range of $\left[D_{k,1_k-}, D_{k,1_k+}\right] = 0.1 - 1.0$ µm, such that we create a new particle bin defined by $\left[D_{\min}, D_{k,1_k+}\right] = 0.2 - 1.0$ µm, and estimate the equivalent dust mass fraction in that new bin. For all model simulations, we can denote this procedure mathematically as:

$$\hat{f}_k\left(x, y, z, \left[D_{\min}, D_{k,1_k+}\right]\right) = \hat{f}_k\left(x, y, z, \left[D_{k,1_k-}, D_{k,1_k+}\right]\right) \cdot \delta_{D_{\min}} \quad (3)$$

$$where \quad \delta_{D_{\min}} = \frac{\int_{D_{\min}}^{D_{k,1_k+}} \left[\frac{d\hat{V}(D)}{dD}\right]_g dD}{\int_{D_{k,1_k-}}^{D_{k,1_k+}} \left[\frac{d\hat{V}(D)}{dD}\right]_g dD}$$

The modelled dust size distribution is relatively invariant for fine particles because of the consistent emitted dust size distribution (Kok, 2011a & b), and because removal processes for fine dust (wet deposition) do not strongly depend on particle size (e.g. Zender et al., 2003). Therefore, we simply estimate $\delta_{D_{\min}}$ in Eqn. 3 as the ratio between the fractional values of the K17 globally-averaged size distribution in the desired new bin $[D_{\min}, D_{k,1_k+}]$ and in the model's original bin $[D_{k,1_k-}, D_{k,1_k+}]$.

We also create a new bin with the upper diameter equal to $D_{\max}$ for model simulations with an upper diameter limit (D_{k,N_k+}) that differs from $D_{\max}$. We do so by scaling the nearest bin by a factor ($\delta_{D_{\max}}$) that also depends, in part, on the constrained K17 globally-averaged size distribution. Because the main removal process for large dust particles ($D > 10\mu m$) is dry deposition, which depends strongly on particle size, the relative contribution to the size distribution of different particle bins of large particles has substantial spatial variability. To account for this, we use simulations of bins with $D > D_{k,N_k+}$ from other model simulations in order to estimate what model k would have predicted for a hypothetical $\left[D_{k,N_k+}, D_{\max}\right]$ particle bin. That is:

$$\hat{f}_k\left(x, y, z, \left[D_{k,N_k+}, D_{\max}\right]\right) = \hat{f}_k\left(x, y, z, \left[D_{k,N_k-}, D_{k,N_k+}\right]\right) \cdot \delta_{D_{\max}}(x, y, z) \quad (4a)$$

$$where \quad \delta_{D_{\max}}(x, y, z) = \frac{\int_{D_{k,N_k+}}^{D_{\max}} \left[\frac{d\hat{V}(D)}{dD}\right]_g dD}{\int_{D_{k,N_k-}}^{D_{k,N_k+}} \left[\frac{d\hat{V}(D)}{dD}\right]_g dD} \cdot \beta_r(x, y, z)$$

The factor β_r thus quantifies the ratio of the mass fractions between the model's largest particle bin ($[D_{k,N_k-}, D_{k,N_k+}]$) and the newly created particle bin to extend the simulation to $D_{\max} = 20\ \mu m$ ($[D_{k,N_k+}, D_{\max}]$), as estimated from the GISS and ARPEGE-Climat simulations, which have particle bins extending to $D_{\max}$ (Table 1). We denote these latter model simulations with a subscript r for the purpose of clarity, and to separate them from the model simulation that is being adjusted to the $[D_{\min}, D_{\max}]$ size range, which is denoted by a subscript k in Eqn. 4a above. We thus estimate β_r as:

$$\beta_r(x,y,z) = \frac{\hat{f}_r\left(x,y,z,\left[D_{r,N_r-}, D_{r,N_r+}\right]\right)}{\int_{D_{r,N_r-}}^{D_{r,N_r+}} \left[\frac{d\hat{V}(D)}{dD}\right]_g dD} \Bigg/ \frac{\hat{f}_r\left(x,y,z,\left[D_{r,j_r-}, D_{r,j_r+}\right]\right)}{\int_{D_{r,j_r-}}^{D_{r,j_r+}} \left[\frac{d\hat{V}(D)}{dD}\right]_g dD} \qquad (4b)$$

Where $[D_{r,N_r-}, D_{r,N_r+}]$ is the bin in model r with dust mass that overlaps in size with the new bin $[D_{k,N_k+}, D_{\max}]$ we want to estimate for model k; and $[D_{r,j_r-}, D_{r,j_r+}]$ is the bin that similarly overlaps with $[D_{k,N_k-}, D_{k,N_k+}]$. To account for the bin-range mismatch between the model simulation that resolved dust up to $D_{\max}$ (with subscript r) and the model simulation being adjusted to the dust size range up to $D_{\max}$ (with subscript k), we normalize each bin mass fraction by its contribution to the constrained K17 globally-averaged size distribution. For cases where model r is the same as model k (i.e. for GISS and ARPEGE-Climat), β_r reduces to one everywhere. It should be noted that the correction of Eqn. 4 takes into account the potential difference in the dust deposition between models k and r, by considering the differences in the spatial variability of dust loading between similar bins of $[D_{k,N_k-}, D_{k,N_k+}]$ and $[D_{r,j_r-}, D_{r,j_r+}]$. After the dust mass fractions are corrected, they are re-normalized such that the discrete sum between $D_{\min}$ and $D_{\max}$ equals unity over each location and height.

This procedure described above (Eqns. 3-4) can be used to correct either the original modelled dust size distribution (section 2.1), or the bias-corrected modelled dust size distribution of Eqn. 2.

2.3.1.2 Estimating the sub-bin distribution of the dust size distribution

After setting the corrected dust size distribution from each model to a common diameter range, $[D_{\min}, D_{\max}]$, we next estimate the sub-bin distribution in order to combine estimates from different models into one dust size distribution product. To do this, we fit a generalized theoretical function of the dust size distribution to the estimated bias-corrected dust size distribution from each model over each location and height level (Eqn. 2). Although fitting lognormal modes are appropriate for several other aerosol species, Mahowald et al., (2014) highlighted that dust size distributions are usually not lognormal and are thus better characterized by a generalized function based on mechanistic understanding of dust emission and deposition processes. Therefore, we describe in this section the generalized function and the fitting procedure used to constrain the dust size distributions.

We define the generalized function for the atmospheric size distribution by considering the theoretical expressions that characterize the processes affecting the dust size distribution. The degree of the impact of any of these processes on the dust size distribution will depend on the location. For example, the impact of emission processes on the shape

of the dust size distribution is expected to be large close to major dust source regions but less farther from source regions. Furthermore, farther from dust source regions, deposition processes are expected to have more impact on the size distribution. We therefore assume that the atmospheric size distribution over any location is proportional to the dust size distribution at emission, $\frac{dV_{emit}(D)}{dD}$, the size-resolved dust lifetime in the atmosphere, $T(D)$, and any other changes to the dust particle size distribution during transport, A(D) (e.g. Weinzierl et al., 2009; Schladitz et al., 2011; Kok et al., 2017). That is:

$$\frac{dV_{atm}(D)}{dD} \propto \frac{dV_{emit}(D)}{dD} \cdot T(D) \cdot A(D) \tag{5a}$$

For the dust size distribution at emission, Kok (2011) suggested that $\frac{dV_{emit}(D)}{dD}$ can be represented by a simple theoretical expression based on brittle fragmentation theory, which shows good agreement with measurements (e.g. Mahowald et al., 2014; Rosenberg et al., 2014). To better represent the variability in dust emission affecting the emitted size distribution in the different simulations, here we generalize this expression such that:

$$\frac{dV_{emit}(D)}{dD} = \frac{1}{C_v} \cdot \left[1 + \mathrm{erf}\left(\frac{\ln\left(\frac{D}{D_v}\right)}{\sqrt{2}\ln(\sigma_v)}\right)\right] \cdot e^{\left[-\left(\frac{D}{\omega}\right)^{\alpha}\right]} \tag{5b}$$

Where D_v and σ_v are respectively the geometric median diameter by volume and the geometric standard deviation of a typical desert soil, ω denotes the propagation distance of main cracks in dust aggregates during fragmentation, α is a tunable parameter primarily affecting the large dust particles, and C_v is a normalization constant.

The second term in our generalized dust size distribution describes the size-resolved dust lifetime, which global model results compiled in Kok et al. (2017) suggest can analytically be approximated as an exponential function of particle diameter, such that:

$$T(D) \cong T_0 \cdot e^{-\left(\frac{D}{\kappa}\right)} \tag{5c}$$

Where T_0 is a constant associated with the lifetime for vanishingly small dust particles, which is determined by depositional processes, and κ is a constant that scales the exponential decay of the dust lifetime with particle size. This exponential decay of dust lifetime with size is caused by the increase of the gravitational settling speed with particle size (e.g. van der Does et al., 2016, 2018).

Finally, we account for other changes to the dust size distribution during transport, by assuming that such changes are likely described by power-law distribution (e.g. Seinfeld & Pandis, 2016). Maring et al. (2003) highlighted that between emission and deposition, changes in dust size distribution can not be accounted for by simple preferential removal of dust particles by gravitational settling. Since such changes in the dust size distribution are difficult to account for, we represent them with a parameter that can affect the entire size range. In addition, $T(D)$ and $\frac{dV_{emit}(D)}{dD}$ represent expressions that describe the globally-averaged size distributions, and applying them to a specific location requires additional parameter that captures the loss rate as a function of location. To represent all other changes to the dust size distribution between emission and deposition, we thus define:

$$A(D) \propto D^b \tag{5d}$$

Combining Eqns. 5b—5d, we obtain:

$$\frac{dV_{atm}(D)}{dD} = \frac{1}{C_v}\left[1 + \mathrm{erf}\left(\frac{\ln\left(\frac{D}{D_s}\right)}{\sqrt{2}\ln(\sigma_s)}\right)\right] e^{\left[-\left(\frac{D}{\omega}\right)^{\alpha}\right]} \cdot T_0 e^{-\left(\frac{D}{\kappa}\right)} \cdot D^b \quad (5e)$$

We combine the two exponential terms in Eqn. 5e in order to reduce the number of fitting parameters. It is worth noting that both parameters κ and ω are sensitive to the larger particles, as they remain highly uncertain and poorly constrained by observation (e.g. Mahowald et al., 2014). The parameter ω depends on the soil moisture, mineralogy and other processes (e.g. Mahowald et al., 2014; Rosenberg et al., 2014; Kok et al., 2017), while the parameter κ depends on the dust wet and dry deposition rates, as the dust particles are transported away from the source (e.g. Han & Zender, 2010; van der Does et al., 2016). To combine them, we define Λ to account for the uncertainty in the atmospheric large-size dust particles over every location. The generalized theoretical function for atmospheric size distribution therefore becomes:

$$\frac{dV_{atm}(D)}{dD} = \frac{1}{C_v^*} \cdot \left[1 + \mathrm{erf}\left(\frac{\ln\left(\frac{D}{D_s}\right)}{\sqrt{2}\ln(\sigma_s)}\right)\right] \cdot e^{\left[-\left(\frac{D}{\Lambda}\right)^{\alpha}\right]} \cdot D^b \quad (6)$$

where C_v^* is a new normalization constant that is obtained from requiring that the integral over Eqn. (6) from D_{min} to D_{max} yields unity.

To determine the parameters in Eqn. 6 for each height, horizontal location, season, and model simulation, we fit the generalized size distribution of Eqn. 6 to the corresponding corrected dust size distribution from Eqn. 2 above. To do this, we minimize the chi-squared (χ_k^2) value for each height, location, and for each model k, such that:

$$\chi_k^2 = \sum_i^{N_k}\left[\log\left(\int_{D_{k,i-}}^{D_{k,i+}} \frac{dV_{atm}}{dD} dD\right) - \log\left(\hat{f}_{k,i}\right)\right]^2 \quad (7)$$

In each case, we estimate the constrained dust size distribution, $\frac{d\hat{V}_{\mathrm{atm}}}{dD}(\mathrm{x,y,z})$, based on the parameters we determine from Eqn. 7. In order to restrict the fitted function to physically realistic dust size distributions, we set the following bounds for the five parameters of Eqn. 6: $D_s = 0.25$ to 6.0 μm; $\sigma_s = 1.6$ to 4.0; $\Lambda = 1$ to 30 μm; $\alpha = 1$ to 6; and $b = -10$ to 4, consistent with previous studies (e.g. Kok, 2011; Kok et al., 2017; Rosenberg et al., 2014;). The probabilty distribution of these parameters for all heights, horizontal locations, and model simulations of the annually-averaged dust size distribution is shown in the supplementary Fig. S-2. Finally, we note here that although our generalized theoretical function of Eqn. 6 builds on the brittle fragmentation theory of Kok 2011, it adds analytical expressions of dust deposition and dust changes during transport that allow us to better fit different shapes of dust size distribution over different locations.

2.3.2 Constraining the 3-D dust mass extinction efficiency

After obtaining the constrained atmospheric dust size distributions (section 2.3.1 above), we combine it with constraints on size-resolved single-particle extinction efficiency at 550 nm, to obtain constraints on the 3-D dust mass extinction efficiency ($\hat{\epsilon}_\tau$ $-m^2g^{-1}$). That is (see also Kok et al., 2017):

$$\hat{\epsilon}_\tau(x,y,z) = \int_{D_{min}}^{D_{\max}} \frac{d\hat{V}_{\text{atm}}(x,y,z,D)}{dD} \frac{3}{2\rho_d D} \hat{Q}_{\text{ext}}(D) dD \quad (8)$$

where $\frac{d\hat{V}_{\text{atm}}(x,y,z,D)}{dD}$ is the constrained atmospheric dust size distribution at a given location and height with sub-bin distribution (Eqn. 6); $\rho_d = 2.5 \pm 0.2$ g cm^{-3} is the globally-averaged density of dust aerosols (Fratini et al., 2007; Reid et al., 2008; Kaaden et al., 2009; Sow et al., 2009; Kok et al., 2017) and its error range is expected to account for the spatial and temporal variability of dust density (e.g. Tegen & Fung, 1994; Li et al., 2008); and $\hat{Q}_{\text{ext}}(D)$ is the globally-averaged size-resolved single-particle extinction efficiency at 550nm wavelength, with the extinction cross-section normalized by $\pi D^2/4$ – the projected area of a sphere with diameter *D*.

We obtain $\hat{Q}_{\text{ext}}$ from Kok et al. (2017), which constrained the dust extinction efficiency by combining measurements of the dust index of refraction and probability distribution of dust particle shape with the single-scattering database of Meng et al., (2010). Specifically, Kok et al. (2017) estimated the globally-averaged values of the real and imaginary dust index of refraction as $n = 1.53 \pm 0.03$ and $\log(-k) = -2.5 \pm 0.3$ (Sokolik et al., 1993; Patterson et al., 1977; Dubovik et al., 2002; K. Kandler et al., 2009; Kim et al., 2011; Denjean et al., 2016), and both are assumed to be normally distributed. Dust particle shapes were represented by the dust aspect ratio – the ratio of the major and minor axes of an ellipsoid best fit to the irregularly-shaped 2-D image of a dust particle – and the height-to-width ratio. Kandler et al., (2007) showed that the deviation of measured dust aspect ratios from a sphere can be approximated by a log-normal distribution, with typical values ranging from 1 – a perfect sphere – to about 3, and median between ~1.5—1.9. Based on aggregates of measurements (Okada et al., 2001; Reid et al., 2003; Kandler et al., 2007; Chou et al., 2008; Kandler et al., 2009, 2011; Scheuvens et al., 2011; Scheuvens & Kandler, 2014), Kok et al. (2017) estimated the median and geometric standard deviation for the distribution of the dust aspect ratio as – 1.7 ± 0.3 and 0.6 ± 0.2, respectively. Similarly, based on limited available measurements of dust height-to-width ratio (Okada et al., 2001; Chou et al., 2008; Veghte & Freedman, 2014), Kok et al. (2017) used a mean value of 0.333 (see details in the supplementary document of Kok et al., 2017). By combining these constraints on the optical properties and shape of the ensemble of dust particles in Earth's atmosphere with the single-scattering database of Meng et al. (2010), Kok et al. (2017) obtained a constraint on the globally-averaged size-resolved extinction efficiency $\hat{Q}_{\text{ext}}(D)$, which explicitly accounts for the enhancement of extinction by the asphericity of dust. Specifically, they found that accounting for dust asphericity enhances the extinction produced by a unit mass loading of dust by 29 ± 5% over the extinction calculated from Mie theory for spherical dust particles, which is used in most climate models.

We use this constrained K17 globally-averaged $\widehat{Q}_{\text{ext}}$ to constrain $\hat{\epsilon}_\tau$ (Eqn. 8) for every location. We thus neglect any regional variation in $\widehat{Q}_{\text{ext}}$ because measurements of dust shapes and index of refraction are currently insufficient to constrain $\hat{\epsilon}_\tau$ on a regional basis. In addition, since measurements of dust refractive index needed to constrain $\hat{\epsilon}_\tau$ at other wavelengths are also scarce, we limit our estimate here only to the 550 nm wavelength. We use 550 nm as the

wavelength of choice because measurements to validate our estimate of $\hat{\epsilon}_\tau$ and the observational constraints to estimate the dust atmospheric loading are mostly available at mid-visible wavelength.

2.3.3 Constraining the 2-D atmospheric dust loading

We now combine the above-estimated mass extinction efficiency at 550 nm (section 2.3.2) with dust aerosol optical depth at the same wavelength, to constrain the atmospheric column dust loading ($\hat{L} - g\ m^{-2}$) (Kaufman et al., 2005; Kok et al., 2017). Because our constraints on dust size distributions are normalized to unity, and also to ensure that our estimates of dust loading produce the same extinction as those from reanalysis dataset or satellite measurements, we use this approach to estimate the atmospheric dust loading, such that:

$$\hat{L}(x,y) = \frac{\hat{\tau}_d(x,y)}{\hat{\epsilon}_m(x,y)} \tag{9}$$

where $\hat{\epsilon}_m$ (unit: $m^2\ g^{-1}$) is the vertically-integrated 2-D mass extinction efficiency calculated from $\hat{\epsilon}_\tau$, and $\hat{\tau}_d(x,y)$ is obtained from an ensemble of reanalysis dust aerosol optical depth products.

The ensemble dust aerosol optical depth (AOD) climatology is obtained from the average of four different reanalysis products (MERRA-2, JRAero, NAAPS, and CAMSiRA; see section 2.2 for details). This individual reanalysis dataset assimilate several satellite and ground-based measurements from multiple platforms, including MODIS (*Terra* and *Aqua*), AVHRR and MISR satellites, as well as from the ground-based AERONET stations (Lynch et al., 2016; Mccarty et al., 2016; Flemming et al., 2017; Yumimoto et al., 2017). As such the assimilation procedure takes advantage of the best features in both the observations and model simulations, thus producing column-integrated dust AOD that is largely representative of what is observed, based on validation studies (e.g. Buchard et al., 2017).

Despite the advantage of assimilating observational datasets, estimating a realistic overall error in the dust AOD across the reanalysis datasets is difficult, yet important. Here, we estimate the total error (σ_d) by considering both the systematic error (σ_{sys}) and random error (σ_{rand}) inherent in the reanalysis-derived dust AOD. As such, we estimate the uncertainty in dust AOD as: $\sigma_d(x,y) = \sqrt{\sigma_{sys}^2(x,y) + \sigma_{rand}^2(x,y)}$. We define the σ_{rand} as the standard error between the four datasets, which represents that part of the total uncertainty that does not correlate across the four reanalysis dust AOD data sets. For instance, σ_{rand} may be associated with differences in the assimilating systems for the different reanalysis products. In contrast, the σ_{sys} is expected to correlate between the four data sets since most of the reanalysis datasets use similar observational datasets. Hence, we assume that the σ_{sys} will be proportional to the mean dust AOD, such that $\frac{\sigma_{sys}(x,y)}{\tau_d(x,y)} = C_d$. We estimate the proportionality constant, C_d, by requiring that the relative error is the same as the relative error obtained from annually-averaged climatology of dust AOD from Ridley et al. (2016), which leveraged observational datasets similar to those used for the reanalysis dataset, but propagated many of the relevant uncertainties. From that, we deduce that $C_d = \sqrt{\frac{\sigma_o^2}{\tau_o^2} - \frac{\sigma_{rand}^2}{\tau_d^2}}$, where τ_o and σ_o are the mean and error estimates of the observationally-constrained dust AOD from Ridley et al. (2016) respectively. We estimate $C_d = 0.26$

for annual climatology (between 2004-2008), averaged over regions that are constrained by Ridley et al. (2016) and account for about 95% of the global dust AOD. Similarly, we estimate 0.31, 0.22, 0.24, 0.28 for December-February, March-May, June-August, and September-November seasonal climatologies, respectively.

2.3.4 Quantifying the uncertainties in DustCOMM products

For each DustCOMM product above – the constrained dust size distribution, dust mass extinction efficiency and dust atmospheric loading - we describe here how we estimate the most likely value and quantify the uncertainty over each location. Specifically, we use a non-parametric procedure based on the bootstrap method (Efron & Gong, 1983; Chernick, 2007). We use this method because the complexity of the equations (Eqns. 1-9) prevents a parametric quantification of error, and the bootstrap approach allows us to nonetheless propagate the uncertainty in the various physical variables used to estimate each product. Using this method, we further assume that the set of input variables in relevant equations above are independent, and are represented by defined probability distributions. Thus, we estimate the probability distribution of the resulting products by randomly sampling (with replacement) the probability distribution of each of the input variables for a large number of times ($n \approx 1{,}500$).

In practice, the procedure uses the following steps to determine the dust size distribution, mass extinction efficiency and atmospheric loading, and their uncertainties:

1. We randomly-select a realization of the globally-averaged size distribution from Kok et al. (2017), which in turn was obtained in that study by randomly-selecting a realization of the emitted dust size distribution and the dust lifetime (Eqn. 1).
2. We use this randomly-selected constrained K17 globally-averaged size distribution to correct a randomly-selected model simulation (Eqn. 2).
3. After this model simulation is corrected, we then scale the resulting 3-D dust size distribution between D_{min} and D_{max} following Eqns. 3 & 4.
4. We thereafter estimate the constrained dust size distribution, $\frac{d\hat{V}_{\mathrm{atm}}}{dD}(x, y, z, D)$, and obtain the sub-bin distribution by fitting the generalized theoretical expression (Eqn. 6) and minimizing the chi-square over each location (Eqn. 7).
5. We randomly select a realization of the globally-averaged size-resolved single-particle extinction efficiency, $\hat{Q}_{\mathrm{ext}}(D)$, from Kok et al. (2017). This realization is also similarly estimated by randomly-selecting from the distribution of the dust index of refraction and dust shape distribution parameters, as explained in section 2.3.2.
6. We then use the randomly-selected $\hat{Q}_{\mathrm{ext}}(D)$ and $\frac{d\hat{V}_{\mathrm{atm}}}{dD}(x, y, z, D)$ to estimate the dust mass extinction efficiency over each location, $\hat{\epsilon}_{\tau}(x, y, z, D)$, following Eqn. 8. This uses a randomly-selected dust density value (ρ_d) from its assumed normal distribution.
7. Similarly, assuming a normal distribution for the dust AOD, we randomly estimate the $\hat{\tau}_d(x, y)$ value within the range of its uncertainty, $\sigma_d(x, y)$.

8. We use this $\hat{\tau}_d(x,y)$ and the vertically-integrated value of dust mass extinction efficiency, $\hat{\epsilon}_m(x,y)$, to estimate the atmospheric dust loading, $\hat{L}(x,y)$, following Eqn. 9.
9. We repeated step 1-8 for n = 1500 times, thereby producing a probability distribution for $\frac{d\hat{V}_{\text{atm}}}{dD}(x,y,z,D)$, $\hat{\epsilon}_\tau(x,y,z,D)$, and $\hat{L}(x,y)$ for each location and height. We report the mean, median, 1-sigma uncertainty range (68% of the distribution), and the 95% confidence interval (95% CI) of those distributions (Adebiyi et al., 2019a).

The above procedure propagates various uncertainties in the estimation of each product. These include the measurement uncertainties and the uncertainties in model simulations. First, the measurement uncertainties are associated with the K17 globally-averaged size distribution and the globally-averaged extinction efficiency (Fig. 1), and these are propagated equally to every location. In addition, we estimated the correlated systematic error in the dust AOD (section 2.3.3), associated with the assimilated observational dataset, and this is also propagated. Second, the uncertainty in model simulations is associated with the spread of the model dust size distribution which is different for every location. This model uncertainty is, in turn, a result of many processes, such as dust emission, deposition, and transport processes in the models (Ginoux et al., 2001; Huneeus et al., 2011; Zhao et al., 2013). Our procedure constrains these model uncertainties (see supplementary Fig. S-1), while retaining the spatial distribution of the model ensemble.

To quantify the size-resolved discrepancies in the DustCOMM size distribution, we quantify the bias with respect to independent measurements as follows (e.g. Lee et al., 2009):

$$\psi_i^{bias} = \frac{1}{N_m}\sum_{m=1}^{N_m} log_{10}\left(\frac{M_{i,m}^f}{O_{i,m}^f}\right) \tag{10}$$

where m sums over the N_m *in-situ* measurements of the dust size distribution available in the literature (see Table 2), $O_{i,m}^f$ is the mth measurement of the mass fraction contained in measurement bin i, and $M_{i,m}^f$ is the corresponding mth DustCOMM dust mass fraction for the same diameter range as measured and collocated with the measurement – i.e. $M_{i,m}^f = \int_{D_{i-}}^{D_{i+}} \frac{d\hat{V}_{\text{atm}}}{dD} dD$. ψ_i^{bias} is the log-mean normalized bias and it represents the average number of orders of magnitude bias for each bin i.

We also estimate the performance of DustCOMM mass extinction efficiency by quantifying the reduced chi-square (χ_ε^2) defined as the chi-squared per degree of freedom (e.g. Bevington et al., 1993):

$$\chi_\varepsilon^2 = \frac{1}{\upsilon_\varepsilon}\sum_{m=1}^{N_m}\left(\frac{O_m^\varepsilon - \hat{\epsilon}_{\tau,m}}{\sigma_m^\varepsilon}\right) \tag{11}$$

where O_m^ε is the mth measurement of the dust mass extinction efficiency with error defined as σ_m^ε, $\hat{\epsilon}_{\tau,m}$ is the corresponding mth DustCOMM dust extinction efficiency ($\hat{\epsilon}_\tau$) collocated with the measurement, and υ_ε is the number of degrees of freedom given as $N_m - 1$. A value of $\chi_\varepsilon^2 \approx 1$ in Eqn. 11 indicates there is agreement between

DustCOMM and observations that is in accordance with the measurement errors, while $\chi_{\varepsilon}^{2} \gg 1$ indicates that DustCOMM estimates do not fully capture the observations (e.g. Andrae et al., 2010).

To facilitate comparison between DustCOMM and model evaluations, Eqns. 10 & 11 are also used to evaluate the performance and calculate the discrepancies between the measurements and the model ensemble.

2.3.5 DustCOMM at other timescales

While we describe above the procedure that constrains the annually-averaged dust size distribution, dust mass extinction efficiency and atmospheric dust loading, a similar procedure as highlighted above can also be used to constrain the three products at any other timescale, such as at daily, monthly, or seasonal timescale. For this study, we only consider the seasonally-averaged and annually-averaged products.

First, to constrain the dust size distribution at any specific timescales, we correct an ensemble of model size distributions at that timescale in a way similar to Eqn. 2 above. However, unlike Eqn. 2 that uses the constrained globally-averaged size distribution, here we use the constrained annually-averaged dust size distribution over every location. That is:

$$\hat{f}^{t}{}_{k,i}\left(x,y,z,D_{k,i}\right) = \tilde{f}^{t}{}_{k,i}\left(x,y,z,D_{k,i}\right) \cdot \frac{\int_{D_{k,i-}}^{D_{k,i+}} \frac{d\hat{V}_{\text{atm}}}{dD}\left(x,y,z,D\right) dD}{\tilde{f}_{k,i}\left(x,y,z,D_{k,i}\right)} \tag{12}$$

where $\frac{d\hat{V}_{\text{atm}}}{dD}$ is the DustCOMM annually-averaged dust size distribution at a given 3-D location, obtained from the procedure described in Section 2.3.1, while $\tilde{f}$ and $\tilde{f}^{t}$ are the annually-averaged and specific time-averaged model simulations of the dust size distribution respectively. Using an ensemble of model simulations, as we do above, the resulting corrected time-averaged dust size distributions, $\hat{f}^{t}$, are also taken through the steps highlighted in section 2.3.4 to calculate the mean and the uncertainty of the constrained dust size distribution ($\frac{dV_{atm}^{t}}{dD}$) at that particular timescale.

Second, to constrain the dust mass extinction at any specific timescale ($\hat{\epsilon}^{t}{}_{\tau}$), we combine the constrained dust size distribution at that timescale, $\frac{dV_{atm}^{t}}{dD}$, with the globally-averaged extinction efficiency, $\hat{Q}_{\text{ext}}$. This similarly follows Eqn. 8 above. We note here that the uncertainty range of $\hat{Q}_{\text{ext}}$ also accommodates the location-dependent and time-dependent variability in the dust index of refraction and dust particle shape, consistent with previous studies (e.g. Dubovik et al., 2002). Hence, using $\hat{Q}_{\text{ext}}$ propagates the uncertainty in the measurements that determine the dust mass extinction efficiency estimate at that timescale. Finally, we constrain the dust loading at any specific timescale ($\hat{L}^{t}$) using the constrained $\hat{\epsilon}^{t}{}_{\tau}$ and dust AOD at that same timescale, similarly following Eqn. 9.

2.4 Description of measurements used for evaluation

We use several types of published measurements to evaluate the dust size distribution and dust mass extinction efficiency from both DustCOMM and the model ensemble. We select 21 studies that measured dust properties – 14 of these reported dust size distributions, and 11 of these reported dust mass extinction or scattering efficiencies (Table 2). These measurements were taken both near and far from dust-dominated regions (Table 2 and supplementary Fig. S-3). While some measurements were taken close to (or over) some of the northern hemisphere deserts – such as the Sahara, Middle East, and Asian deserts - no measurements were taken close to the southern hemisphere deserts. 12 of the 21 studies obtained measurements near the Sahara Desert, while one measurement each was taken near the Middle East (Sde Boker, Israel), and Asian (Qinghai Province, China) deserts. Other measurements represent dust properties at different distances of transport away from the dust sources.

Except for four measurements, most of the data are taken during airborne field campaigns that often occur over a wide geographical area, several altitude levels, and several days (Table 2). As such, studies often report measurements that represent the averages of the dust properties taken during the campaign. Details of the flight path, showing the locations where dust particles are encountered, are not always reported. To use these measurements, we therefore define a representative location and altitude for each measurement based on the area where the majority of dust was encountered. In addition, since the measurements often represent average of several days and sometimes multiple months, we also compare them against seasonal averages of the DustCOMM and model ensemble estimates.

Below, we give a broad overview of the measurements of the dust size distribution and mass extinction efficiency, and further information on each study, including the instruments used, can be found in the supplementary document.

2.4.1 Dust size distribution measurements

Dust size distribution measurements are taken using a variety of instruments with different sizing methodologies (e.g. Reid et al., 2003). These instruments generally fall within the categories of sample collectors (e.g. D'Almeida, 1987; McConnell et al., 2008), cascade impactors (e.g. Chou et al., 2008; Kandler et al., 2009) and aerodynamic particle sizers (e.g. Otto et al., 2007), and optical particle counters or spectrometers (e.g. Chou et al., 2008; Clarke et al., 2004; Otto et al., 2007). The first category of instruments, sample collectors, are usually installed behind filters or thermal denuders to remove non-dust particles. The aerosol samples are then analysed using electron or light microscopy techniques, where they are counted and sized either manually or using an automated software. This type of measurement yields dust size distribution with respect to geometric diameters. For the second category of instruments, cascade impactors and particle sizers, aerosol particles are usually accelerated through a jet outlet, and sometimes collected on a substrate. Using these instruments, the aerosols are sized based on the mass-to-drag characteristics of the particles. Dust particle sizes measured using these types of instruments are associated with the aerodynamic diameter. Finally, the optical particle counters generally determine particle sizes in optical diameters based on the amount of light they scatter. Another category is the imaging probe whereby the particle image is detected by linear photodiode array providing a two-dimensional projection of the particle (Baumgardner et al., 2017; Ryder et al., 2018). For many of the studies we use here, these instruments are sometimes combined to verify the accuracy of the

measurements (e.g. Ryder et al., 2013a). For all dust size distribution measurements, the studies that used aerodynamic or optical sizing instruments eventually report the measured size distribution in geometric diameters.

An important consideration is the elevation at which the dust size distributions are measured. With the exception of two studies (D'Almeida, 1987; Kandler et al., 2011) that took measurements at ground stations, most measurements were performed solely aboard aircrafts with in-cabin or wing-mounted instruments. Ground stations were equipped with stationary instruments to collect aerosol samples or stationary optical particle counters to measure size distributions directly. For aircraft measurements, size distributions are often measured during flight segments at constant altitude – also called horizontal legs. For the dust size distributions, our criteria for selection of studies are as follows: (1) the measured size range of the data should extend into the coarse dust (D > 5 um) size range; (2) the study should report the original in-situ measurements, instead of (lognormal) fits to the actual measurements; and (3) each study's measurements should be taken with commonly-used instrumentation in order to ensure some consistency with measurements taken by other studies.

Regardless of the instrument used, most dust size distribution measurements are subject to uncertainties associated with measurement type or presence of other aerosol species, such as biomass burning aerosols. The contamination by other aerosol species is common for fine-mode dust particles, especially dust particles less than ~0.5μm (e.g. Dubovik et al., 2000; Clarke et al., 2004), since to the instruments these aerosols are indistinguishable from dust particles of the same size. This causes a high bias in the fine-mode of measured dust size distributions (e.g. Clarke et al., 2004). Another important measurement error arises from assumptions made about the non-sphericity of dust particles. For example, during the microscopy analysis, particle diameters are usually determined as the volume-equivalent geometric diameters based on 2-dimensional images (Chou et al., 2008). Because of the asphericity of dust aerosols, this could introduce biases (e.g. Huang et al, in prep.; Okada et al., 2001). Since dust particles have a small height-to-width ratio (Okada et al., 2001), the resulting size distribution may overestimate dust particle diameters. In the case of cascade impactors and particle sizers, unusual dust particle shapes and the possibility of particle bouncing off the substrate may lead to significant bias, especially for coarse-mode particles. For in-cabin measurements, studies have shown that the loss rate of coarse dust particles can be substantial due to the aircraft's instrument inlet, therefore leading to lower sampling rate and size bias (e.g. von der Weiden et al., 2009). For dust measurements that used optical particle counters, irregularly-shaped dust particles are often assumed to be spherical in order to convert them to volume-equivalent geometric diameters, but light scattering between spherical and non-spherical particles are different. In addition, optical particle counters also make assumptions about the refractive index to derive the dust size distribution, and are affected by the non-monotonic increase in the intensity of scattered light with particle size (e.g. Weinzierl et al., 2011; Ryder et al., 2018). Unlike the optical particle counters that require assumption regarding dust refractive index and shape to convert scattered light intensity to particle size, the imaging probes are not subject to these uncertainties (Baumgardner et al., 2017; Ryder et al., 2018). Nevertheless, these assumptions often lead to biases, that many studies try to account for to various degrees (e.g. Ryder et al., 2013a, 2013b, 2018).

2.4.2 Mass extinction efficiency measurements

In the literature, the term dust mass extinction efficiency (MEE) is sometimes used interchangeably with the mass scattering efficiency (MSE; e.g. Hand & Malm, 2007). This is because, for typical solar wavelength at 550 nm, dust particles scatter more radiation than they absorb for $D \leq 10$ μm. Despite the strong scattering by these particles, larger particles ($D \geq 10$ μm) often exhibit substantial absorption relative to scattering in the visible wavelength (e.g. Ryder et al., 2018). In order to put all the measurements in the same equal footing, we convert the reported dust MSE in some of these studies to dust MEE, by using measured scattering albedo value of 0.95 ± 0.03 (e.g. Haywood, 2003; Clarke et al., 2004; Ryder et al., 2018).

Mass extinction efficiencies (MEE) that are reported in the literature are generally derived using two methods: regression and theoretical methods (e.g. Hand & Malm, 2007). The regression method calculates the dust MEE as the slope between the dust extinction coefficient (m^{-1}) and the dust mass concentration (g m^{-3}). In this case, the dust samples are typically collected using filters, while aerosol extinction is measured using nephelometers. The difficulty, however, is that measured total aerosol extinction from the nephelometer may be influenced by several aerosol species other than dust particles. Some studies ignore the impact of other aerosol species, and derive the dust MEE using the total aerosol extinction and the collected dust mass concentration (e.g. Li et al., 1996). Others take advantage of the linear relationship between the aerosol extinction and mass concentrations in order to separate the column MEE into constituents that correspond to each aerosol species, using a multivariate linear regression method (e.g. Andreae et al., 2002; Maring et al., 2003). Such calculations therefore require that all the aerosol species contributing to the extinction are included. With this in mind, the regression-derived MEE is therefore subject to several systematic and random errors, including instrument uncertainties (Hand and Malm, 2007).

The theoretical method calculates the dust MEE using the measured size distributions of dust mass or number concentration (Seinfeld & Pandis, 2016). This may take the form of calculating the dust MEE directly using the dust size distribution and the estimate of single-particle extinction efficiency, or indirectly by first calculating the size-resolved dust extinction coefficient, using dust size distribution, and then combining the result with dust mass concentration. In either case, the dust density, shape and index of refraction are needed. While assumptions of dust density and index of refraction are typically based on previously reported measurements, dust shapes are generally assumed to be spherical, which is contrary to observations (e.g., Okada et al., 2001; Kandler et al., 2007). This is a major disadvantage that may result in an underestimation of the derived dust extinction efficiency (e.g. Kok et al., 2017). Another source of error is associated with the instrument used to measure the aerosol size distribution, which may assume certain mixing properties of the observed aerosols. For mobility measurements (differential mobility analyzer, DMA), optical measurements (optical particle counter, OPC) or aerodynamic measurements (aerodynamic particle sizer, APS), aerosols are often assumed to be internally mixed (e.g. Quinn et al., 2002; Clarke et al., 2004). In contrast, for an impactor, aerosols are often assumed to be externally mixed (e.g. Chiapello et al., 1999; Osborne et al., 2008).

Despite the differences between both methods used to derive dust MEE from observed quantities, previous studies have highlighted that they both produce similar values within measurement uncertainties (e.g. Maring et al., 2000; Quinn et al., 2004). In addition, for measurements where only the mean dust MEE/MSEs are reported, but not the

uncertainty estimates, we estimate here in this study what the measured uncertainty estimate could be by assuming that its relative uncertainty (that is the ratio of the presumed uncertainty to the reported mean) is proportional to the mean relative uncertainty that is calculated from other measurements. While this estimated uncertainty may likely not be representative of the specific field campaign to which the measurement was taken, they are likely representative of the seasonal values over the region.

3 Results

In this section, we present the DustCOMM products obtained using the methodology and data described above. We first present the dust particle size distribution (PSD; section 3.1) and then the dust mass extinction efficiency (MEE; section 3.2). In each case, we evaluate the DustCOMM and the model ensemble products against available *in-situ* measurements. We show that DustCOMM products generally reproduce observations better than model ensemble estimates. We then compare the spatial variability of the DustCOMM products against the model ensemble. In section 3.3, we compare the atmospheric dust loading obtained from both DustCOMM and the model ensemble, and we examine the spatial distribution of the uncertainty in all DustCOMM products in section 3.4.

3.1 Dust Size Distribution

3.1.1 Evaluation of DustCOMM against measurements

We evaluate DustCOMM and the model ensemble PSD against available in-situ measurements taken during field campaigns (Figs. 2 & 3). We compare these location-based measurements against season-averaged DustCOMM and model ensemble estimates. The reason for using the seasonal averages is justified in section 2.4 above. An additional justification for the comparison between the individual measurements and the season-averaged DustCOMM and model ensemble estimates is that the variability of the normalized dust PSD within each season is relatively small, especially for dust with $D \leq 10\ \mu m$ (e.g. McConnell et al., 2008; Mahowald et al., 2014). Furthermore, most of these measurements are campaign averages often over a variety of cases that could be representative of the season-averaged size distribution.

Model simulations of dust PSD generally show substantial errors when compared against measurements. In each of the 12 studies used in Fig. 2, the model ensemble overestimates the observed fine-mode particles (defined here as $D \leq 2.5\mu m$) and underestimates the coarse-mode particles (defined here as $D \geq 5\ \mu m$). In some of the cases, the overestimation extends above $D = 2.5\mu m$ and the underestimation below $D = 5\mu m$. Nevertheless, these differences are apparent in all the comparisons, and consistent with previous studies indicating more coarse-mode dust particles are in the atmosphere than models account for (e.g. van der Does et al., 2016, 2018; Kok et al., 2017; Ryder et al., 2018).

In contrast, the DustCOMM dust PSD shows overall better agreement against measurement than the model ensemble (Fig. 2). This improved agreement includes a substantial reduction of the underestimation of coarse-mode dust, as well as a reduction of the overestimation of some fine-mode particle sizes. Although DustCOMM better reproduces

the measurements for $D \geq 0.5\mu m$, it shows poorer agreement for $D \leq 0.5\ \mu m$ (e.g. Fig. 2e, h, i, j), underestimating the measurements by about one to two orders of magnitude. For example, during DARPO (Fig. 2e; Wagner et al., 2009) and BACEX (Fig. 2h; Jung et al., 2013), the differences between DustCOMM PSD and the measurements are about two orders of magnitude. The $D \leq 0.5\ \mu m$ size range is also the size range in which measurements of dust PSD are potentially contaminated by the presence of other aerosol species (see section 2.3.1 and section 4.1). In addition to the disagreement for $D \leq 0.5\ \mu m$, there is also some disagreement for $D \geq 10\ \mu m$ (e.g. Fig. 2d, e, h), although for fewer cases. Overall, the DustCOMM dust PSDs significantly better represent the measurements in the $0.5 \leq D \leq 20\ \mu m$ size range than the model ensemble.

DustCOMM also shows better agreement than the model ensemble against measurements of the dust PSD as a function of altitude (Fig. 3). We highlight here measurements taken from three campaigns: (1) the ACE-2 campaign (June/July, 1997) in the vicinity of Canary Islands (Otto et al., 2007); (2) the Fennec project (June 2011) between the Canary Islands and Mauritania/Mali (Ryder et al., 2013a); and (3) the AER-D campaign in August 2015 near Cape Verde Island (Ryder et al., 2018). All three cases show that a significant fraction of coarse-mode dust particles, including with $D \geq 10\ \mu m$, are transported off the coast of North Africa. We compare these measurements at selected altitude of 2500 m (2700 m for ACE-2), 4000 m, 5500 m, and 6000 m (7000 m for ACE-2). Similar to Fig. 2 above, the DustCOMM dust PSD agrees better with the measurements than the model ensemble for these measurements at similar 2-D location but at different altitudes. For dust particles with $D \leq 0.5\ \mu m$, the DustCOMM size distributions also differ from the measurements by about an order of magnitude (similar to Fig. 2) for altitude at 2500 m. However, this difference increases to more than two orders of magnitude above ~4000 m altitude.

In summary, the overall differences between the in-situ measurements and DustCOMM are significantly smaller than the differences between the measurements and the model ensemble, especially for $D \geq 0.5\ \mu m$. To quantify this, we report the log-mean bias in each bin following Eqn. 10 and using all the measurements shown in Fig. 2 & 3. DustCOMM shows an overall reduction in the bias relative to the model ensemble, except for dust particles with $D \leq 0.5\ \mu m$ (Fig. 4). For $D \leq 0.5\ \mu m$, model shows an average (95% CI) positive log-mean bias of 0.26 (-0.08 — +0.6), while DustCOMM shows an average negative log-mean bias of -0.92 (-1.18 — -0.73). In contrast, DustCOMM shows a remarkable reduction in the average log-mean bias in the $0.5 \leq D \leq 10\ \mu m$ size range; for instance, the bias for the $5 - 10\ \mu m$ bin is ~90% less than it is for the model ensemble. DustCOMM also shows a substantially reduced bias in the $10 \leq D \leq 20\ \mu m$ size range, although the bias here remains substantially negative, indicating a persistent underestimation of these coarse particles. On average, DustCOMM reduces the log-mean bias for dust particles with $D \geq 0.5\ \mu m$ by about 46%, relative to the model ensemble.

3.1.2 Global comparison between DustCOMM and the model ensemble

Considering that the DustCOMM dust PSD agrees better with in-situ measurements than the model ensemble, we now compare the differences between DustCOMM and model ensemble PSDs. Specifically, we first compare the differences in the shape of the globally-averaged dust size distribution between DustCOMM and the model ensemble

(section 3.1.2.1). Second, we examine the changes in the spatial variability of the DustCOMM and model dust mass fraction as a function of particle size range (section 3.1.2.2).

3.1.2.1 Differences in dust size distribution

As we already concluded based on in-situ measurements, climate models globally overestimate fine-mode dust particles ($D \leq 2.5\ \mu m$) and under-estimate coarse-mode dust particles ($D \geq 5\ \mu m$), relative to globally-averaged DustCOMM dust PSD (compare black and coloured lines in Fig. 5a). On average, simulations in our model ensemble overestimate the dust mass fraction of the fine mode by ~14%, and underestimate that of the coarse mode by ~15%. The degree of this deviation from DustCOMM depends on the model, and can be as much as 50% in the fine mode or 37% in the coarse mode.

While the globally-averaged dust PSDs clearly show marked differences, it is also important to quantitatively examine the variability of the dust PSD for all locations. The variability of dust PSDs in the atmosphere is influenced by dust emission, transport, and deposition processes, and it can be assessed by considering metrics such as the volume median diameter (e.g. Maring et al., 2003; Formenti et al., 2011; Mahowald et al., 2014). Thus, the probability distributions of the volume median diameters (VMD) for the model simulations are generally biased towards smaller VMD values, with different peak diameters for each model. WRFChem and IMPACT show the lowest VMD at ~1.9 μm, and ARPEGE-Climat shows the highest VMD at ~5.5μm (Fig. 5a). In contrast, the DustCOMM VMD peaks around 5 μm. The probability distribution also shows that that the DustCOMM VMD lies between approximately 2.5 μm and 6.5 μm at most heights and locations (Fig. 5b). This range is consistent with the range of measured VMD (3-6 μm) for coarse-mode dust particles generally reported in the literature and compiled by Reid et al. (2003; see their Table 1). It also falls within the range of values measured at near-source regions and farther downwind. For instance, the VMD calculated from dust particle size distributions measured at Cape Verde, off the coast of North Africa (Ryder et al., 2018) is about 5.5μm. Farther downstream where dust particles are likely to deposit after long-range transport, the VMD values near Puerto Rico is approximately 4μm (Maring et al, 2003). It is noteworthy however, that some studies (e.g. Carlson & Caverly, 1977; Weinzierl et al., 2009) have reported measured VMD values that exceed 13 μm, but these studies often include giant-mode dust particles with $D \geq 20\mu m$, whereas we limited our analysis to dust with $D \leq 20\mu m$ (see Section 2.3.1.1). Overall, DustCOMM shows better consistency with observations of VMD than model simulations.

3.1.2.2 Changes in spatial variability of dust mass fraction

Although coarse-mode particles dominate the dust mass fraction near source regions and fine-mode particles dominate the dust mass fraction in the far remote regions, there are considerable changes in the spatial variability of the dust mass fraction between DustCOMM and the model ensemble (left and middle panels of Fig. 6). As highlighted above in section 3.1.2.1, there is a general decrease of DustCOMM dust mass fraction for particles between $0.2 - 2.5\mu m$ and $2.5 - 5\mu m$, relative to the model ensemble (right panel of Fig. 6). In contrast, there is an overall increase of DustCOMM dust mass fraction for particles between $5 - 10\mu m$ and $10-20\mu m$. These changes cause DustCOMM to

produce generally better agreement against in-situ measurements than the model ensemble, as shown in section 3.1.1 above. Overall, the most significant changes in DustCOMM dust mass fraction, relative to the model ensembles, are near dust-dominated regions, resulting in a decrease of up to 26% and an increase of up to 29% for dust particles between $2.5-5\mu m$ and $10-20\mu m$ respectively.

These changes in the dust mass fraction gradually decrease away from the dust-dominated regions. This is evident, for example, over the North Atlantic basin, where dust from the Sahara Desert is transported to the Caribbean and South America. Models generally simulate fewer large dust particles ($D \geq 5\mu m$), and thus transport only a small fraction to the Caribbean. But observational evidence shown earlier in Figs. 2h & l indicates that dust in Barbados includes a significant fraction of coarse dust. Thus, the east-west gradient and the overall increase of the DustCOMM dust mass fraction over the North Atlantic helps resolve the underestimation of long-range transported coarse particles, such as near Barbados (Fig. 6; e.g. Weinzierl et al., 2017).

The vertical distribution of the DustCOMM dust mass fraction shows differences with the model ensemble that are consistent with the globally-averaged differences (Fig. 7) – that is, DustCOMM dust mass fractions are lower than for the model ensemble for particles between $0.2-2.5\mu m$ and $2.5-5\mu m$, and higher for particles between $5-10\mu m$ and $10-20\mu m$. It is noteworthy here that vertical changes in the dust PSD in DustCOMM are based on model simulations, causing a similarity in the shape of the vertical profile of the dust mass fraction between DustCOMM and the model ensemble. Finally, similar changes in the spatial variability of the annually-averaged dust mass fraction are apparent in the seasonally-averaged values.

3.2 Dust Mass Extinction Efficiency

3.2.1 Evaluation of DustCOMM against measurements

We evaluate the dust mass extinction efficiency (MEE – m^2g^{-1}) of DustCOMM and the model ensemble against measurement (Fig. 8). These measurements span from those taken near dust source regions such as the Saharan, Middle East and Asian deserts, to those taken farther downwind from source regions (Table 2). Higher values of dust MEE are expected where fine-mode dust particles dominate, because smaller dust particles scatter light more efficiently per unit mass at visible wavelengths. In contrast, dust MEE decreases as the coarse-mode fraction increases. Thus, observed dust MEE values generally range between ~0.3-0.8 m^2g^{-1} at approximately 550 nm.

DustCOMM shows better agreement with measurements of dust MEE than the model ensemble (Fig. 8). DustCOMM dust MEE estimates are within the measurement uncertainty range for most of the 11 studies used here. Notable exceptions are the comparison at Sde Boker, Israel (Andreae et al., 2002) and Qinghai Province, China (Li et al., 2000), where both the DustCOMM and the model ensemble underestimate the measured MEE. Nevertheless, the DustCOMM estimates better reproduce the lower values of dust MEE near dust sources, and the higher values farther downstream. For example, lower dust MEE values near the Sahara Desert, between Niamey and the Canary Islands (generally below 0.6 m^2g^{-1}), and higher values farther downstream, such as over Barbados, are better reproduced by DustCOMM. DustCOMM dust MEE also compares well against measurements at the same location but for different

seasons. An example is the measurements over Cape Verde, off the coast of North Africa (Haywood et al., 2003; Ryder et al., 2018), taken in September 2000 and August 2015. For both cases, DustCOMM estimates compare better with the observed dust MEE, while the model ensemble over-estimates the values in both cases.

DustCOMM also reproduces the observed dust MEE values with strong spatial gradient, measured during the same campaign (INDOEX) over the Arabian Sea and Indian Ocean (Quinn et al., 2002). Dust particles emitted from Middle East deserts can get transported over the Arabia sea, and are deposited over the Indian Ocean where strong precipitation occurs year-round (e.g. Kulshrestha et al., 1996). Since dust MEE increases with distance from source regions due to deposition of larger dust particles, the measured dust MEE values increase from 0.5 m^2g^{-1} measured in the Arabian Sea to 0.75 m^2g^{-1} in the Indian Ocean, south of the equator. DustCOMM captures much of this gradient, and is in better quantitative agreement than the model ensemble estimate (Fig. 8).

DustCOMM also shows better agreement than the model ensemble against the observed dust MEE averaged over all measurements (see the last column of Fig. 8). DustCOMM shows a very small difference with the mean of the measurement estimates [0.007 m^2g^{-1} (95% CI is -0.04—0.08)], whereas the model ensemble mean (95% CI) overestimates the measurements by 0.12 (-0.17 – 0.4) m^2g^{-1} – that is about 94% reduction in the mean bias. We further assess DustCOMM performance by calculating the reduced chi-square (χ_ϵ^2; Eqn. 11); a value of $\chi_\epsilon^2 > 1$ highlights the degree that a model does not fit the observations within the uncertainty range (e.g. Andrae et al., 2010). DustCOMM shows a χ_ϵ^2 value of 1.19 , in comparison to the model ensemble with χ_ϵ^2 value of 8.70 (Fig. 8), thereby showing a substantial improvement.

3.2.2 Global comparison between DustCOMM and model ensemble

After showing that DustCOMM better reproduces measurements of dust MEE than the model ensemble, we now compare the spatial variability of the DustCOMM and model ensemble dust MEE. To do so, we estimate the column-integrated dust MEE for DustCOMM and model ensembles over each location (Fig. 9 a & b). Both DustCOMM and model estimates show smaller values of dust MEE over dust-dominated regions and higher values farther downwind – like over the Inter Tropical Convergence Zone (ITCZ), the eastern Pacific Ocean and the polar regions. Although DustCOMM and model ensemble estimates are thus spatially similar, important differences exist. Near dust-dominated regions, DustCOMM dust MEE values are lower than model ensembles, but farther downstream, DustCOMM values are higher than model ensembles. This regional difference in dust MEE values corresponds to similar difference in dust mass fraction, with fractional increase in coarse-mode dust over dust-dominated regions than farther downstream (compare Fig. 9 & 6). In addition, there is also a gradual east-to-west changes in the dust MEE values as coarser dust particles are deposited away from dust sources, consistent with similar changes in dust mass fraction shown earlier in Fig. 6. The globally-averaged DustCOMM dust MEE values are lower than predicted by the model ensemble. The global mean of dust MEE for DustCOMM and model ensembles are 0.68 (Min-Max: 0.22—1.1) $m^2\ g^{-1}$ and 0.95 (Min-Max: 0.30— 1.98) $m^2\ g^{-1}$ respectively.

3.3 Global comparison of atmospheric dust load between DustCOMM and models

After obtaining the DustCOMM dust MEE as described in the previous section, we combine this with the reanalysis-derived dust AOD (Eqn. 9; see also section 2.3.3) to obtain the atmospheric dust loading. We find that the DustCOMM dust column loading is generally larger than the model ensemble estimate (Fig. 10a & b). DustCOMM shows substantially larger dust column loading than the model ensemble over desert regions, such as the Middle East, and Asian deserts. The relative increase of dust load in DustCOMM over the Asian desert is more than twice the increases over the Middle East desert. DustCOMM also shows larger dust column loading over most parts of the North African desert, except some parts that includes the north-western section and the coastal regions which show smaller dust column loading than the model ensemble. Although reanalysis-derived mean dust AOD over North Africa is substantially lower than the model ensemble, it is within the uncertainty estimates, which is higher over this region (see supplementary Fig. S-4; see also Ridley et al., 2016). In addition, DustCOMM estimates over the Australian deserts show a lower dust column loading than the model ensemble, similarly corresponding to lower reanalysis-derived dust AOD (Fig. 10c & supplementary Fig. S-4). Overall, globally-averaged DustCOMM dust column loading is about 46% higher than the model ensemble.

3.4 Spatial distribution of DustCOMM relative uncertainty

We examine here the spatial distribution of the DustCOMM relative uncertainty– that is, the uncertainty characterizing 68% of the distribution of each variable over each location divided by the mean value of that variable at that location. We do this for the dust mass fraction for the particle bins shown in Fig. 6 & 7, the dust MEE, and the dust load (Fig. 11).

The relative uncertainties in the DustCOMM fine-mode fraction ($D = 0.2 - 2.5\mu m$) are higher mostly near emission regions (Fig. 11a), while the relative uncertainties in the coarse-mode fractions are higher over remote regions, especially for $D = 10 - 20\mu m$ (Fig. 11d). These uncertainties are, in part, directly associated with the uncertainties in the measurement constraints. The globally-averaged constrained dust size distribution (Eqn. 1) has a higher relative uncertainty for the $D \leq 1\ \mu m$ and $D \geq 10\ \mu m$ diameter range than for the $1 \leq D \leq 10\ \mu m$ diameter range (see Fig. 2 in Kok et al., 2017), and we propagate these uncertainties over every location. In addition, the spatial distribution for the relative uncertainties in the dust mass fraction is similar to that of the model ensembles (supplementary Fig. S-5), which is also propagated into the DustCOMM product.

The relative uncertainties in DustCOMM dust MEE are mostly higher over dust-dominated regions (Fig. 11e). The dust MEE is influenced by the uncertainty in the constrained globally-averaged extinction efficiency, which in-turn is partially due to uncertainties in the in-situ emission measurements of index of refraction and dust particle shapes (see Fig. 1b in Kok et al., 2017), all of which are propagated into the DustCOMM dust MEE. In addition, the relative uncertainties in the dust MEE are also affected by the uncertainty in the dust size distribution. Thus, the spatial distribution of dust MEE relative uncertainty is particularly informed by the uncertainties in the fine-mode and coarse-mode dust particles (compare Fig. 11a & d with 11e). For the most part, uncertainties in the fine-mode dust fraction appears to dominate the uncertainties in dust MEE, more than the uncertainties in the coarse-mode dust fractions.

The relative uncertainties in the DustCOMM dust column loading are mostly higher over remote regions, where the mean dust load is small (Fig. 11f). Though the dust column loading is influenced by the uncertainties in dust MEE, the spatial distribution of the relative uncertainties in dust load is largely informed by the uncertainties in the reanalysis dust AOD (see supplementary Fig. S-4).

4 Discussion

We presented the DustCOMM products in the previous section, where we showed that both the dust particle size distribution (PSD) and the dust mass extinction efficiency (MEE) are reproduced more accurately than by an ensemble of model simulations. Despite the overall agreement with observations, there are some disagreements highlighting potential limitations of our methodology. In this section, we discuss these disagreements between DustCOMM and measurements and provide possible insights into these discrepancies (section 4.1). We also discuss the impact of dust sizes and asphericity on DustCOMM dust mass extinction efficiency (section 4.2), and we highlight the limitations in using modelling constraints as part of DustCOMM estimates (section 4.3). We end by highlighting how our constrained DustCOMM products can be used by the research community to potentially improve estimates of dust impacts on the Earth system (section 4.4).

4.1 Cause of discrepancy between DustCOMM and size distribution measurements

The evaluation of the DustCOMM PSD shows an underestimation of dust with $D \leq 0.5\mu m$ and $D \geq 10\mu m$ (Figs. 2, 3 & 4). This is in contrast to the ensemble of model simulations overestimating the dust mass fractions for $D \leq 0.5\mu m$, and underestimating the dust mass fraction substantially more than DustCOMM for $D \geq 10\mu m$. Although the comparison between date-specific individual measurements and season-averaged DustCOMM dust PSD is expected to induce errors, this difference cannot explain the apparently systematic difference between measurements and the DustCOMM dust PSD for both $D \leq 0.5\mu m$ and $D \geq 10\mu m$ (Fig. 4). We provide here possible reasons for this disagreement between DustCOMM and observations.

First, DustCOMM's underestimation of dust with $D \leq 0.5\mu m$ may be caused by contamination of the measured size distributions by other aerosol species for $D \leq 0.5\mu m$. Studies have shown that a substantial fraction of aerosols with $D \leq 0.5\mu m$ are not mineral dust, even in dust-dominated regions (Chou et al., 2008; Kandler et al., 2009; Weinzierl et al., 2009). For example, during the Saharan Mineral Dust Experiment (SAMUM) over southern Morocco, Kandler et al. (2009) showed that more than 50% of the measured particles with $D \leq 0.5\mu m$ are ammonium sulphates or mixture of sulphate and dust. Even when strict measurement techniques are used to separate other non-mixing aerosol components, the aerosol mixing state for $D \leq 0.5\mu m$ often leads to outer coating of available dust particles, thus leading to a higher particle volume that overestimates the true dust size (Weinzierl et al., 2009). In addition, campaign logistics often require that some measurements of dust properties are taken close to major cities, where contaminations by other aerosol species, such as biomass-burning aerosols or urban pollutions are possible (e.g. McConnell et al.,

2008; Wagner et al., 2009). For example, Clarke et al. (2004) highlighted that the presence of biomass-burning aerosols (e.g. soot) led to a variability of about 2 orders of magnitude for measured size distributions with diameter less than $D \leq 0.6\mu m$ during the ACE-Asia campaign. This variability is consistent with the average difference between our estimates and the observations for $D \leq 0.5\mu m$. After separating out the contamination of the soot-mode from the dust size distribution, their resulting dust PSD generally agrees with our estimate within the uncertainty range (Fig. 2f). Thus, the large variability of the measured size distribution is indicative of the potential problems with the representation of dust particles with $D \leq 0.5\mu m$.

Second, the constraint on the globally-averaged dust size distribution could also underestimate the contribution from dust with $D \leq 0.5\mu m$. A key input to this constraint is the emitted dust size distribution, but there is a dearth of measurements of the mass fraction of emitted dust with $D \leq 0.5\mu m$, leading to uncertainty in constraining the globally-averaged emitted dust size distribution with $D \leq 0.5\mu m$ (Kok et al, 2017). Moreover, the measurements of emitted dust size distribution with $D \leq 0.5\mu m$ that do exist (e.g. Fratini et al., 2007; Sow et al., 2009; see Fig. 1c in Kok et al., 2017) indeed show a larger dust mass fraction than represented in the constraint on the globally-averaged emitted dust size distribution. Therefore, more measurements of the size distribution of emitted dust particles extending to very fine sizes are needed.

Third, the underestimation of dust with $D \geq 10\ \mu m$ by both DustCOMM and the model ensemble might be caused by biases in both global model simulations and the constraints on the global dust size distribution used by DustCOMM. Similar to $D \leq 0.5\mu m$, the experimental constraint on the emitted dust size distribution with $D \geq 10\ \mu m$ also has a large uncertainty because of limited available measurements (Kok 2011). In addition, since spatial and temporal variability of large dust particles ($D \geq 10\mu m$) strongly depend on the model simulation of dust emission and deposition processes, uncertainties in these processes will influence the constraints on DustCOMM dust size distribution. For example, if the giant mineral dust particles are transported far away from the source regions as suggested by observations (e.g., van der Does et al., 2018), the lack of this mechanism would result in a negative bias of the simulated dust atmospheric lifetime (e.g. Huneeus et al., 2011). And since modelling constraints of globally-averaged dust lifetime are used to constrain the globally-averaged size distribution (Eqn. 1), such systematic negative bias may have contributed to the underestimation of dust particles with $D \geq 10\mu m$. Although our methodology partly constrains dust deposition globally, it does not constrain regional variability in dust deposition, and we expect that such uncertainties may increase as a function of distance away from dust-dominated regions. We note here that regional observational constraints on dust lifetime are currently not available, and stronger modelling constraints that may account for the underestimation of coarse dust particles in the atmosphere are a subject for future work.

4.2 Impacts of dust sizes and asphericity on DustCOMM dust mass extinction efficiency

The dust MEE is partially determined by the dust size distribution (Eqn. 8). Despite the good agreement between DustCOMM and the measurements of dust MEE (Fig. 8), the size discrepancies in the dust size distribution for particles with $D \leq 0.5\ \mu m$ and $D \geq 10\ \mu m$ (Figs. 2, 3 & 4) affect the estimation of dust MEE. Dust with $D \leq 0.5\ \mu m$ has a large single-particle MEE, whereas dust with $D \geq 10\ \mu m$ has a small single particle MEE (see supplementary

Fig. S-6). Consequently, errors due to the possible overestimation of both size fractions at least partially cancel each other.

In addition to the impact of dust sizes, dust asphericity also has a substantial impact on the dust MEE. The DustCOMM constraint on dust MEE leverages measurements of dust shape to represent dust particles as an ensemble of tri-axial ellipsoids (Meng et al., 2010; Kok et al., 2017). In contrast, most models use Mie theory, which approximates dust as spherical particles. Thus, the difference between single-particle dust MEE used in DustCOMM and calculated using Mie theory shows the impact of dust asphericity is substantial for both small and lager dust particles, increasing extinction for particles with $D \geq 1\mu m$ (supplementary Fig. S-6). This implies that typical global model simulations, which contain too much fine-mode dust particles and approximate dust as spherical, the overestimation of the dust extinction due to the fine size bias could (partially) cancel out the underestimation of the dust extinction due to the treatment as dust spherical shapes, leading to nonetheless reasonable agreement with measured dust MEE. However, for DustCOMM, both the size bias and dust asphericity are accounted for, thereby producing better agreement with measurements (Fig. 8). In addition, accounting for dust asphericity could allow dust particles to stay longer in the atmosphere because asphericity reduces dust settling speed (Ginoux, 2003), which may in turn lead to a more accurate estimation of dust deposition mass fluxes onto land and ocean ecosystems (e.g. van der Does et al., 2016; 2018).

4.3 Limitations in using modelling constraints

We used modelling constraints in DustCOMM where observational constraints were either not available or insufficient. For example, modelling constraints are used for the regional differences in dust size distribution and extinction efficiency because the measurements to constrain these parameters on a regional basis across the different dust-source regions are currently insufficient. To further reduce the uncertainty associated with using modelling constraints, we used an ensemble of six model simulations. In addition to the uncertainties associated with model simulations of dust emission and deposition processes that may influence the constraints on dust size distributions as highlighted in section 4.1, there are other limitations in the modelling constraints that can influence DustCOMM estimates.

First, one such limitation is the uncertainty in the dust mass spatial distribution of the model ensemble, which directly determines the spatial distribution of dust mass for DustCOMM estimates. Variability in dust emission rates influence the distribution of simulated size-resolved atmospheric dust loading, and consequently the 3-D dust mass fractions. In addition, ensemble model simulations of dust emission and transport are driven by different meteorological datasets (Table 1), which represent the actual historical meteorology with various degrees of accuracy (e.g. Evan, 2018). Dust transport is also influenced by model resolution and sub-grid parameterizations of wind and turbulence, which differ between models (e.g., Zender et al., 2003; Cakmur et al., 2004). Although averaging over multiple models and over long time periods reduces random errors, systematic errors that affect different models similarly would affect the model ensemble (e.g. Ridley et al., 2012), and would impact the spatial distribution of dust mass (e.g. Johnson et al. 2012; Ridley et al., 2016). In addition, uncertainties in the vertical distribution of size-resolved dust mass fractions directly affect DustCOMM dust size distributions. Since we use the globally-averaged size-resolved extinction

efficiency to constrain the dust MEE over every location (Eqn. 8), the spatial distribution of dust MEE is thus partially determined by the dust size distribution, effectively propagating any uncertainty in model simulations of the spatial distribution.

Second, some errors may have been introduced while scaling and fitting the different model dust size distributions to a common diameter range (section 2.3.1). For the scaling procedure (section 2.3.1.1), the variance of the dust mass fraction in all the bins, including the newly-created ones, are of similar orders of magnitude, thus errors introduced through this process are small relative to the magnitude of errors in the dust mass fraction. In addition, the resulting dust size distributions are dependent on the specific function and set of parameters used in the fitting procedure (section 2.3.1.2), which may also introduce some errors.

Third, our constraints on the dust atmospheric loading use ensemble estimates of reanalysis-derived dust AOD, which depends in part on the assimilated aerosol observations, in part on the numerical simulation of dust sources and sinks, and in part on the numerical simulation of other aerosol species. Although some of the reanalysis products try to constrain these dust processes using space-based observations (e.g. Lynch et al., 2016; see supplementary information), the impact of the uncertainties associated with each process on the DustCOMM estimates of the atmospheric dust loading is beyond the scope of the study.

Finally, this study primarily uses climatologies of modelled dust size distribution between 2004-2008, except for WRF-Chem and IMPACT (see Table 1), and it also scales dust mass loading using the 2004-2008 reanalysis products (see section 2.3.3 & 2.2). Thus, any application of our methodology to a different time periods is expected to have some errors. While these errors are expected to be small for the dust size distribution and dust mass extinction efficiency, they may have a substantial impact on the dust mass loading, depending on the inter-annual variability in the reanalysis-derived products and also on the assimilated observations

4.4 Possible use of DustCOMM to improve estimates of dust impacts on the Earth system.

Given that DustCOMM estimates of dust aerosol properties are in better agreement with measurements than the model ensemble, DustCOMM could be used to obtain improved constraints on dust impacts on the Earth system than is possible from current global models. Specifically, DustCOMM dust properties could be used as an alternative to global model simulations in constraining dust impacts, such as the dust direct radiative impact or dust impacts on biogeochemistry and human health. For instance, dust radiative heating rates in the atmosphere strongly depend on the ability of dust particles to absorb shortwave and longwave radiation (e.g. Perlwitz and Miller, 2010). In turn, such absorption depends on the dust size distribution, which strongly influences the optical parameters like the dust absorption optical thickness (e.g. Tegen and Lacis, 1996). With improved constraints on the dust size distribution and therefore the dust optical properties, DustCOMM could be used to determine the dust (shortwave and longwave) heating rates in the atmosphere more accurately than possible with current global model simulations. As a result, our constraints on dust size distribution could be used to better quantify radiative effects of dust, especially in the longwave spectrum which have remained very uncertain (Dufresne et al., 2002; Di Biagio et al., 2017a; Kok et al.,

2017; Song et al., 2018). Furthermore, since recent studies associate much of the biases in dust properties, such as the dust aerosol optical depth, deposition fluxes and surface dust concentration, to model biases in dust size distribution (Evan et al., 2014; Huneeus et al., 2011), DustCOMM estimates can therefore serve as a better alternative. For example, DustCOMM's improved constraints on atmospheric dust loading and dust size distribution could contribute to better estimates of size-resolved dust concentration near the surface (e.g. Whicker et al., 2018). Over the ocean, such constraints on size-resolved dust concentration could potentially be used for constraints on dust deposition fluxes that are more accurate than possible from global model simulations.

In addition to being used as an alternative to global model simulations, DustCOMM could also be used to improve the simulation of dust aerosol properties in global models. Incorporating DustCOMM products in the simulation process can potentially be achieved when the aerosol module is coupled with the global model in either the so-called online or offline modes (e.g. Tegen, 2003; Pérez et al., 2011; Han et al., 2012). In the online mode, the simulated dust size distributions could be adjusted ("nudged") to match the DustCOMM constraints on dust size distribution, similar to what is often done with meteorological fields (e.g. Kooperman et al., 2012). Alternatively, the 3-D dust size distribution could also be corrected offline after the simulated size distribution is obtained but before dust impacts such as on radiation are estimated (e.g. Weaver et al., 2002). Specifically, the modelled dust size distribution can be corrected by minimizing the differences between the DustCOMM and the modelled size distributions for a specific timescale (see section 2.3.5). Whether simulated dust properties are corrected in the online or offline modes, using DustCOMM to bias correct global model simulations could produce better estimation of dust impacts, such as dust impacts on radiation, clouds and precipitation, biogeochemistry, and human health.

An example of dust impacts that can be substantially improved by DustCOMM product are dust radiative effects. These radiative effects are sensitive to dust particle sizes and shapes, which are both constrained substantially more accurately in DustCOMM than in models (Fig. 2-6). Smaller dust particles ($D \leq 2.5\mu m$) scatter more shortwave radiation and cool the climate while larger dust particles ($D \geq 5\mu m$) absorb more longwave radiation and warm the climate. Thus, correcting both biases of too much fine dust and not enough coarse dust in models (Figs. 4 & 5), as we do here in DustCOMM, decreases the shortwave cooling and increases the longwave warming (e.g. Otto et al., 2011; Kok et al., 2017). Using the 3-D DustCOMM size distribution to correct modelled dust properties could yield more accurate estimates of dust radiative effects.

In addition, simulated dust impacts on clouds and precipitation can also be improved using DustCOMM dust aerosol properties. For the interactions of dust particles with clouds, it is important to know the number of particles that are activated above a given particle size as cloud condensation nuclei or ice nuclei (e.g. Andreae & Rosenfeld, 2008; DeMott et al., 2015). Therefore, in regions with significant dust loading, accurate estimates of dust size distribution can be key to accurate simulations of precipitation initiation and aerosol-cloud interactions, including dust aerosol indirect and semi-direct effects (e.g. Sassen, 2003; Doherty and Evan, 2014). Since DustCOMM represent the dust size distribution more accurately than model simulations, it could be used to improve the simulated dust impacts on clouds, precipitation and aerosol-cloud interactions.

Another key advantage of DustCOMM over global model simulations is that it propagates many observational, experimental, and modelling uncertainties of dust properties, which can be propagated into the calculation of dust impacts on the Earth system. For instance, experimental uncertainties associated with the emitted dust size distributions are propagated into the DustCOMM 3D dust size distribution, and experimental uncertainties in the dust index of refraction and dust particle shapes are propagated into the DustCOMM mass extinction efficiency at 550 nm wavelength (e.g,. Kok et al. 2017). In addition, our methodology propagates the uncertainty due to the spread in model predictions of the dust spatial distribution, although substantial biases in the model ensemble might exist (see section 4.3 for example).

Finally, it is worth noting that DustCOMM can be readily updated as more accurate constraints on dust properties and abundance become available. Current constraints in DustCOMM can also be expanded to include more information about dust properties. For instance, a next step could be to include constraints on the dust vertical concentration profile over every location, in order to more accurately estimate dust deposition, and dust concentration at the surface and in 3D. For this, lidar-based retrieval of vertical dust extinction profiles from Cloud-Aerosol Lidar and Infrared Pathfinder Satellite Observations (CALIPSO) can be combined with the corresponding constraints on dust mass extinction efficiency from this study to obtain constraints on the dust vertical concentration profile. Another addition could be constraining the relative contribution of each dust source region to the 3D dust load, which can be combined with constraints on optical properties of dust emitted from each region (Di Biagio et al., 2017, 2019; Green et al., 2018) to obtain more accurate quantifications of dust radiative impacts. Given that dust particles with $D \geq 20$ μm can contribute substantially to dust extinction both in the shortwave and longwave spectrum (Ryder et al., 2019), future versions of DustCOMM could be extended to a diameter range beyond 20 μm as more measurements of dust size distribution with $D \geq 20$ μm become available.

5 Summary and Conclusions

In this study, we presented a new dataset of atmospheric dust aerosol properties called the 'Dust Constraints from Joint Observational-Modelling-experiMental Analysis' – DustCOMM. DustCOMM combines observational and experimental constraints on dust properties and abundance with an ensemble of global model simulations of dust spatial distribution to obtain more accurate 3-D annual and seasonal climatologies of dust properties and abundance than possible with global model simulations alone. Here, we presented three DustCOMM products: the three-dimensional (3-D) dust size distribution, 3-D dust mass extinction efficiency, and two-dimensional dust loading. First, we obtained constraints on the 3-D dust size distribution by combining constraints on the globally-averaged dust size distribution with an ensemble of model simulations of the spatial variability of the dust size distribution. Second, we combined the resulting 3-D dust size distribution with constraints on the size-resolved globally-averaged dust extinction efficiency, which accounts for the substantial asphericity of dust aerosols, to constrain the 3-D dust mass extinction efficiency. Finally, we used the resulting column-integrated dust mass extinction efficiency with an ensemble of reanalysis-derived dust aerosol optical depth to constrain the atmospheric dust column loading.

By comparing DustCOMM estimates of dust size distribution and dust mass extinction efficiency against independent *in-situ* measurements, we showed that DustCOMM reproduces observations substantially better than an ensemble of model simulations (Figs. 2-4, & 8). Models generally overestimate the contribution of fine-mode dust ($D \leq 2.5\mu m$) and underestimate the contribution of coarse-mode dust ($D \geq 5\mu m$), consistent with previous studies (e.g. Mahowald et al., 2014; Kok et al., 2017). In contrast, the DustCOMM size distribution is in substantially better agreement with measurements for different locations, heights and seasons over the $0.5 \leq D \leq 20\ \mu m$ size range. However, there remain some discrepancies between DustCOMM and measurements, notably an underestimation of dust with $D \leq 0.5\mu m$. Potential reasons for these discrepancies include contamination of measured dust size distribution by other aerosol species for $D \leq 0.5\mu m$, and biases in observational and modelling constraints for $D \leq 0.5\mu m$ (section 4.1). Because DustCOMM underestimates the measurements for $D \leq 0.5\mu m$, it shows a more negative bias (~50% more) over the full size range (between $D = 0.2 - 20\mu m$), although the error is markedly lower (~15 %), when compared to the ensemble of model simulations. Overall for $D \geq 0.5\mu m$, DustCOMM shows a bias against measured size distributions that is significantly less (about 46% less) than for an ensemble of global model simulations.

DustCOMM similarly shows better agreement against measurements of the dust mass extinction efficiency (MEE) than an ensemble of model estimates. Because DustCOMM predicts a coarser dust size distribution, as supported by the comparison against *in situ* size distribution measurements, it yields a global-mean dust MEE that is about 28% lower than that from the model ensemble, driven by large reductions in MEE over dust-dominated regions, where coarse particles dominate. For specific locations and seasons, DustCOMM estimates consistently show smaller errors relative to dust MEE measurements than an ensemble of model results, including in regions with strong spatial gradients in dust loading. On average, there is a negligible difference (~1%) between DustCOMM and measurements of MEE, while the model ensemble overestimates MEE by about 23% relative to measurements.

DustCOMM estimates of spatially-varying dust properties and abundance can be used to constrain various dust impacts on the Earth system in a manner that is more robust than possible with current global models. This is because DustCOMM reproduces dust properties more accurately than global model simulations, and also because DustCOMM explicitly propagates uncertainties in experimental, observational, and modelling constraints used in obtaining the DustCOMM products, and these uncertainties can be propagated in calculations of dust impacts on global climate, biogeochemistry, and human health.

List of some acronyms.

GISS	Goddard Institute for Space Studies (GISS) ModelE atmospheric general circulation model
WRF-Chem	Weather Research and Forecasting model coupled with Chemistry
CESM	Community Earth System Model
GEOS-Chem	Goddard Earth Observing System coupled with Chemistry
IMPACT	Integrated Massively Parallel Atmospheric Chemical Transport
INDOEX	Indian Ocean Experiment Intensive Field Phase
SHADE	Saharan Dust Experiment
ACE-Asia	Asian Pacific Regional Aerosol Characterization Experiment

TRACE-P	Transport and Chemical Evolution over the Pacific
ACE-2	Aerosol Characterisation Experiment
DABEX	Dust and Biomass-burning Experiment
AMMA	African Monsoon Multidisciplinary Analysis
DODO	Dust Outflow and Deposition to the Ocean project
SAMUM	Saharan Mineral Dust Experiment
DARPO	Desert Aerosols over Portugal
BACEX	Barbados Aerosol Cloud Experiment
SALTRACE	Saharan Aerosol Long-Range Transport And Aerosol–Cloud-Interaction Experiment
AER-D	AERosol Properties – Dust
MERRA-2	Modern-Era Retrospective analysis for Research and Applications, Version 2
NAAPS	Navy Aerosol Analysis and Prediction System
JRAero	Japanese Reanalysis for Aerosol
CAMSiRA	Copernicus Atmosphere Monitoring Service interim Reanalysis

Data availability

Annually-averaged and seasonally-averaged DustCOMM dust size distribution, dust mass extinction efficiency and dust loading are publicly available at http://doi.org/10.5281/zenodo.2620475. The model dust mass concentration, Kok et al. 2017 datasets, as well as other input dataset used to generate the DustCOMM dataset presented here can be found at http://doi.org/10.5281/zenodo.2620547 (Adebiyi et al., 2019b).

Code availability

The codes used to generate DustCOMM size distribution, dust mass extinction efficiency and the atmospheric loading are available at http://doi.org/10.5281/zenodo.2620556.

Author contribution.

A.A.A and J.F.K designed the project. A.A.A performed the analysis and wrote the paper with contribution from J.F.K. Y.W helped with gathering the literature that reported dust size distribution, and A.I, P.N and C.Z contributed global model simulations outputs. D.A.R provided observationally-constrained dust aerosol optical depth data used in the analysis. All authors discussed the results and commented on the manuscript.

Competing interests.

The authors declare that they have no conflict of interest.

Acknowledgements.

This work was developed with support from the University of California President's Postdoctoral Fellowship awarded to A.A.A. We also acknowledge support from National Science Foundation (NSF) grants 1552519 and 1856389 awarded to J.F.K. Chun Zhao is supported by the National Natural Science Foundation of China NSFC (Grant No. 41775146), and Akinori Ito is supported by the Japan Society for the Promotion of Science KAKENHI Grant Number JP16K00530 and Integrated Research Program for Advancing Climate Models (MEXT). The authors thank Claire L.

Ryder for providing access to the Fennec and AER-D data which are both available at http://www.met.reading.ac.uk/~jp902366/research/. We also thank Bruce Albrecht and Eunsil Jung for providing access to the size distribution collected during the Barbados Aerosol Cloud Experiment (BACEX). The MERRA-2 reanalysis datasets are acquired from the NASA Goddard Earth Sciences (GES) Data and Information Services Center (DISC) and available at https://gmao.gsfc.nasa.gov/reanalysis/MERRA-2/. NAAPS data was obtained through the USGODAE Data Catalog at https://usgodae.org/cgi-bin/datalist.pl?generate=summary and CAMSiRA data was obtained through the ECMWF's Meteorological Archiving and Retrieval System at http://apps.ecmwf.int/data-catalogues/cams-reanalysis. Finally, we thank Yumimoto, K. for providing access to the Japanese Reanalysis dataset through their website at https://www.riam.kyushu-u.ac.jp/taikai/JRAero/.

References

Adebiyi, A. A., Kok, J. F., Wang, Y., Ito, A., Ridley, D. A., Nabat, P. and Chun Zhao: Dust Constraints from joint Observational-Modelling-experiMental analysis – DustCOMM Version 1, Zenodo, [Data set], doi:10.5281/zenodo.2620475, 2019a.

Adebiyi, A. A., Kok, J. F., Wang, Y., Ito, A., Ridley, D. A., Nabat, P. and Zhao, C.: DustCOMM_v1 Input Dataset, Zenodo, [Data set], doi:10.5281/ZENODO.2620547, 2019b.

Albani, S., Mahowald, N. M., Perry, A. T., Scanza, R. A., Zender, C. S., Heavens, N. G., Maggi, V., Kok, J. F. and Otto-Bliesner, B. L.: Improved dust representation in the Community Atmosphere Model, J. Adv. Model. Earth Syst., 6(3), 541–570, doi:10.1002/2013MS000279, 2014.

Altman, D. G. and Bland, J. M.: Standard deviations and standard errors., BMJ, 331(7521), 903, doi:10.1136/bmj.331.7521.903, 2005.

Amiri-Farahani, A., Allen, J. R., Neubauer, D. and Lohmann, U.: Impact of Saharan dust on North Atlantic marine stratocumulus clouds: Importance of the semidirect effect, Atmos. Chem. Phys., 17(10), 6305–6322, doi:10.5194/acp-17-6305-2017, 2017.

Andrae, R., Schulze-Hartung, T. and Melchior, P.: Dos and don'ts of reduced chi-squared, 2010.

Andreae, M. O. O. and Rosenfeld, D.: Aerosol-cloud-precipitation interactions. Part 1. The nature and sources of cloud-active aerosols, Earth-Science Rev., 89(1–2), 13–41, doi:10.1016/j.earscirev.2008.03.001, 2008.

Andreae, T. W., Andreae, M. O., Ichoku, C., Maenhaut, W., Cafmeyer, J., Karnieli, A. and Orlovsky, L.: Light scattering by dust and anthropogenic aerosol at a remote site in the Negev desert, Israel, J. Geophys. Res., 107(D2), 4008, doi:10.1029/2001JD900252, 2002.

Baumgardner, D., Abel, S. J., Axisa, D., Cotton, R., Crosier, J., Field, P., Gurganus, C., Heymsfield, A., Korolev, A., Krämer, M., Lawson, P., McFarquhar, G., Ulanowski, Z., Um, J., Baumgardner, D., Abel, S. J., Axisa, D., Cotton, R., Crosier, J., Field, P., Gurganus, C., Heymsfield, A., Korolev, A., Krämer, M., Lawson, P., McFarquhar, G., Ulanowski, Z. and Um, J.: Cloud Ice Properties: In Situ Measurement Challenges, Meteorol. Monogr., 58, 9.1-9.23, doi:10.1175/AMSMONOGRAPHS-D-16-0011.1, 2017.

Bevington, P. R., Robinson, D. K. and Bunce, G.: Data Reduction and Error Analysis for the Physical Sciences, 2nd ed., Am. J. Phys., 61(8), 766–767, doi:10.1119/1.17439, 1993.

Di Biagio, C., Formenti, P., Balkanski, Y., Caponi, L., Cazaunau, M., Pangui, E., Journet, E., Nowak, S., Caquineau,

S., Andreae, M. O., Kandler, K., Saeed, T., Piketh, S., Seibert, D., Williams, E. and Doussin, J.-F.: Global scale variability of the mineral dust long-wave refractive index: a new dataset of in situ measurements for climate modeling and remote sensing, Atmos. Chem. Phys., 17(3), 1901–1929, doi:10.5194/acp-17-1901-2017, 2017.

Di Biagio, C., Formenti, P., Balkanski, Y., Caponi, L., Cazaunau, M., Pangui, E., Journet, E., Nowak, S., Andreae, M. O., Kandler, K., Saeed, T., Piketh, S., Seibert, D., Williams, E. and Doussin, J.-F.: Complex refractive indices and single scattering albedo of global dust aerosols in the shortwave spectrum and relationship to iron content and size, Atmos. Chem. Phys. Discuss., 1–42, doi:10.5194/acp-2019-145, 2019.

Blain, S., Quéguiner, B., Armand, L., Belviso, S., Bombled, B., Bopp, L., Bowie, A., Brunet, C., Brussaard, C., Carlotti, F., Christaki, U., Corbière, A., Durand, I., Ebersbach, F., Fuda, J.-L., Garcia, N., Gerringa, L., Griffiths, B., Guigue, C., Guillerm, C., Jacquet, S., Jeandel, C., Laan, P., Lefèvre, D., Lo Monaco, C., Malits, A., Mosseri, J., Obernosterer, I., Park, Y.-H., Picheral, M., Pondaven, P., Remenyi, T., Sandroni, V., Sarthou, G., Savoye, N., Scouarnec, L., Souhaut, M., Thuiller, D., Timmermans, K., Trull, T., Uitz, J., van Beek, P., Veldhuis, M., Vincent, D., Viollier, E., Vong, L. and Wagener, T.: Effect of natural iron fertilization on carbon sequestration in the Southern Ocean, Nature, 446(7139), 1070–1074, doi:10.1038/nature05700, 2007.

Boucher, O., Randall, D., Artaxo, P., Bretherton, C., Feingold, G., Forster, P., Kerminen, V.-M. V.-M., Kondo, Y., Liao, H., Lohmann, U., Rasch, P., Satheesh, S. K., Sherwood, S., Stevens, B., Zhang, X. Y. and Zhan, X. Y.: Clouds and Aerosols, Clim. Chang. 2013 Phys. Sci. Basis. Contrib. Work. Gr. I to Fifth Assess. Rep. Intergov. Panel Clim. Chang., 571–657, doi:10.1017/CBO9781107415324.016, 2013.

Buchard, V., Randles, C. A., da Silva, A. M., Darmenov, A., Colarco, P. R., Govindaraju, R., Ferrare, R., Hair, J., Beyersdorf, A. J., Ziemba, L. D., Yu, H., Buchard, V., Randles, C. A., Silva, A. M. da, Darmenov, A., Colarco, P. R., Govindaraju, R., Ferrare, R., Hair, J., Beyersdorf, A. J., Ziemba, L. D. and Yu, H.: The MERRA-2 Aerosol Reanalysis, 1980 Onward. Part II: Evaluation and Case Studies, J. Clim., 30(17), 6851–6872, doi:10.1175/JCLI-D-16-0613.1, 2017.

Carlson, T. N. and Caverly, R. S.: Radiative characteristics of Saharan dust at solar wavelengths, J. Geophys. Res., 82(21), 3141–3152, doi:10.1029/JC082i021p03141, 1977.

Chernick, M. R.: Bootstrap Methods: A Guide for Practitioners and Researchers, Hoboken, NJ, USA., 2007.

Chiapello, I., Bergametti, G., Chatenet, B., Dulac, F., Jankowiak, I., Liousse, C. and Soares, E. S.: Contribution of the different aerosol species to the aerosol mass load and optical depth over the northeastern tropical Atlantic, J. Geophys. Res. Atmos., 104(D4), 4025–4035, doi:10.1029/1998JD200044, 1999.

Chou, C., Formenti, P., Maille, M., Ausset, P., Helas, G., Harrison, M. and Osborne, S.: Size distribution, shape, and composition of mineral dust aerosols collected during the African Monsoon Multidisciplinary Analysis Special Observation Period 0: Dust and Biomass-Burning Experiment field campaign in Niger, January 2006, J. Geophys. Res., 113(D23), D00C10, doi:10.1029/2008JD009897, 2008.

Clarke, A. D., Shinozuka, Y., Kapustin, V. N., Howell, S., Huebert, B., Doherty, S., Anderson, T., Covert, D., Anderson, J., Hua, X., Moore, K. G., McNaughton, C., Carmichael, G. and Weber, R.: Size distributions and mixtures of dust and black carbon aerosol in Asian outflow: Physiochemistry and optical properties, J. Geophys. Res., 109(D15), D15S09, doi:10.1029/2003JD004378, 2004.

Colarco, P. R., Nowottnick, E. P., Randles, C. A., Yi, B., Yang, P., Kim, K.-M., Smith, J. A. and Bardeen, C. G.: Impact of radiatively interactive dust aerosols in the NASA GEOS-5 climate model: Sensitivity to dust particle shape

and refractive index, J. Geophys. Res. Atmos., 119(2), 753–786, doi:10.1002/2013JD020046, 2014.

D'Almeida, G. A.: On the variability of desert aerosol radiative characteristics, J. Geophys. Res., 92(D3), 3017, doi:10.1029/JD092iD03p03017, 1987.

DeMott, P. J., Prenni, A. J., McMeeking, G. R., Sullivan, R. C., Petters, M. D., Tobo, Y., Niemand, M., Möhler, O., Snider, J. R., Wang, Z. and Kreidenweis, S. M.: Integrating laboratory and field data to quantify the immersion freezing ice nucleation activity of mineral dust particles, Atmos. Chem. Phys., 15(1), 393–409, doi:10.5194/acp-15-393-2015, 2015.

Denjean, C., Formenti, P., Desboeufs, K., Chevaillier, S., Triquet, S., Maillé, M., Cazaunau, M., Laurent, B., Mayol-Bracero, O. L., Vallejo, P., Quiñones, M., Gutierrez-Molina, I. E., Cassola, F., Prati, P., Andrews, E. and Ogren, J.: Size distribution and optical properties of African mineral dust after intercontinental transport, J. Geophys. Res. Atmos., 121(12), 7117–7138, doi:10.1002/2016JD024783, 2016.

van der Does, M., Korte, L. F., Munday, C. I., Brummer, G.-J. A. and Stuut, J.-B. W.: Particle size traces modern Saharan dust transport and deposition across the equatorial North Atlantic, Atmos. Chem. Phys., 16(21), 13697–13710, doi:10.5194/acp-16-13697-2016, 2016.

van der Does, M., Knippertz, P., Zschenderlein, P., Giles Harrison, R. and Stuut, J.-B. W.: The mysterious long-range transport of giant mineral dust particles, Sci. Adv., 4(12), eaau2768, doi:10.1126/sciadv.aau2768, 2018.

Doherty, O. M. and Evan, A. T.: Identification of a new dust-stratocumulus indirect effect over the tropical North Atlantic, Geophys. Res. Lett., 41(19), 6935–6942, doi:10.1002/2014GL060897, 2014.

Dubovik, O., Smirnov, A., Holben, B. N., King, M. D., Kaufman, Y. J., Eck, T. F. and Slutsker, I.: Accuracy assessments of aerosol optical properties retrieved from Aerosol Robotic Network (AERONET) Sun and sky radiance measurements, J. Geophys. Res. Atmos., 105(D8), 9791–9806, doi:10.1029/2000JD900040, 2000.

Dubovik, O., Holben, B., Eck, T. F., Smirnov, A., Kaufman, Y. J., King, M. D., Tanré, D., Slutsker, I., Dubovik, O., Holben, B., Eck, T. F., Smirnov, A., Kaufman, Y. J., King, M. D., Tanré, D., Slutsker, I., Sciences, G. E. and Directorate, E. S.: Variability of Absorption and Optical Properties of Key Aerosol Types Observed in Worldwide Locations, J. Atmos. Sci., 59(3), 590–608, doi:10.1175/1520-0469(2002)059<0590:VOAAOP>2.0.CO;2, 2002.

Duce, R. A., Unni, C. K., Ray, B. J., Prospero, J. M. and Merrill, J. T.: Long-range atmospheric transport of soil dust from Asia to the tropical north pacific: temporal variability., Science, 209(4464), 1522–4, doi:10.1126/science.209.4464.1522, 1980.

Dufresne, J.-L., Gautier, C., Ricchiazzi, P. and Fouquart, Y.: Longwave Scattering Effects of Mineral Aerosols, J. Atmos. Sci., 59(12), 1959–1966, doi:10.1175/1520-0469(2002)059<1959:LSEOMA>2.0.CO;2, 2002.

Efron, B. and Gong, G.: A Leisurely Look at the Bootstrap, the Jackknife, and Cross-Validation, Am. Stat., 37(1), 36–48, doi:10.1080/00031305.1983.10483087, 1983.

Evan, A. T.: Surface Winds and Dust Biases in Climate Models, Geophys. Res. Lett., 45(2), 1079–1085, doi:10.1002/2017GL076353, 2018.

Evan, A. T., Flamant, C., Fiedler, S. and Doherty, O.: An analysis of aeolian dust in climate models, Geophys. Res. Lett., 41(16), 5996–6001, doi:10.1002/2014GL060545, 2014.

Flemming, J., Benedetti, A., Inness, A., Engelen, R. J., Jones, L., Huijnen, V., Remy, S., Parrington, M., Suttie, M., Bozzo, A., Peuch, V.-H., Akritidis, D. and Katragkou, E.: The CAMS interim Reanalysis of Carbon Monoxide, Ozone and Aerosol for 2003–2015, Atmos. Chem. Phys., 17(3), 1945–1983, doi:10.5194/acp-17-1945-2017, 2017.

Formenti, P., Schütz, L., Balkanski, Y., Desboeufs, K., Ebert, M., Kandler, K., Petzold, A., Scheuvens, D., Weinbruch, S. and Zhang, D.: Recent progress in understanding physical and chemical properties of African and Asian mineral dust, Atmos. Chem. Phys., 11(16), 8231–8256, doi:10.5194/acp-11-8231-2011, 2011.

Fratini, G., Ciccioli, P., Febo, A., Forgione, A. and Valentini, R.: Size-segregated fluxes of mineral dust from a desert area of northern China by eddy covariance, Atmos. Chem. Phys., 7(11), 2839–2854, doi:10.5194/acp-7-2839-2007, 2007.

Gelaro, R., McCarty, W., Suárez, M. J., Todling, R., Molod, A., Takacs, L., Randles, C. A., Darmenov, A., Bosilovich, M. G., Reichle, R., Wargan, K., Coy, L., Cullather, R., Draper, C., Akella, S., Buchard, V., Conaty, A., da Silva, A. M., Gu, W., Kim, G.-K., Koster, R., Lucchesi, R., Merkova, D., Nielsen, J. E., Partyka, G., Pawson, S., Putman, W., Rienecker, M., Schubert, S. D., Sienkiewicz, M., Zhao, B., Gelaro, R., McCarty, W., Suárez, M. J., Todling, R., Molod, A., Takacs, L., Randles, C. A., Darmenov, A., Bosilovich, M. G., Reichle, R., Wargan, K., Coy, L., Cullather, R., Draper, C., Akella, S., Buchard, V., Conaty, A., Silva, A. M. da, Gu, W., Kim, G.-K., Koster, R., Lucchesi, R., Merkova, D., Nielsen, J. E., Partyka, G., Pawson, S., Putman, W., Rienecker, M., Schubert, S. D., Sienkiewicz, M. and Zhao, B.: The Modern-Era Retrospective Analysis for Research and Applications, Version 2 (MERRA-2), J. Clim., 30(14), 5419–5454, doi:10.1175/JCLI-D-16-0758.1, 2017.

Giannadaki, D., Pozzer, A. and Lelieveld, J.: Modeled global effects of airborne desert dust on air quality and premature mortality, Atmos. Chem. Phys., 14(2), 957–968, doi:10.5194/acp-14-957-2014, 2014.

Ginoux, P.: Effects of nonsphericity on mineral dust modeling, J. Geophys. Res., 108(D2), 4052, doi:10.1029/2002JD002516, 2003.

Ginoux, P., Chin, M., Tegen, I., Prospero, J. M., Holben, B., Dubovik, O. and Lin, S.-J.: Sources and distributions of dust aerosols simulated with the GOCART model, J. Geophys. Res. Atmos., 106(D17), 20255–20273, doi:10.1029/2000JD000053, 2001.

Green, R. O., Mahowald, N. M., Clark, R. N., Ehlmann, B. L., Ginoux, P. A., Kalashnikova, O. V., Miller, R. L., Okin, G., Painter, T. H., Pérez García-Pando, C., Realmuto, V. J., Swayze, G. A., Thompson, D. R., Middleton, E., Guanter, L., Ben Dor, E. and Phillips, B. R.: NASA's Earth Surface Mineral Dust Source Investigation, Am. Geophys. Union, Fall Meet. 2018, Abstr. #A24D-01, 2018.

Han, Q. and Zender, C. S.: Desert dust aerosol age characterized by mass-age tracking of tracers, J. Geophys. Res., 115(D22), D22201, doi:10.1029/2010JD014155, 2010.

Han, Z., Li, J., Xia, X. and Zhang, R.: Investigation of direct radiative effects of aerosols in dust storm season over East Asia with an online coupled regional climate-chemistry-aerosol model, Atmos. Environ., 54, 688–699, doi:10.1016/J.ATMOSENV.2012.01.041, 2012.

Hand, J. L. and Malm, W. C.: Review of aerosol mass scattering efficiencies from ground-based measurements since 1990, J. Geophys. Res., 112(D16), D16203, doi:10.1029/2007JD008484, 2007.

Haywood, J.: Radiative properties and direct radiative effect of Saharan dust measured by the C-130 aircraft during SHADE: 1. Solar spectrum, J. Geophys. Res., 108(D18), 8577, doi:10.1029/2002JD002687, 2003.

Hu, Z., Zhao, C., Huang, J., Leung, L. R., Qian, Y., Yu, H., Huang, L. and Kalashnikova, O. V.: Trans-Pacific transport and evolution of aerosols: evaluation of quasi-global WRF-Chem simulation with multiple observations, Geosci. Model Dev., 9(5), 1725–1746, doi:10.5194/gmd-9-1725-2016, 2016.

Huang et al, Y.: Climate models and remote sensing retrievals underestimate desert dust asphericity, n.d.

Huneeus, N., Schulz, M., Balkanski, Y., Griesfeller, J., Prospero, J., Kinne, S., Bauer, S., Boucher, O., Chin, M., Dentener, F., Diehl, T., Easter, R., Fillmore, D., Ghan, S., Ginoux, P., Grini, a., Horowitz, L., Koch, D., Krol, M. C., Landing, W., Liu, X., Mahowald, N., Miller, R., Morcrette, J. J., Myhre, G., Penner, J., Perlwitz, J., Stier, P., Takemura, T. and Zender, C. S.: Global dust model intercomparison in AeroCom phase i, Atmos. Chem. Phys., 11(15), 7781–7816, doi:10.5194/acp-11-7781-2011, 2011.

Hurrell, J. W., Holland, M. M., Gent, P. R., Ghan, S., Kay, J. E., Kushner, P. J., Lamarque, J.-F., Large, W. G., Lawrence, D., Lindsay, K., Lipscomb, W. H., Long, M. C., Mahowald, N., Marsh, D. R., Neale, R. B., Rasch, P., Vavrus, S., Vertenstein, M., Bader, D., Collins, W. D., Hack, J. J., Kiehl, J., Marshall, S., Hurrell, J. W., Holland, M. M., Gent, P. R., Ghan, S., Kay, J. E., Kushner, P. J., Lamarque, J.-F., Large, W. G., Lawrence, D., Lindsay, K., Lipscomb, W. H., Long, M. C., Mahowald, N., Marsh, D. R., Neale, R. B., Rasch, P., Vavrus, S., Vertenstein, M., Bader, D., Collins, W. D., Hack, J. J., Kiehl, J. and Marshall, S.: The Community Earth System Model: A Framework for Collaborative Research, Bull. Am. Meteorol. Soc., 94(9), 1339–1360, doi:10.1175/BAMS-D-12-00121.1, 2013.

Ito, A. and Kok, J. F.: Do dust emissions from sparsely vegetated regions dominate atmospheric iron supply to the Southern Ocean?, J. Geophys. Res. Atmos., 122(7), 3987–4002, doi:10.1002/2016JD025939, 2017.

Ito, A., Myriokefalitakis, S., Kanakidou, M., Mahowald, N. M., Scanza, R. A., Hamilton, D. S., Baker, A. R., Jickells, T., Sarin, M., Bikkina, S., Gao, Y., Shelley, R. U., Buck, C. S., Landing, W. M., Bowie, A. R., Perron, M. M. G., Guieu, C., Meskhidze, N., Johnson, M. S., Feng, Y., Kok, J. F., Nenes, A. and Duce, R. A.: Pyrogenic iron: The missing link to high iron solubility in aerosols, Sci. Adv., 5(5), eaau7671, doi:10.1126/sciadv.aau7671, 2019.

Johnson, M. S., Meskhidze, N., Praju Kiliyanpilakkil, V. and Kiliyanpilakkil, V. P.: A global comparison of GEOS-Chem-predicted and remotely-sensed mineral dust aerosol optical depth and extinction profiles, J. Adv. Model. Earth Syst., 4(7), 1–15, doi:10.1029/2011MS000109, 2012.

Jung, E., Albrecht, B., Prospero, J. M., Jonsson, H. H. and Kreidenweis, S. M.: Vertical structure of aerosols, temperature, and moisture associated with an intense African dust event observed over the eastern Caribbean, J. Geophys. Res. Atmos., 118(10), 4623–4643, doi:10.1002/jgrd.50352, 2013.

Kaaden, N., Massling, A., Schladitz, A., MüLLER, T., Kandler, K., SchüTZ, L., Weinzierl, B., Petzold, A., Tesche, M., Leinert, S., Deutscher, C., Ebert, M., Weinbruch, S. and Wiedensohler, A.: State of mixing, shape factor, number size distribution, and hygroscopic growth of the Saharan anthropogenic and mineral dust aerosol at Tinfou, Morocco, Tellus B Chem. Phys. Meteorol., 61(1), 51–63, doi:10.1111/j.1600-0889.2008.00388.x, 2009.

Kalashnikova, O. V. and Sokolik, I. N.: Importance of shapes and compositions of wind-blown dust particles for remote sensing at solar wavelengths, Geophys. Res. Lett., 29(10), 38-1-38–4, doi:10.1029/2002GL014947, 2002.

Kalashnikova, O. V. and Sokolik, I. N.: Modeling the radiative properties of nonspherical soil-derived mineral aerosols, J. Quant. Spectrosc. Radiat. Transf., 87(2), 137–166, doi:10.1016/J.JQSRT.2003.12.026, 2004.

Kandler, K., Benker, N., Bundke, U., Cuevas, E., Ebert, M., Knippertz, P., Rodríguez, S., Schütz, L. and Weinbruch, S.: Chemical composition and complex refractive index of Saharan Mineral Dust at Izaña, Tenerife (Spain) derived by electron microscopy, Atmos. Environ., 41(37), 8058–8074, doi:10.1016/J.ATMOSENV.2007.06.047, 2007.

Kandler, K., SchüTZ, L., Deutscher, C., Ebert, M., Hofmann, H., JäCKEL, S., Jaenicke, R., Knippertz, P., Lieke, K., Massling, A., Petzold, A., Schladitz, A., Weinzierl, B., Wiedensohler, A., Zorn, S. and Weinbruch1, S.: Size distribution, mass concentration, chemical and mineralogical composition and derived optical parameters of the boundary layer aerosol at Tinfou, Morocco, during SAMUM 2006, Tellus B Chem. Phys. Meteorol., 61(1), 32–50,

doi:10.1111/j.1600-0889.2008.00385.x, 2009.

Kandler, K., Lieke, K., Benker, N., Emmel, C., Küpper, M., Müller-Ebert, D., Ebert, M., Scheuvens, D., Schladitz, A., Schütz, L. and Weinbruch, S.: Electron microscopy of particles collected at Praia, Cape Verde, during the Saharan Mineral Dust Experiment: particle chemistry, shape, mixing state and complex refractive index, Tellus B Chem. Phys. Meteorol., 63(4), 475–496, doi:10.1111/j.1600-0889.2011.00550.x, 2011.

Kaufman, Y. J., Koren, I., Remer, L. A., Tanré, D., Ginoux, P. and Fan, S.: Dust transport and deposition observed from the Terra-Moderate Resolution Imaging Spectroradiometer (MODIS) spacecraft over the Atlantic Ocean, J. Geophys. Res., 110(D10), D10S12, doi:10.1029/2003JD004436, 2005.

Kim, D., Chin, M., Yu, H., Eck, T. F., Sinyuk, A., Smirnov, A. and Holben, B. N.: Dust optical properties over North Africa and Arabian Peninsula derived from the AERONET dataset, Atmos. Chem. Phys., 11(20), 10733–10741, doi:10.5194/acp-11-10733-2011, 2011.

Kinne, S., Schulz, M., Textor, C., Guibert, S., Balkanski, Y., Bauer, S. E., Berntsen, T., Berglen, T. F., Boucher, O., Chin, M., Collins, W., Dentener, F., Diehl, T., Easter, R., Feichter, J., Fillmore, D., Ghan, S., Ginoux, P., Gong, S., Grini, A., Hendricks, J., Herzog, M., Horowitz, L., Isaksen, I., Iversen, T., Kirkevag, A., Kloster, S., Koch, D., Kristjansson, J. E., Krol, M., Lauer, A., Lamarque, J. F., Lesins, G., Liu, X., Lohmann, U., Montanaro, V., Myhre, G., Penner, J. E., Pitari, G., Reddy, S., Seland, O., Stier, P., Takemura, T. and Tie, X.: An AeroCom initial assessment – optical properties in aerosol component modules of global models, Atmos. Chem. Phys., 6, 1815–1834, doi:10.5194/acpd-5-8285-2005, 2006.

Kok, J. F.: A scaling theory for the size distribution of emitted dust aerosols suggests climate models underestimate the size of the global dust cycle, Proc. Natl. Acad. Sci., 108(3), 1016–1021, doi:10.1073/pnas.1014798108, 2011a.

Kok, J. F.: Does the size distribution of mineral dust aerosols depend on the wind speed at emission?, Atmos. Chem. Phys., 11(19), 10149–10156, doi:10.5194/acp-11-10149-2011, 2011b.

Kok, J. F., Ridley, D. A., Zhou, Q., Miller, R. L., Zhao, C., Heald, C. L., Ward, D. S., Albani, S. and Haustein, K.: Smaller desert dust cooling effect estimated from analysis of dust size and abundance, Nat. Geosci., 10(4), 274–278, doi:10.1038/ngeo2912, 2017.

Kooperman, G. J., Pritchard, M. S., Ghan, S. J., Wang, M., Somerville, R. C. J. and Russell, L. M.: Constraining the influence of natural variability to improve estimates of global aerosol indirect effects in a nudged version of the Community Atmosphere Model 5, J. Geophys. Res. Atmos., 117(D23), n/a-n/a, doi:10.1029/2012JD018588, 2012.

Kulshrestha, U. C., Sarkar, A. K., Srivastava, S. S. and Parashar, D. C.: Investigation into atmospheric deposition through precipitation studies at New Delhi (India), Atmos. Environ., 30(24), 4149–4154, doi:10.1016/1352-2310(96)00034-9, 1996.

Lee, Y. H., Chen, K. and Adams, P. J.: Development of a global model of mineral dust aerosol microphysics, Atmos. Chem. Phys., 9(7), 2441–2458, doi:10.5194/acp-9-2441-2009, 2009.

Li, F., Ginoux, P. and Ramaswamy, V.: Distribution, transport, and deposition of mineral dust in the Southern Ocean and Antarctica: Contribution of major sources, J. Geophys. Res., 113(D10), D10207, doi:10.1029/2007JD009190, 2008.

Li, S.-M., Tang, J., Xue, H. and Toom-Sauntry, D.: Size distribution and estimated optical properties of carbonate, water soluble organic carbon, and sulfate in aerosols at a remote high altitude site in western China, Geophys. Res. Lett., 27(8), 1107–1110, doi:10.1029/1999GL010929, 2000.

Li, X., Maring, H., Savoie, D., Voss, K. and Prospero, J. M.: Dominance of mineral dust in aerosol light-scattering in the North Atlantic trade winds, Nature, 380(6573), 416–419, doi:10.1038/380416a0, 1996.

Lohmann, U. and Diehl, K.: Sensitivity Studies of the Importance of Dust Ice Nuclei for the Indirect Aerosol Effect on Stratiform Mixed-Phase Clouds, J. Atmos. Sci., 63(3), 968–982, doi:10.1175/JAS3662.1, 2006.

Lynch, P., Reid, J. S., Westphal, D. L., Zhang, J., Hogan, T. F., Hyer, E. J., Curtis, C. A., Hegg, D. A., Shi, Y., Campbell, J. R., Rubin, J. I., Sessions, W. R., Turk, F. J. and Walker, A. L.: An 11-year global gridded aerosol optical thickness reanalysis (v1.0) for atmospheric and climate sciences, Geosci. Model Dev., 9(4), 1489–1522, doi:10.5194/gmd-9-1489-2016, 2016.

Mahowald, N., Jickells, T. D., Baker, A. R., Artaxo, P., Benitez-Nelson, C. R., Bergametti, G., Bond, T. C., Chen, Y., Cohen, D. D., Herut, B., Kubilay, N., Losno, R., Luo, C., Maenhaut, W., McGee, K. A., Okin, G. S., Siefert, R. L. and Tsukuda, S.: Global distribution of atmospheric phosphorus sources, concentrations and deposition rates, and anthropogenic impacts, Global Biogeochem. Cycles, 22(4), n/a-n/a, doi:10.1029/2008GB003240, 2008.

Mahowald, N., Albani, S., Kok, J. F., Engelstaeder, S., Scanza, R., Ward, D. S. and Flanner, M. G.: The size distribution of desert dust aerosols and its impact on the Earth system, Aeolian Res., 15, 53–71, 2014.

Mahowald, N. M., Engelstaedter, S., Luo, C., Sealy, A., Artaxo, P., Benitez-Nelson, C., Bonnet, S., Chen, Y., Chuang, P. Y., Cohen, D. D., Dulac, F., Herut, B., Johansen, A. M., Kubilay, N., Losno, R., Maenhaut, W., Paytan, A., Prospero, J. M., Shank, L. M. and Siefert, R. L.: Atmospheric Iron Deposition: Global Distribution, Variability, and Human Perturbations, Ann. Rev. Mar. Sci., 1(1), 245–278, doi:10.1146/annurev.marine.010908.163727, 2009.

Maring, H., Savoie, D. L., Izaguirre, M. A., McCormick, C., Arimoto, R., Prospero, J. M. and Pilinis, C.: Aerosol physical and optical properties and their relationship to aerosol composition in the free troposphere at Izaña, Tenerife, Canary Islands, during July 1995, J. Geophys. Res. Atmos., 105(D11), 14677–14700, doi:10.1029/2000JD900106, 2000.

Maring, H., Savoie, D. L., Izaguirre, M. A., Custals, L. and Reid, J. S.: Mineral dust aerosol size distribution change during atmospheric transport, J. Geophys. Res., 108(D19), 8592, doi:10.1029/2002JD002536, 2003.

Mccarty, W., Coy, L., Gelaro, R., Huang, A., Merkova, D., Smith, E. B., Sienkiewicz, M., Wargan, K. and Koster, R. D.: MERRA-2 Input Observations: Summary and Assessment. Technical Report Series on Global Modeling and Data Assimilation., 2016.

McConnell, C. L., Highwood, E. J., Coe, H., Formenti, P., Anderson, B., Osborne, S., Nava, S., Desboeufs, K., Chen, G. and Harrison, M. A. J.: Seasonal variations of the physical and optical characteristics of Saharan dust: Results from the Dust Outflow and Deposition to the Ocean (DODO) experiment, J. Geophys. Res., 113(D14), D14S05, doi:10.1029/2007JD009606, 2008.

Meng, Z., Yang, P., Kattawar, G. W., Bi, L., Liou, K. N. and Laszlo, I.: Single-scattering properties of tri-axial ellipsoidal mineral dust aerosols: A database for application to radiative transfer calculations, J. Aerosol Sci., 41(5), 501–512, doi:10.1016/J.JAEROSCI.2010.02.008, 2010.

Michou, M., Nabat, P. and Saint-Martin, D.: Development and basic evaluation of a prognostic aerosol scheme (v1) in the CNRM Climate Model CNRM-CM6, Geosci. Model Dev., 8(3), 501–531, doi:10.5194/gmd-8-501-2015, 2015.

Miller, R. L., Cakmur, R. V., Perlwitz, J., Geogdzhayev, I. V., Ginoux, P., Koch, D., Kohfeld, K. E., Prigent, C., Ruedy, R., Schmidt, G. A. and Tegen, I.: Mineral dust aerosols in the NASA Goddard Institute for Space Sciences ModelE atmospheric general circulation model, J. Geophys. Res., 111(D6), D06208, doi:10.1029/2005JD005796,

2006.

Okada, K., Heintzenberg, J., Kai, K. and Qin, Y.: Shape of atmospheric mineral particles collected in three Chinese arid-regions, Geophys. Res. Lett., 28(16), 3123–3126, doi:10.1029/2000GL012798, 2001.

Osborne, S. R., Johnson, B. T., Haywood, J. M., Baran, A. J., Harrison, M. A. J. and McConnell, C. L.: Physical and optical properties of mineral dust aerosol during the Dust and Biomass-burning Experiment, J. Geophys. Res., 113(D23), D00C03, doi:10.1029/2007JD009551, 2008.

Otto, S., de Reus, M., Trautmann, T., Thomas, A., Wendisch, M. and Borrmann, S.: Atmospheric radiative effects of an in situ measured Saharan dust plume and the role of large particles, Atmos. Chem. Phys., 7(18), 4887–4903, doi:10.5194/acp-7-4887-2007, 2007.

Otto, S., Trautmann, T. and Wendisch, M.: On realistic size equivalence and shape of spheroidal Saharan mineral dust particles applied in solar and thermal radiative transfer calculations, Atmos. Chem. Phys., 11(9), 4469–4490, doi:10.5194/acp-11-4469-2011, 2011.

Patterson, E. M., Gillette, D. A. and Stockton, B. H.: Complex index of refraction between 300 and 700 nm for Saharan aerosols, J. Geophys. Res., 82(21), 3153–3160, doi:10.1029/JC082i021p03153, 1977.

Pérez, C., Haustein, K., Janjic, Z., Jorba, O., Huneeus, N., Baldasano, J. M., Black, T., Basart, S., Nickovic, S., Miller, R. L., Perlwitz, J. P., Schulz, M. and Thomson, M.: Atmospheric dust modeling from meso to global scales with the online NMMB/BSC-Dust model – Part 1: Model description, annual simulations and evaluation, Atmos. Chem. Phys., 11(24), 13001–13027, doi:10.5194/acp-11-13001-2011, 2011.

Perlwitz, J. and Miller, R. L.: Cloud cover increase with increasing aerosol absorptivity: A counterexample to the conventional semidirect aerosol effect, J. Geophys. Res. Atmos., 115(8), 1–23, doi:10.1029/2009JD012637, 2010.

Potenza, M. A. C., Albani, S., Delmonte, B., Villa, S., Sanvito, T., Paroli, B., Pullia, A., Baccolo, G., Mahowald, N. and Maggi, V.: Shape and size constraints on dust optical properties from the Dome C ice core, Antarctica, Sci. Rep., 6(1), 28162, doi:10.1038/srep28162, 2016.

Prospero, J. M., Glaccum, R. A. and Nees, R. T.: Atmospheric transport of soil dust from Africa to South America, Nature, 289(5798), 570–572, doi:10.1038/289570a0, 1981.

Quinn, P. K., D. J. Coffman, T. S. Bates, T. L. Miller, J. E. Johnson, E. J. Welton, C. Neusüss, M. Miller and Sheridan, P. J.: Aerosol optical properties during INDOEX 1999: Means, variability, and controlling factors, J. Geophys. Res., 107(D19), 8020, doi:10.1029/2000JD000037, 2002.

Quinn, P. K., Coffman, D. J., Bates, T. S., Welton, E. J., Covert, D. S., Miller, T. L., Johnson, J. E., Maria, S., Russell, L., Arimoto, R., Carrico, C. M., Rood, M. J. and Anderson, J.: Aerosol optical properties measured on board the *Ronald H. Brown* during ACE-Asia as a function of aerosol chemical composition and source region, J. Geophys. Res., 109(D19), D19S01, doi:10.1029/2003JD004010, 2004.

Reid, E. A., Reid, J. S., Meier, M. M., Dunlap, M. R., Cliff, S. S., Broumas, A., Perry, K. and Maring, H.: Characterization of African dust transported to Puerto Rico by individual particle and size segregated bulk analysis, J. Geophys. Res., 108(D19), 8591, doi:10.1029/2002JD002935, 2003a.

Reid, J. S., Jonsson, H. H., Maring, H. B., Smirnov, A., Savoie, D. L., Cliff, S. S., Reid, E. A., Livingston, J. M., Meier, M. M., Dubovik, O. and Tsay, S.: Comparison of size and morphological measurements of coarse mode dust particles from Africa, J. Geophys. Res., 108(D19), 8593, doi:10.1029/2002JD002485, 2003b.

Reid, J. S., Reid, E. A., Walker, A., Piketh, S., Cliff, S., Al Mandoos, A., Tsay, S.-C. and Eck, T. F.: Dynamics of

southwest Asian dust particle size characteristics with implications for global dust research, J. Geophys. Res., 113(D14), D14212, doi:10.1029/2007JD009752, 2008.

Ridley, D. A., Heald, C. L. and Ford, B.: North African dust export and deposition: A satellite and model perspective, J. Geophys. Res. Atmos., 117(D2), n/a-n/a, doi:10.1029/2011JD016794, 2012.

Ridley, D. A., Heald, C. L., Kok, J. F. and Zhao, C.: An observationally-constrained estimate of global dust aerosol optical depth, Atmos. Chem. Phys. Discuss., 16(23), 1–31, doi:10.5194/acp-2016-385, 2016.

Rosenberg, P. D., Parker, D. J., Ryder, C. L., Marsham, J. H., Garcia-Carreras, L., Dorsey, J. R., Brooks, I. M., Dean, A. R., Crosier, J., McQuaid, J. B. and Washington, R.: Quantifying particle size and turbulent scale dependence of dust flux in the Sahara using aircraft measurements, J. Geophys. Res. Atmos., 119(12), 7577–7598, doi:10.1002/2013JD021255, 2014.

Ryder, C. L., Highwood, E. J., Lai, T. M., Sodemann, H. and Marsham, J. H.: Impact of atmospheric transport on the evolution of microphysical and optical properties of Saharan dust, Geophys. Res. Lett., 40(10), 2433–2438, doi:10.1002/grl.50482, 2013a.

Ryder, C. L., Highwood, E. J., Rosenberg, P. D., Trembath, J., Brooke, J. K., Bart, M., Dean, A., Crosier, J., Dorsey, J., Brindley, H., Banks, J., Marsham, J. H., McQuaid, J. B., Sodemann, H. and Washington, R.: Optical properties of Saharan dust aerosol and contribution from the coarse mode as measured during the Fennec 2011 aircraft campaign, Atmos. Chem. Phys., 13(1), 303–325, doi:10.5194/acp-13-303-2013, 2013b.

Ryder, C. L., Marenco, F., Brooke, J. K., Estelles, V., Cotton, R., Formenti, P., McQuaid, J. B., Price, H. C., Liu, D., Ausset, P., Rosenberg, P., Taylor, J. W., Choularton, T., Bower, K., Coe, H., Gallagher, M., Crosier, J., Lloyd, G., Highwood, E. J. and Murray, B. J.: Coarse mode mineral dust size distributions, composition and optical properties from AER-D aircraft measurements over the Tropical Eastern Atlantic, Atmos. Chem. Phys. Discuss., 1–49, doi:10.5194/acp-2018-739, 2018.

Ryder, C. L., Highwood, E. J., Walser, A., Seibert, P., Philipp, A. and Weinzierl, B.: Coarse and Giant Particles are Ubiquitous in Saharan Dust Export Regions and are Radiatively Significant over the Sahara, Atmos. Chem. Phys. Discuss., 1–36, doi:10.5194/acp-2019-421, 2019.

Sassen, K.: Saharan dust storms and indirect aerosol effects on clouds: CRYSTAL-FACE results, Geophys. Res. Lett., 30(12), 1–4, doi:10.1029/2003GL017371, 2003.

Scheuvens, D. and Kandler, K.: On Composition, Morphology, and Size Distribution of Airborne Mineral Dust, in Mineral Dust, pp. 15–49, Springer Netherlands, Dordrecht., 2014.

Scheuvens, D., Kandler, K., Küpper, M., Lieke, K., Zorn, R. S., Ebert, M., Schütz, L. and Weinbruch, S.: Individual-particle analysis of airborne dust samples collected over Morocco in 2006 during SAMUM 1, Tellus B Chem. Phys. Meteorol., 63(4), 512–530, doi:10.1111/j.1600-0889.2011.00554.x, 2011.

Schladitz, A., Müller, T., Nowak, A., Kandler, K., Lieke, K., Massling, A. and Wiedensohler, A.: In situ aerosol characterization at Cape Verde, Tellus B Chem. Phys. Meteorol., 63(4), 531–548, doi:10.1111/j.1600-0889.2011.00569.x, 2011.

Seinfeld, J. H. and Pandis, S. N.: Atmospheric chemistry and physics : from air pollution to climate change., 2016.

Shao, Y.: A model for mineral dust emission, J. Geophys. Res. Atmos., 106(D17), 20239–20254, doi:10.1029/2001JD900171, 2001.

Sokolik, I., Andronova, A. and Johnson, T. C.: Complex refractive index of atmospheric dust aerosols, Atmos.

Environ. Part A. Gen. Top., 27(16), 2495–2502, doi:10.1016/0960-1686(93)90021-P, 1993.

Song, Q., Zhang, Z., Yu, H., Kato, S., Yang, P., Colarco, P., Remer, L. A. and Ryder, C. L.: Net radiative effects of dust in the tropical North Atlantic based on integrated satellite observations and in situ measurements, Atmos. Chem. Phys., 18(15), 11303–11322, doi:10.5194/acp-18-11303-2018, 2018.

Sow, M., Alfaro, S. C., Rajot, J. L. and Marticorena, B.: Size resolved dust emission fluxes measured in Niger during 3 dust storms of the AMMA experiment, Atmos. Chem. Phys., 9(12), 3881–3891, doi:10.5194/acp-9-3881-2009, 2009.

Tegen, I.: Modeling the mineral dust aerosol cycle in the climate system, Quat. Sci. Rev., 22(18–19), 1821–1834, doi:10.1016/S0277-3791(03)00163-X, 2003.

Tegen, I. and Fung, I.: Modeling of mineral dust in the atmosphere: Sources, transport, and optical thickness, J. Geophys. Res., 99(D11), 22897, doi:10.1029/94JD01928, 1994.

Tegen, I. and Lacis, A.: Modeling of particle size distribution and its influence on the radiative properties of mineral dust aerosol, J. Geophys. Res., 101(D14), 19237–19244, doi:10.1029/95jd03610, 1996.

Tegen, I., Lacis, A. a. and Fung, I.: The influence on climate forcing of mineral aerosols from disturbed soils, Nature, 380(6573), 419–422, doi:10.1038/380419a0, 1996.

Veghte, D. P. and Freedman, M. A.: Facile Method for Determining the Aspect Ratios of Mineral Dust Aerosol by Electron Microscopy, Aerosol Sci. Technol., 48(7), 715–724, doi:10.1080/02786826.2014.920484, 2014.

Wagner, F., Bortoli, D., Pereira, S., Costa, M. Jo., Maria Silva, A., Weinzierl, B., Esselborn, M., Petzold, A., Rasp, K., Heinold, B. and Tegen, I.: Properties of dust aerosol particles transported to Portugal from the Sahara desert, Tellus B Chem. Phys. Meteorol., 61(1), 297–306, doi:10.1111/j.1600-0889.2008.00393.x, 2009.

Weaver, C. J., Ginoux, P., Hsu, N. C., Chou, M.-D., Joiner, J., Weaver, C. J., Ginoux, P., Hsu, N. C., Chou, M.-D. and Joiner, J.: Radiative Forcing of Saharan Dust: GOCART Model Simulations Compared with ERBE Data, J. Atmos. Sci., 59(3), 736–747, doi:10.1175/1520-0469(2002)059<0736:RFOSDG>2.0.CO;2, 2002.

von der Weiden, S.-L., Drewnick, F. and Borrmann, S.: Particle Loss Calculator – a new software tool for the assessment of the performance of aerosol inlet systems, Atmos. Meas. Tech., 2(2), 479–494, doi:10.5194/amt-2-479-2009, 2009.

Weinzierl, B., Petzold, A., Esselborn, M., Wirth, M., Rasp, K., Kandler, K., SchüTZ, L., Koepke, P. and Fiebig, M.: Airborne measurements of dust layer properties, particle size distribution and mixing state of Saharan dust during SAMUM 2006, Tellus B Chem. Phys. Meteorol., 61(1), 96–117, doi:10.1111/j.1600-0889.2008.00392.x, 2009.

Weinzierl, B., Sauer, D., Esselborn, M., Petzold, A., Veira, A., Rose, M., Mund, S., Wirth, M., Ansmann, A., Tesche, M., Gross, S. and Freudenthaler, V.: Microphysical and optical properties of dust and tropical biomass burning aerosol layers in the Cape Verde region—an overview of the airborne in situ and lidar measurements during SAMUM-2, Tellus B Chem. Phys. Meteorol., 63(4), 589–618, doi:10.1111/j.1600-0889.2011.00566.x, 2011.

Weinzierl, B., Ansmann, A., Prospero, J. M., Althausen, D., Benker, N., Chouza, F., Dollner, M., Farrell, D., Fomba, W. K., Freudenthaler, V., Gasteiger, J., Groß, S., Haarig, M., Heinold, B., Kandler, K., Kristensen, T. B., Mayol-Bracero, O. L., Müller, T., Reitebuch, O., Sauer, D., Schäfler, A., Schepanski, K., Spanu, A., Tegen, I., Toledano, C., Walser, A., Weinzierl, B., Ansmann, A., Prospero, J. M., Althausen, D., Benker, N., Chouza, F., Dollner, M., Farrell, D., Fomba, W. K., Freudenthaler, V., Gasteiger, J., Groß, S., Haarig, M., Heinold, B., Kandler, K., Kristensen, T. B., Mayol-Bracero, O. L., Müller, T., Reitebuch, O., Sauer, D., Schäfler, A., Schepanski, K., Spanu, A., Tegen, I.,

Toledano, C. and Walser, A.: The Saharan Aerosol Long-Range Transport and Aerosol–Cloud-Interaction Experiment: Overview and Selected Highlights, Bull. Am. Meteorol. Soc., 98(7), 1427–1451, doi:10.1175/BAMS-D-15-00142.1, 2017.

Whicker, C., Adebiyi, A. and Kok, J. F.: Improved Model Estimates of Desert Dust Aerosol Surface Concentration, Am. Geophys. Union, Fall Meet. 2018, Abstr. #A21I-2799, 2018.

Yumimoto, K., Tanaka, T. Y., Oshima, N. and Maki, T.: JRAero: the Japanese Reanalysis for Aerosol v1.0, Geosci. Model Dev., 10(9), 3225–3253, doi:10.5194/gmd-10-3225-2017, 2017.

Zender, C. S., Bian, H. and Newman, D.: Mineral Dust Entrainment and Deposition (DEAD) model: Description and 1990s dust climatology, J. Geophys. Res., 108(D14), 4416, doi:10.1029/2002JD002775, 2003.

Zhao, C., Liu, X., Leung, L. R., Johnson, B., McFarlane, S. A., Gustafson, W. I., Fast, J. D. and Easter, R.: The spatial distribution of mineral dust and its shortwave radiative forcing over North Africa: modeling sensitivities to dust emissions and aerosol size treatments, Atmos. Chem. Phys., 10(18), 8821–8838, doi:10.5194/acp-10-8821-2010, 2010.

Zhao, C., Chen, S., Leung, L. R., Qian, Y., Kok, J. F., Zaveri, R. A. and Huang, J.: Uncertainty in modeling dust mass balance and radiative forcing from size parameterization, , 13(21), 10733–10753, doi:10.5194/acp-13-10733-2013, 2013.

Model	Particle size bins (diameter – μm)	Time Period	Spatial resolution	Meteorology used for simulation	Relevant reference
GISS	0.2-0.36, 0.36-0.6, 0.6-1.2, 1.2-2.0, 2.0-4.0, 4.0-8.0, 8.0-16.0, 16.0-32.0	2004-2008	5° by 4° with 20 levels up to 0.1 hPa	Internal model meteorology	Miller et al. (2006)
WRF-Chem	0.039-0.312, 0.312-0.625, 0.625-1.25, 1.25-2.5, 2.5-5.0, 5.0-10.0	2007-2016	1° by 1° with 35 levels up to 50 hPa.	NCEP/FNL reanalysis	Zhao et al. (2013)
CESM	0.1-1.0, 1.0-2.5, 2.5-5.0, 5.0-10.0	2004-2008	2.5° by 1.89° with 56 levels up to 1.8 hPa.	ERA-Interim reanalysis	Hurrell et al. (2013)
GEOS-Chem	0.2-0.36, 0.36-0.6, 0.6-1.2, 1.2-2.0, 2.0-3.6, 3.6-6.0, 6.0-12.0	2004-2008	2.5° by 2° with 47 levels up to 0.1 hPa.	MERRA reanalysis	See Kok et al., (2017)
ARPEGE-Climat	0.1-0.2, 0.2-0.5, 0.5-1.0, 1.0-2.5, 2.5-10.0, 10.0-100.0	2004-2008	1.4° by 1.4° with 91 levels up to 10 hPa.	Internal model meteorology	Michou et al., 2015
IMPACT	0.1-1.26, 1.26-2.5, 2.5-5.0, 5.0-20.0	2004	2.0°×2.5° with 59 levels up to 0.02 hPa.	Meteorology from GEOS-5 model	Ito & Kok, 2017

Table 1: Details of model simulations used in this study. Shown are the particle bin ranges, time periods of simulations, the spatial resolutions, the meteorology used, and the relevant model reference. We interpolate all model simulations to 2.5° by 1.9° to facilitate comparison and consistency with other datasets. See section 2 for details.

1

Measurement Reference	Project Name	Time Period	Representative Location	Comments
D'Almeida (1987)	N/A (Ground station)	Feb-Mar 1979; Jan-Feb1982	Niamey (Niger): 14.21N,2.5E	PSD only; Z = 0-100m Data taken from their Fig. 3.
Li et al., 1996	N/A (Ground Station)	April-May 1994	Barbados: 13.19N, 59.54W	MEE only; λ = 530 nm See their equation 3.
Li et al., 2000	N/A (Ground Station)	Oct-Nov, 1997 and Jan,1998	Qinghai Province (China): 33.16N, 96.25E	MSE only; λ = 550 nm Data taken from their table 2.
Maring et al., 2000	N/A (Ground Station)	July 1995	Tenerife (Canary Island): 28.29N, 16.63W	MSE only; λ = 532 nm Data taken from their table 4.
Andreae et al., 2002	ARACHNE	Dec, 1995 -Oct, 1997	Sde Boker (Israel): 30N,34.79E	MSE only; λ = 550 nm Data taken from their table 4.
Quinn et al., 2002	INDOEX	Feb- Mar, 1999	Arabia Sea: 15N, 69E Arabia Sea – Indian Ocean: 8N, 72E Indian Ocean: 8S, 74E	MEE only; λ = 550 nm Data taken from their table 10.
Haywood et al., 2003	SHADE	September 2000	Cape Verde: 18N, 21W	MEE only; λ = 550 nm Data taken from their table 2.
Clarke et al. 2004	ACE-Asia/TRACE-P	Feb.-Apr., 2001	Sea of Japan: 38.85N, 130E	PSD and MSE; λ = 550 nm, Z = 0-6000m PSD data taken from their Fig. 5. MSE data taken from the paper.
Otto et al., 2007	ACE-2	Jun-Jul, 1997	Canary Islands: 27.65N, 14.25W	PSD only; Z=2700m, 4000m, 5500m, 7000m Data taken from their Fig. 3
Osborne et al., 2008	DABEX	Jan-Feb, 2006	Niamey (Niger): 15.5N, 5.0E	MEE only; λ = 550 nm Data taken from their table 4.
Chou et al., 2008	AMMA/DABEX	Jan-Feb, 2006	Niamey (Niger): 15.5N, 5.0E	PSD only; Z = 0 – 1,500m Data take from their Fig. 6

McConnell et al., 2008	DODO-1	Feb., 2006	Dakar (Senegal): 14.76N, 17.38W	MEE only; λ = 550 nm Data taken from table 4 of Osborne et al., 2008
McConnell et al., 2008	DODO-2	August 2006	Dakar (Senegal): 19.89N, 12.5W	PSD only; Z = 0 - 1000m Data taken from their Fig. 7
Weinzierl et al., 2009	SAMUM-1	May-Jun, 2006	Morocco: 31.26N 7.5W	PSD only; Z = 3700-4900m Data taken from their Fig. 8
Wagner et al., 2009	DARPO	May 2006	Évora (Portugal): 38.57N 7.91 W	PSD only; Z = 2300-5000m Data taken from their Fig. 9
Kandler et al., 2009	SAMUM-1	May 2006	Morocco: 31.26N 7.5W	PSD only; Z = 0-700 m Data taken from their Fig. 8
Kandler et al., 2011	SAMUM-2	Jan-Feb, 2008	Praia (Cape Verde): 14.21N, 22.5W	PSD only; Z = 0-110m Data taken from their Fig. 6
Jung et al., 2013	BACEX	Mar–Apr, 2010	Barbados: 12.32N, 60W	PSD only; Z = 1250-2700m Data taken from their Fig. 14
Ryder et al., 2013a	Fennec 2011	June 2011	Canary Islands: 27.65N, 14.25W	PSD and MEE; λ = 550 nm; Z = 0 – 6000m; PSD data obtained from the author MEE data taken from their section 3.4
Ryder et al., 2013b	Fennec 2011	June, 2011	Mauritania-Mali.: 24N, 6W	PSD only; λ = 550 nm; Z = 0 – 3000m; Data taken from their Fig. 5b
Weinzierl et al., 2017	SALTRACE	June, 2013	Cape Verde: 14.21N, 22.5W Barbados: 13.19N, 59.54W	PSD only; Z=0-2600m Data taken from their Fig. 9
Ryder et al., 2018	AER-D	August, 2015	Cape Verde: 18N, 21W	PSD and MEE; λ = 550 nm; Z = 0-6000m PSD data obtained from the author MEE data taken from their table 6.

Table 2: Overview of in-situ measurements used to evaluate DustCOMM and model ensemble estimates of the dust size distribution and dust mass extinction efficiency (see section 2.4 for details). The label PSD in the last column indicates that we take dust size distribution values from the study. MSE and MEE similarly indicates that we take dust mass scattering or extinction efficiency values.

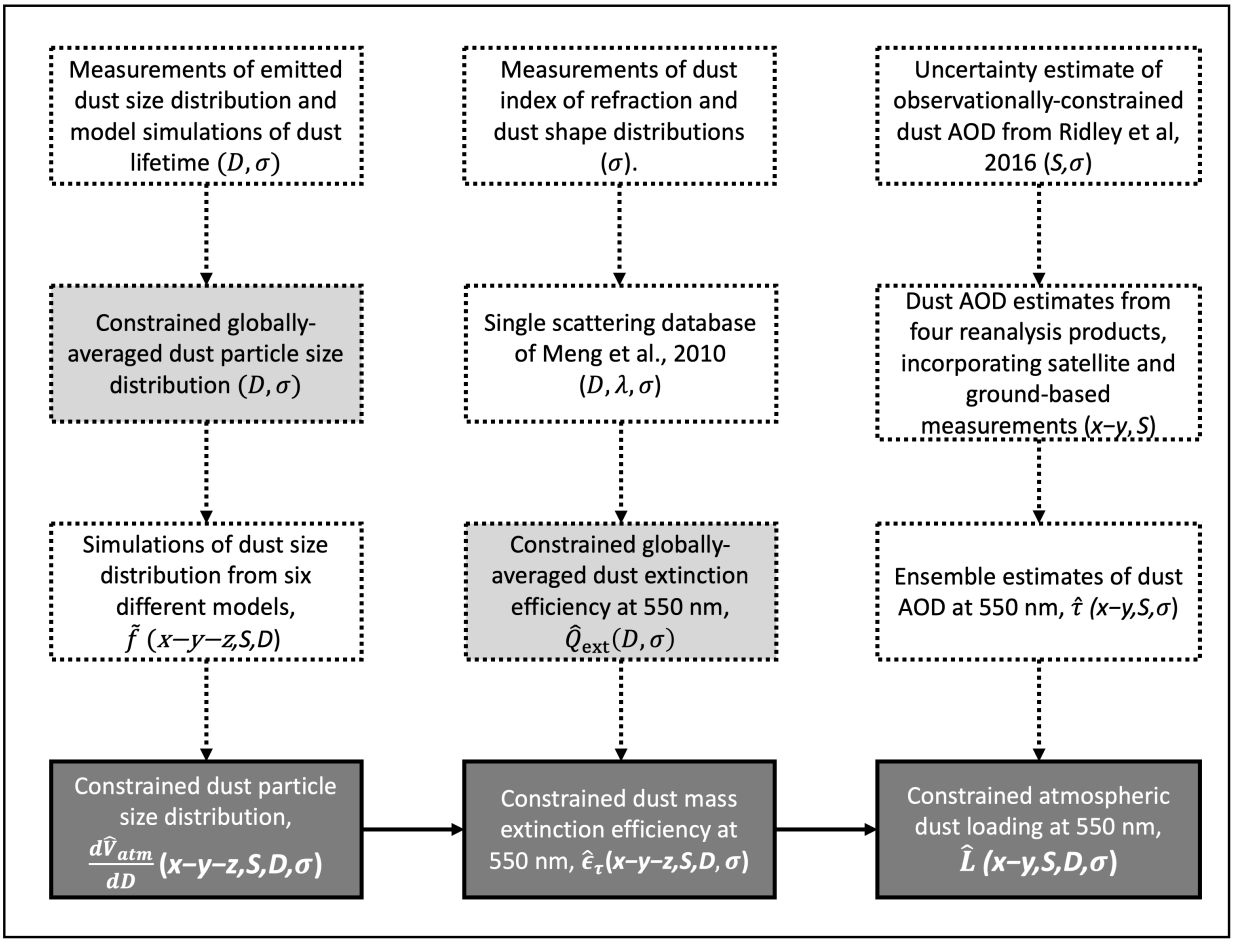

Figure 1: Schematic of the key steps to obtain the DustCOMM products (dark shaded boxes): constraints on the 3-D dust size distribution, 3-D mass extinction efficiency and the 2-D atmospheric loading. The variables are a function of the following: x-y-z (three-dimensional field), x-y (two-dimensional field), S (seasonally-resolved), D (size-resolved), σ (includes uncertainties). The variables in the light grey boxes are obtained from Kok et al (2017). See section 2 for details.

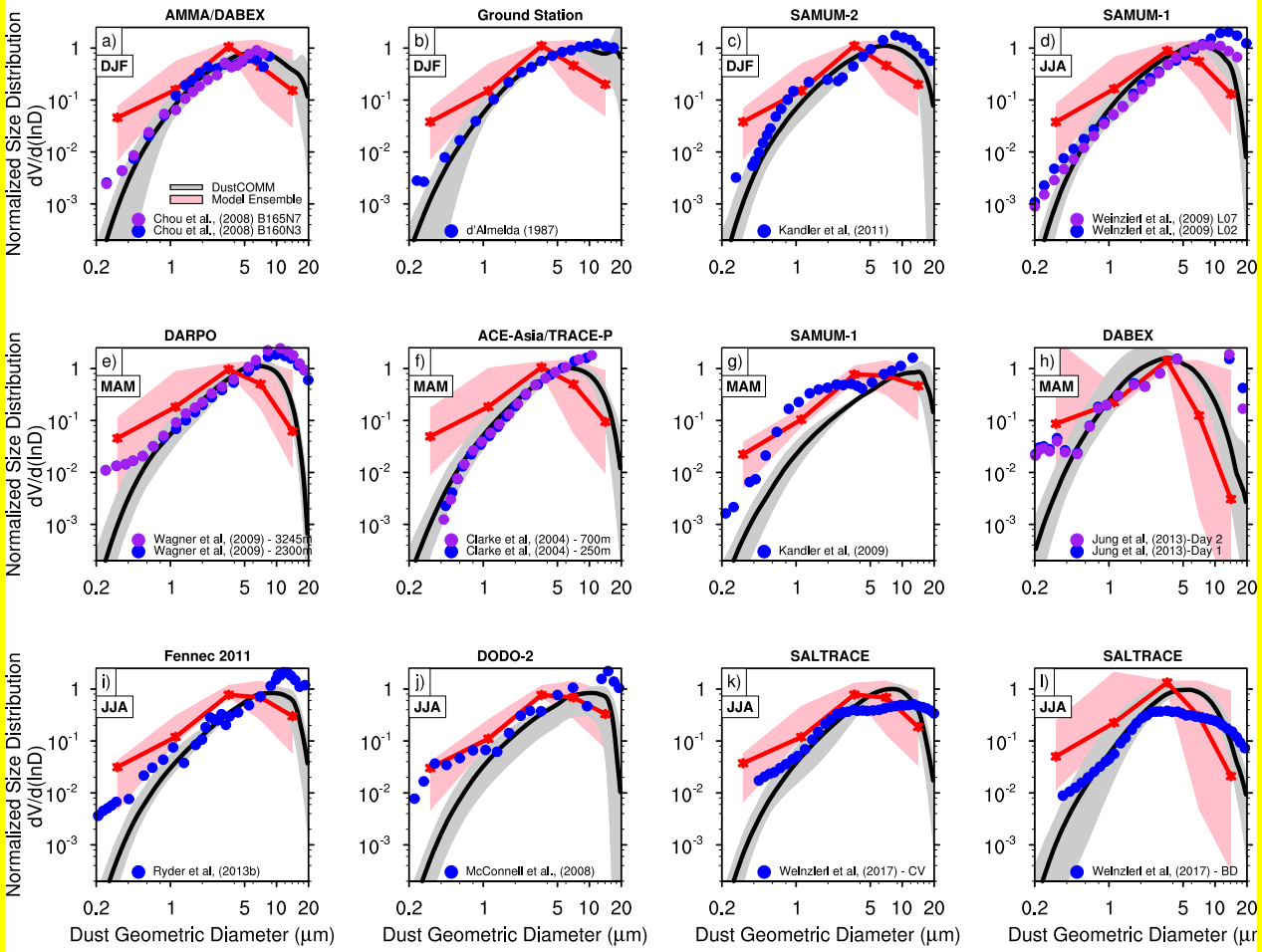

Figure 2: Comparison of normalized dust size distributions between published in-situ measurements (blue and purple dots; see Table 2) and season-averaged DustCOMM (black lines) and model ensemble (red lines) estimates. The grey shading shows the 95% confidence interval for the DustCOMM dust size distributions, whereas the pink shading shows the range of the model ensemble size distributions. The size distributions are normalized between 2.5-10 µm. The comparisons are made at the nearest model grid-points to the representative location and height level of the measurements.

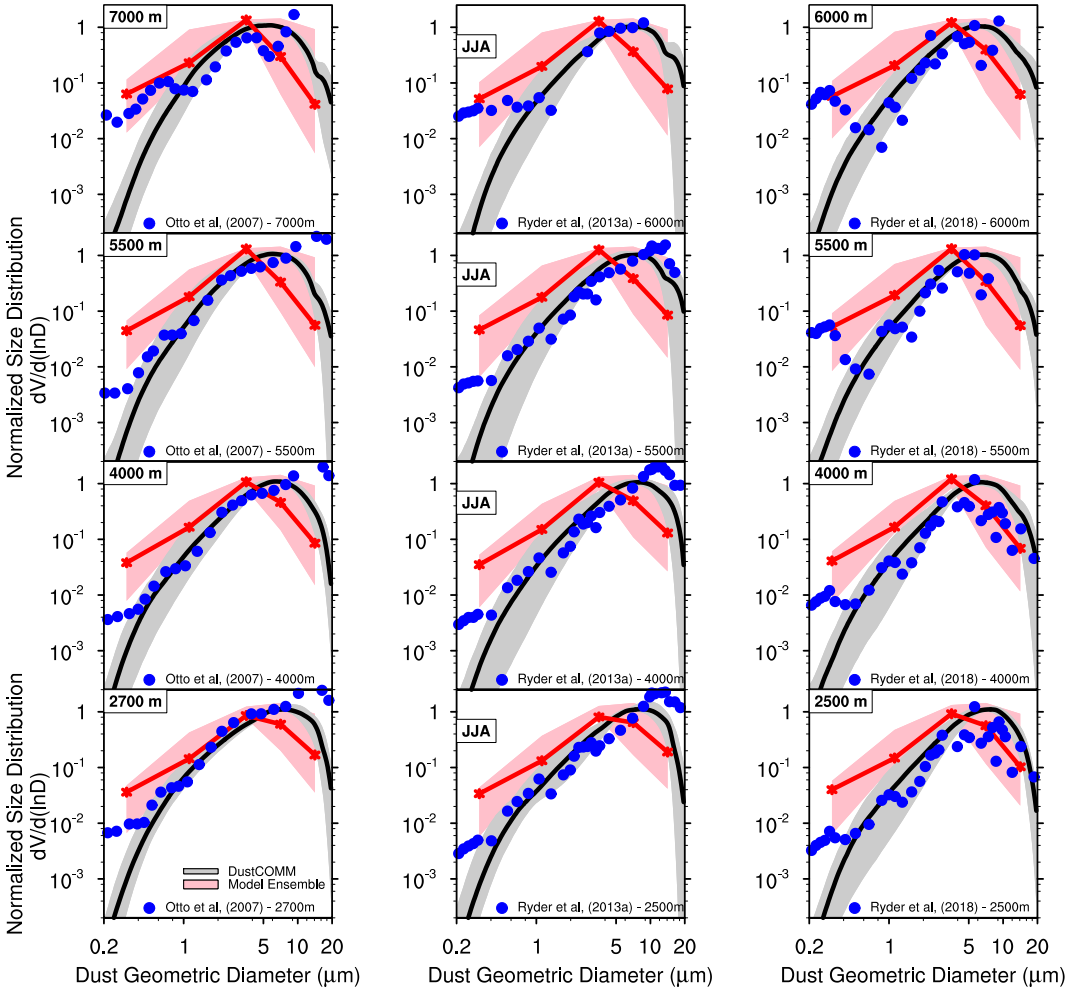

Figure 3: Same as Figure 2 above, but as a function of height, which increases from bottom to top. The measurements plotted on the left panels are from Otto et al., (2007) taken during the ACE-2 campaign (June/July, 1997) in the vicinity of Canary Islands; the measurements plotted on the middle panels are from Ryder et al., (2013a) taken during Fennec project (June 2011) near the Canary Islands; and the measurements plotted on the right panels are from Ryder et al., (2018) taken during the AER-D campaign in August 2015 near Cape Verde Island.

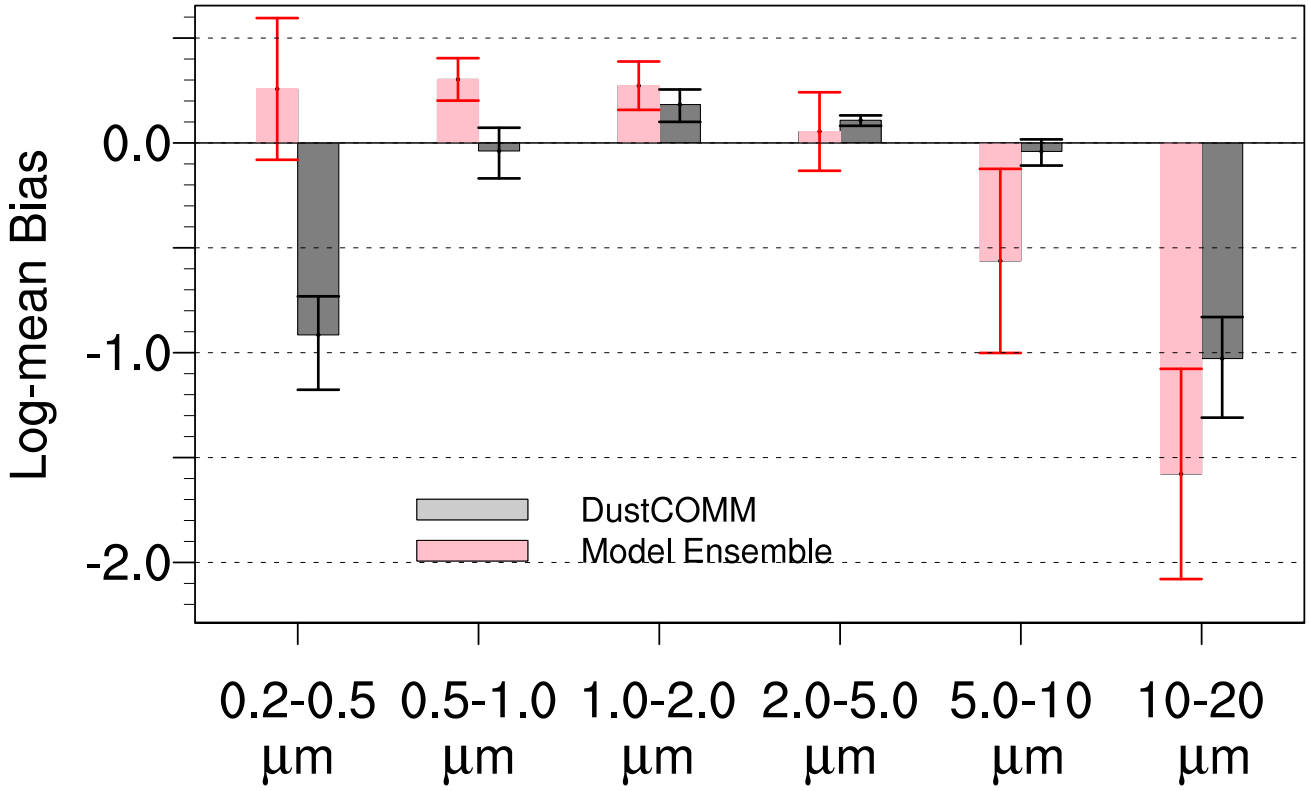

Figure 4: Average log-mean bias between measurements and DustCOMM (grey) or model ensemble (pink) estimates of dust size distributions (shown in Figures 2 and 3), for different particle bins. The vertical bars represent the 95% confidence interval.

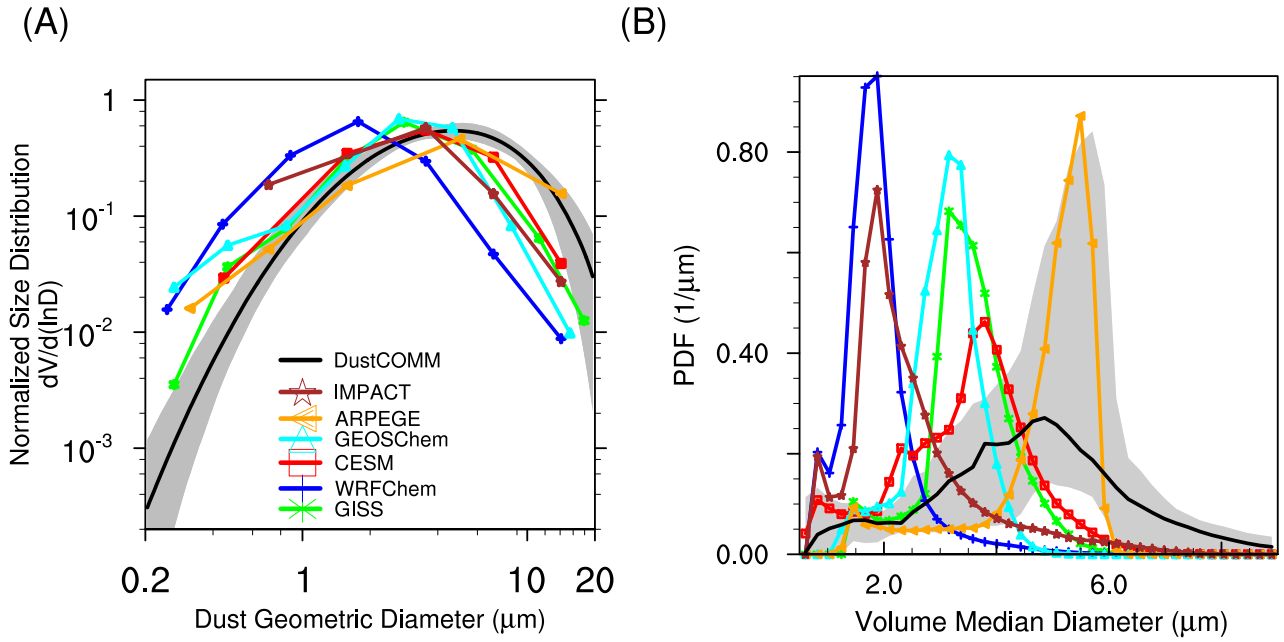

Figure 5: (A) Comparison between DustCOMM (black line) and model simulations (colored lines) of the globally-averaged dust particle size distribution (PSD). The grey shading denotes the 95% confidence interval for the DustCOMM product. (B) The probability distribution of the volume median diameter (µm) of the PSD for DustCOMM (black line) and the individual model simulations (colored lines) over all locations and height levels.

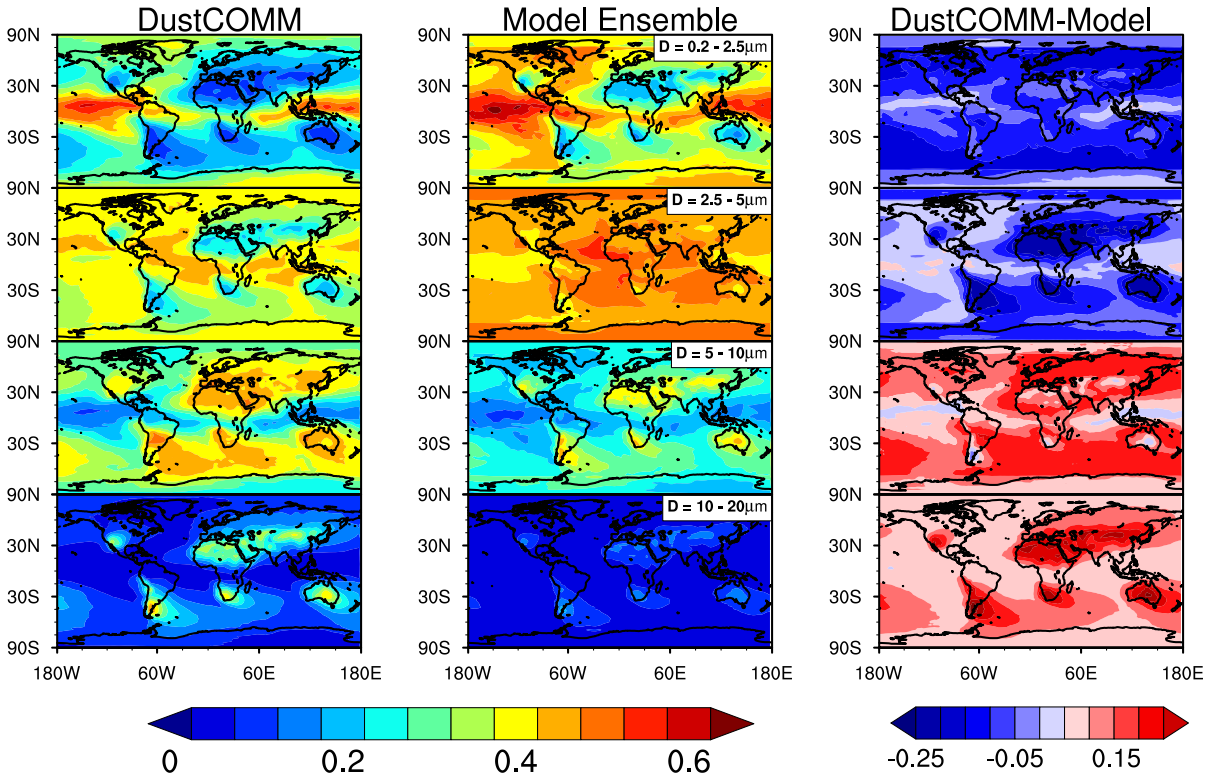

Figure 6: Differences in the spatial variability of the dust mass fraction between DustCOMM and the model ensemble. Shown are the spatial distributions of the vertically-integrated dust mass fractions for different particle bins for DustCOMM (left panel), the model ensemble (middle panel), and the difference between the two (right panel; DustCOMM -Model Ensemble).

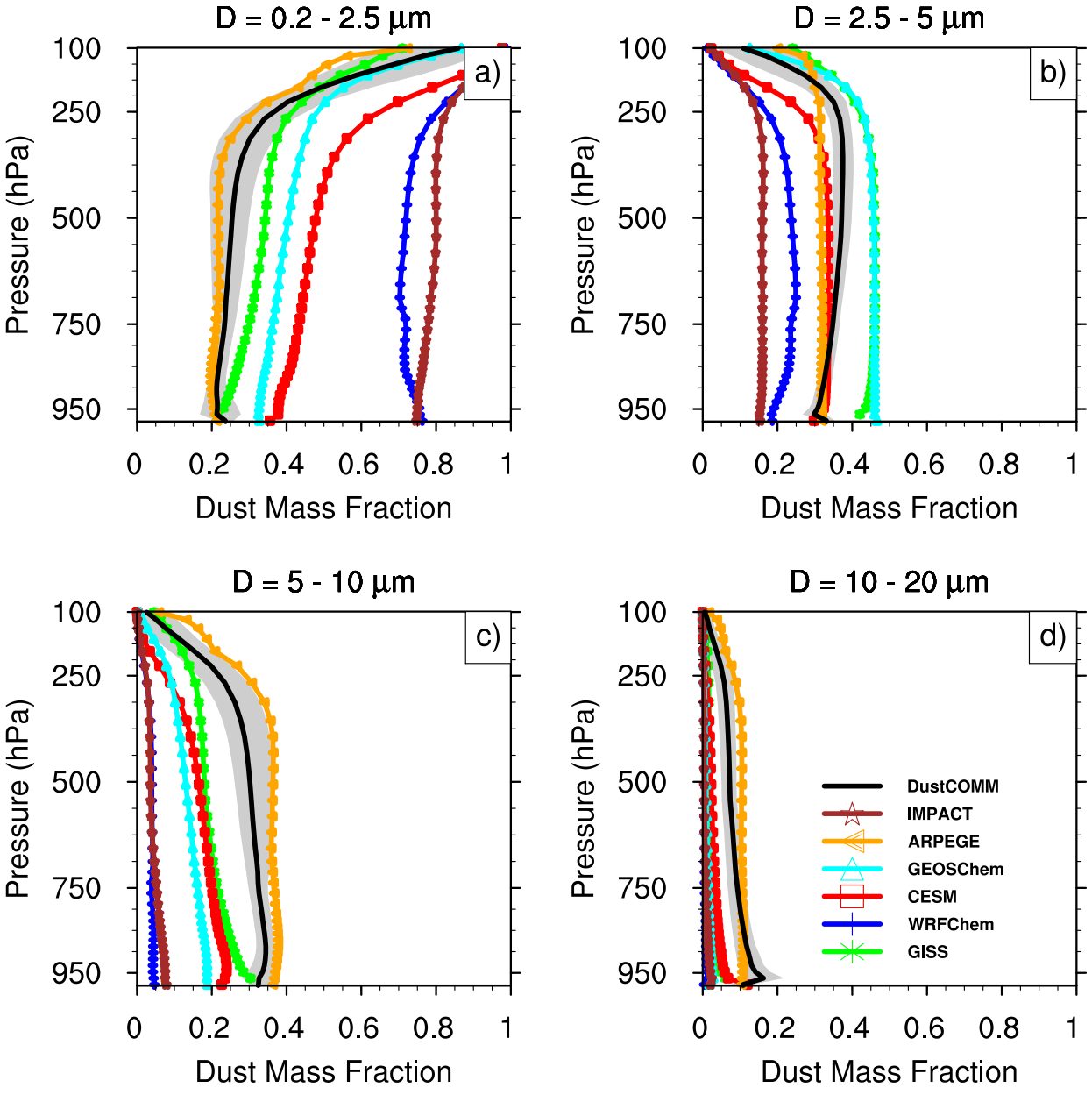

Figure 7: Vertical distributions of dust mass fractions as a function of particle size for the individual model simulation (colored lines) and DustCOMM (black lines) estimates. The grey shading shows the 95% uncertainty confidence interval for DustCOMM.

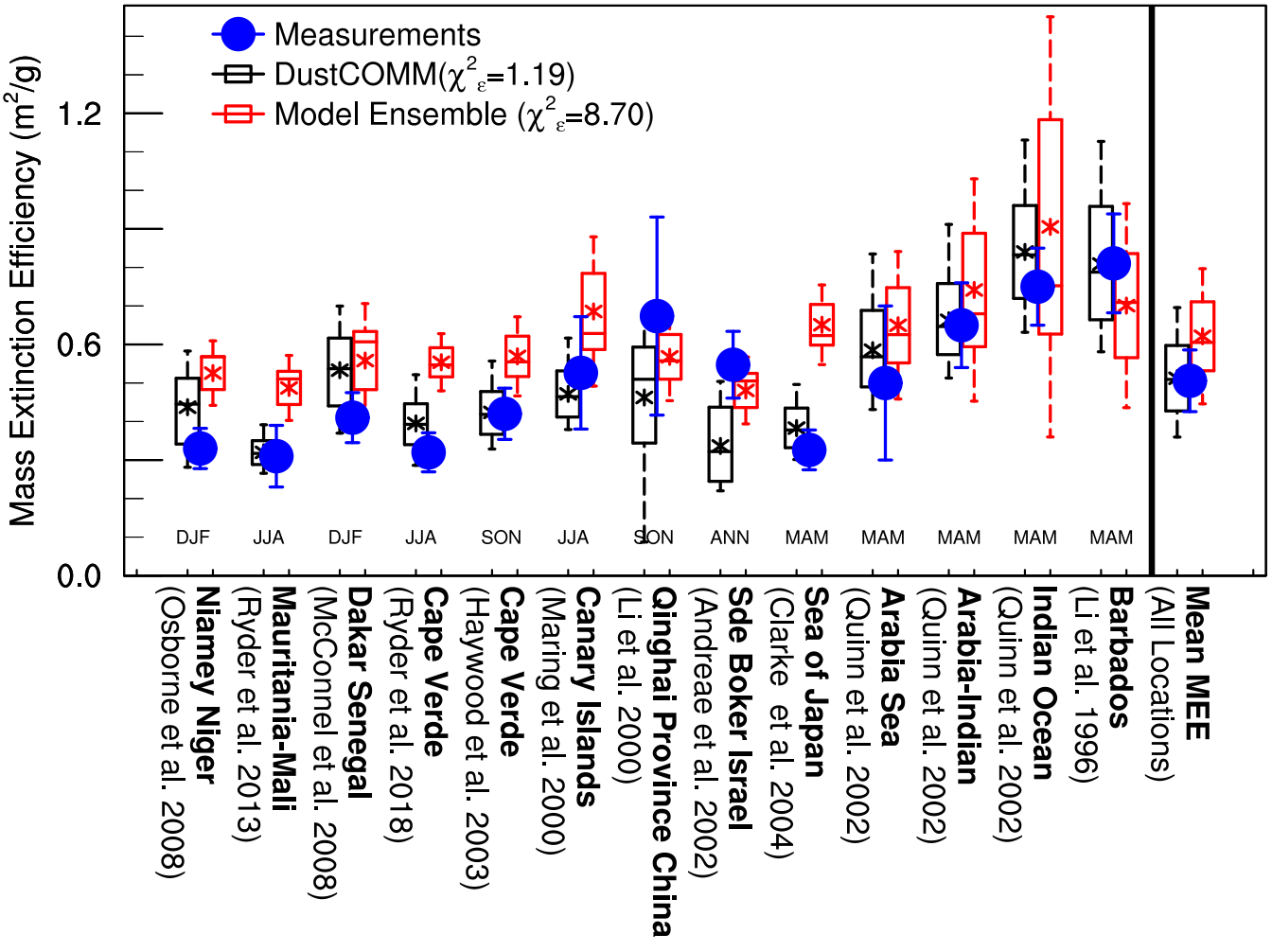

Figure 8: Comparison of measurements (blue dots) of dust mass extinction efficiencies (MEE – m^2g^{-1}) against column-integrated DustCOMM (black bars) and model ensemble (red bars) estimates. Vertical bars on the measurements represent reported uncertainty. For the DustCOMM and model ensemble estimates, the black and red boxes show one standard error, whereas the vertical dotted lines show the 95% confidence interval; the middle horizontal bar and star shows the median and mean values, respectively. The DustCOMM and model ensemble values are season-averaged values corresponding to the observation time period (see Table 2 for details). These seasons are labelled DJF— Dec-Feb., MAM—Mar-May, JJA – Jun.-Jul., SON – Sep.-Nov; ANN represents an annually-averaged value. The model ensemble MEE is calculated from the ratio between individual model dust aerosol optical depth and the dust mass loading, while the DustCOMM MEE is calculated using the constrained dust size distributions and single-particle extinction efficiency that takes into account the asphericity of dust aerosols. χ^2_ϵ is the reduced chi-squared (Eqn. 10b), and quantifies the performance of a model in representing observations (e.g. Andrae et al., 2010).

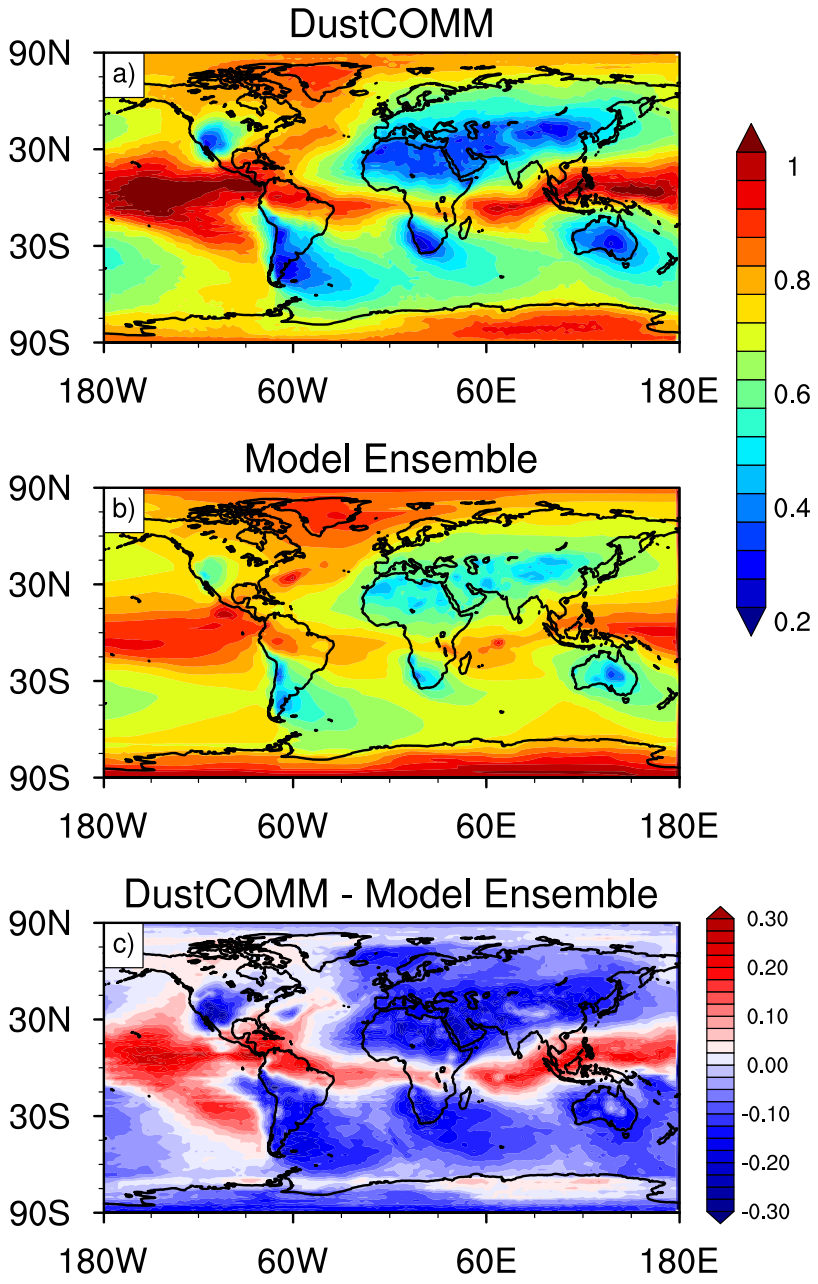

Figure 9: Spatial distributions of column-integrated dust mass extinction efficiency (MEE – m^2g^{-1}), weighted by the dust vertical distribution, for (a) DustCOMM, (b) the model ensemble, and (c) the difference between the two (DustCOMM -Model Ensemble).

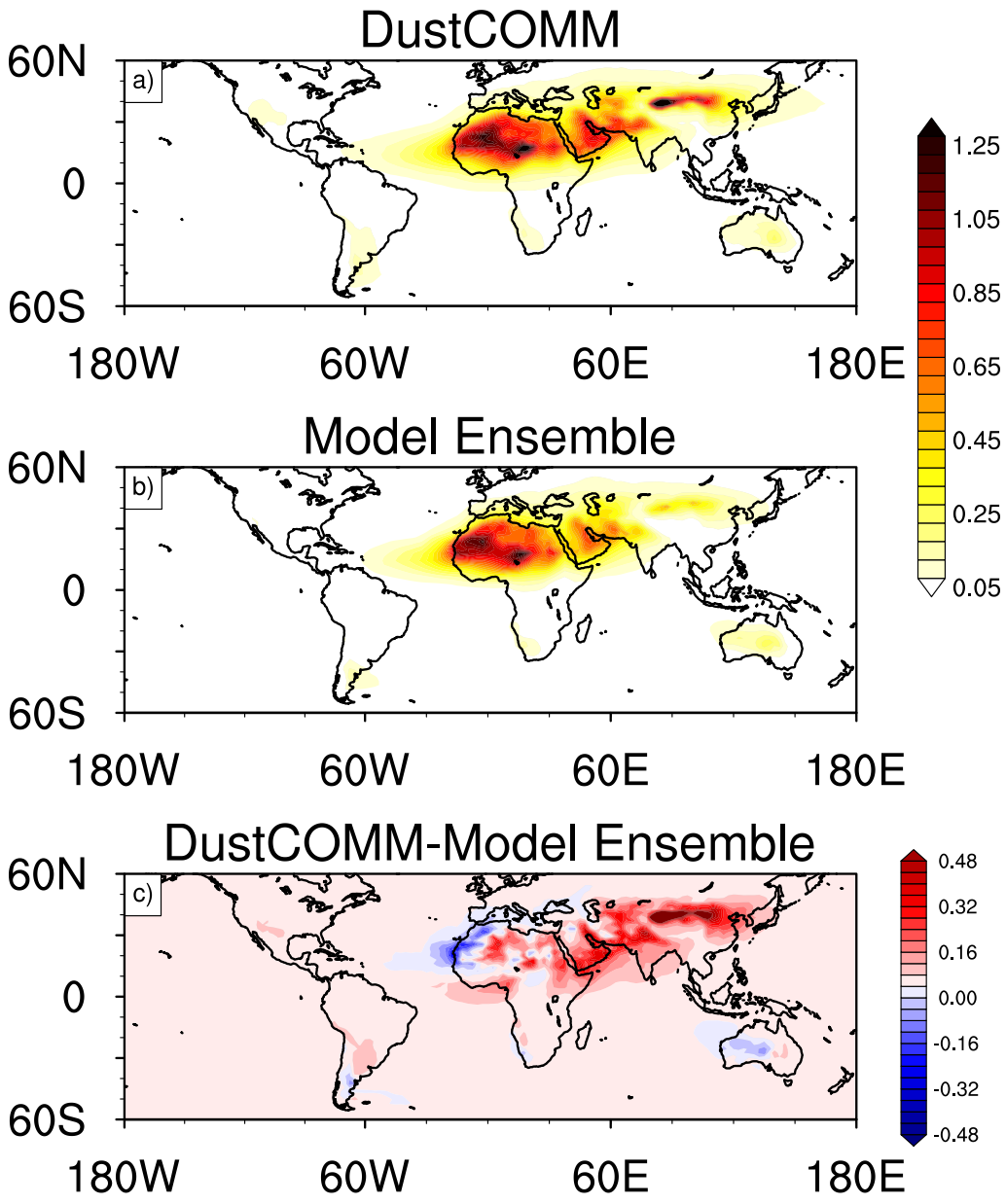

Figure 10: Spatial distributions of the atmospheric dust column loading (g m^{-2}) for the (a) DustCOMM and (b) model ensemble estimates, and (c) the difference between the two (DustCOMM -Model Ensemble).

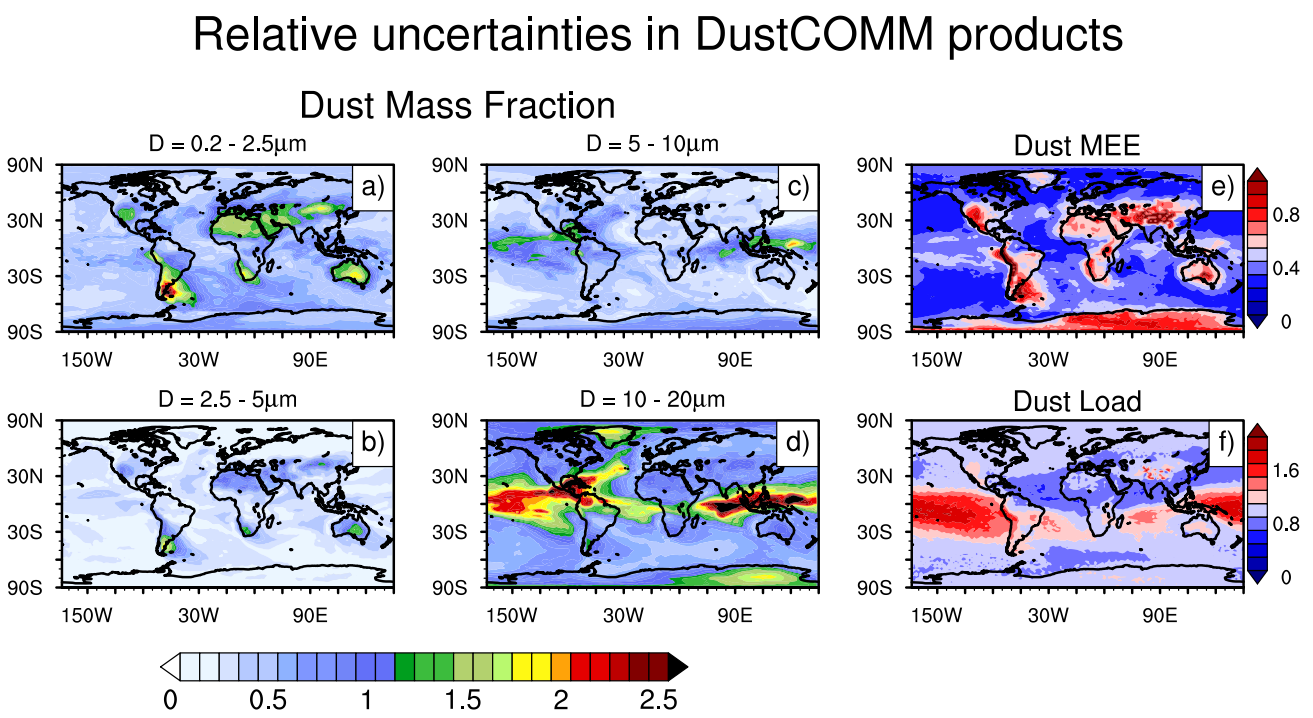

Figure 11: Spatial distributions of DustCOMM relative uncertainties for (a-d) the dust mass fraction in the diameter ranges of $0.2-2.5\mu m$, $2.5-5\mu m$, $5-10\mu m$, and $10-20\mu m$; (e) the dust mass extinction efficiency (MEE); and (f) dust load. The relative uncertainties are calculated as the ratio of the uncertainty characterizing 68% of the distribution of each variable, divided by the mean value.

Supplementary Document for "Dust Constraints from joint Observational-Modelling-experiMental analysis (DustCOMM): Comparison with measurements and model simulations"

Adeyemi A. Adebiyi[1], Jasper F. Kok[1], Yang Wang[1], Akinori Ito[2], David A. Ridley[3], Pierre NABAT[4], Chun Zhao[5]

[1]Department of Atmospheric and Oceanic Sciences, University of California Los Angeles, CA, USA
[2]Yokohama Institute for Earth Sciences, JAMSTEC, Yokohama, Kanagawa, 236-0001, Japan
[3]Monitoring & Laboratory Division, California Air Resources Board, Sacramento, CA, USA
[4]Centre National de Recherches Météorologiques, UMR3589, Météo-France-CNRS, Toulouse, France
[5]School of Earth and Space Sciences, University of Science and Technology of China, Hefei, Anhui 230026, China.

Correspondence to: Adeyemi A. Adebiyi (aadebiyi@ucla.edu)

1. Supplementary Figures

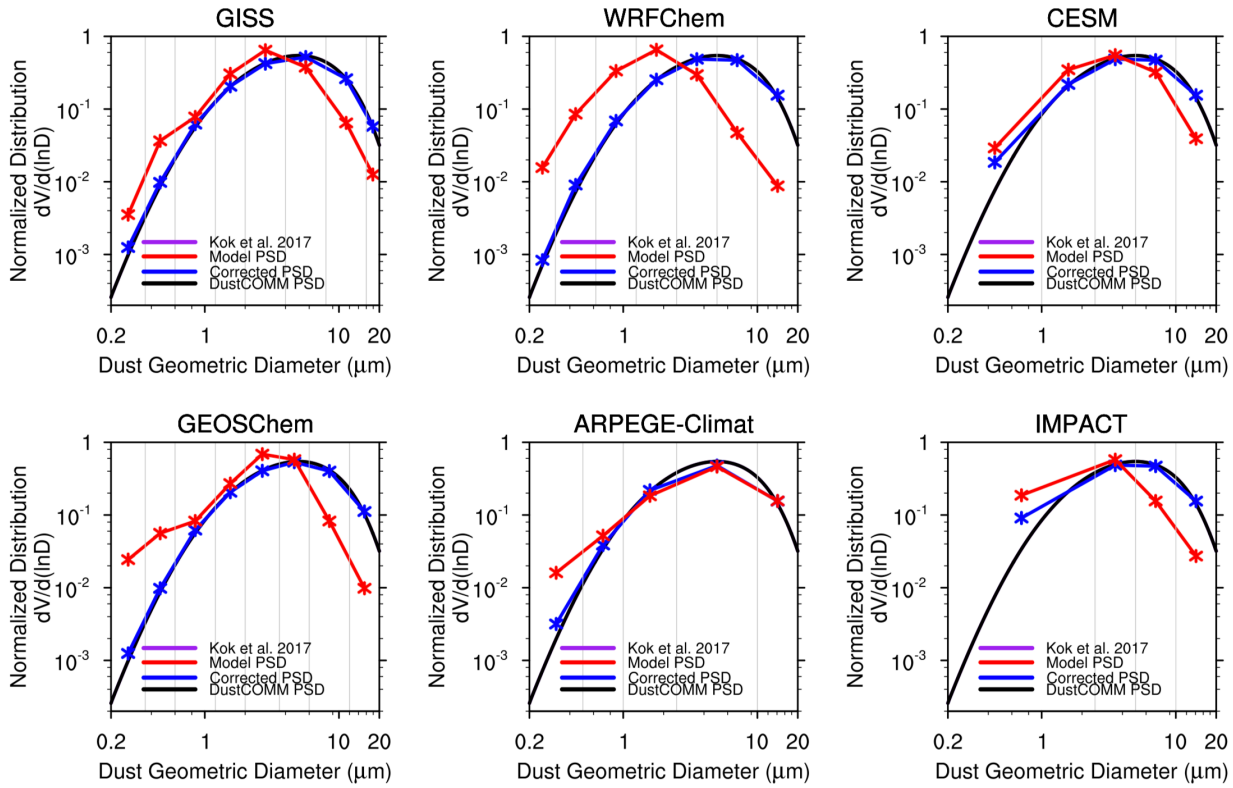

Figure S-1: The globally-averaged size distributions for each model normalized between 0.2 and 20 µm. It shows the model uncorrected dust size distribution (red lines), corrected dust size distribution (blue lines), Kok et al. 2017, and the final constrained DustCOMM dust size distribution with the sub-bins (black lines). Note that since the constrained DustCOMM dust size distribution forced to that of Kok et al., 2017, the lines overlap.

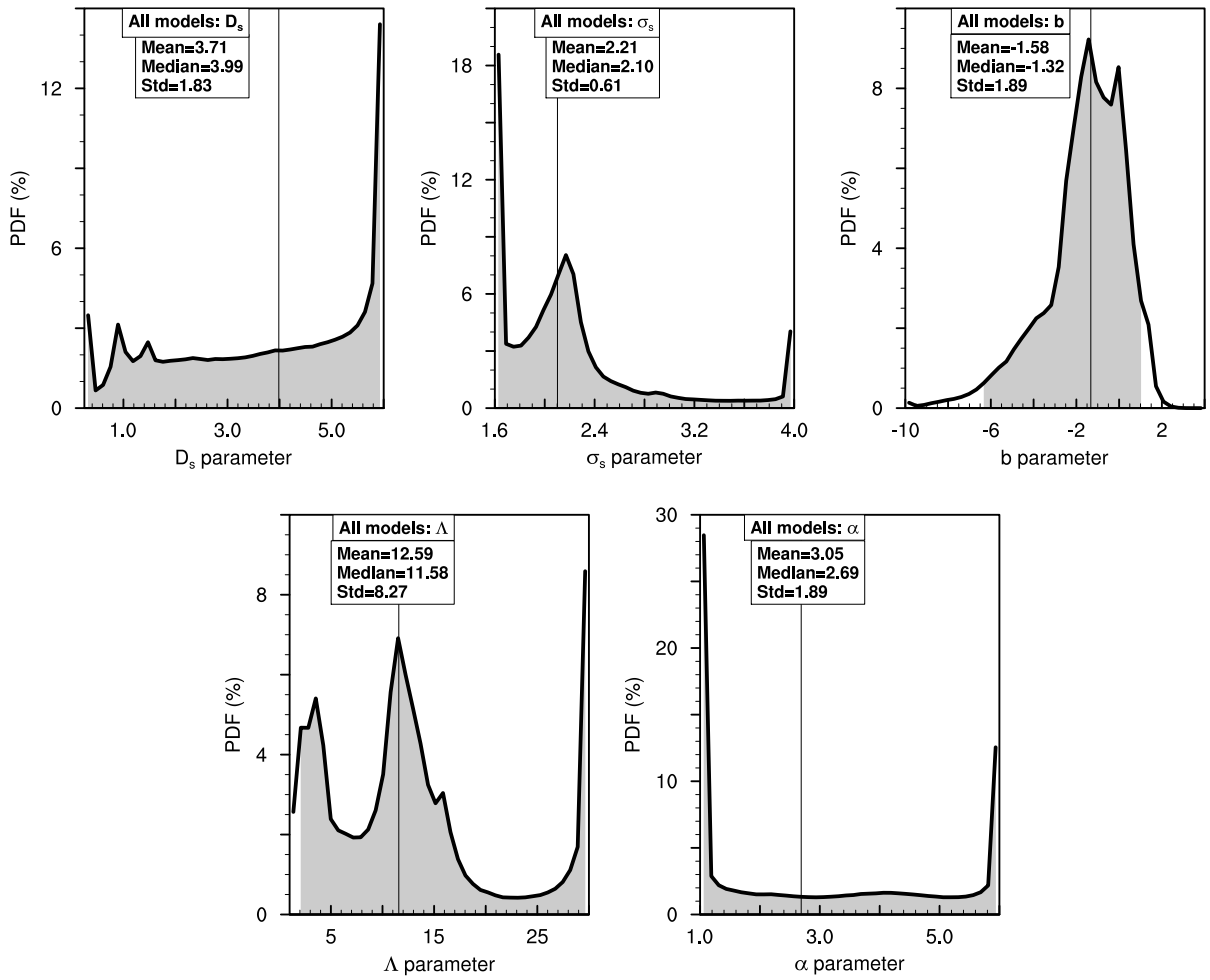

Figure S- 2: Probability distribution of the parameters for the generalized analytical function describing the atmospheric dust size distribution. See section 2.1.2 for details. The shaded regions denote the 95% confidence intervals of each distribution.

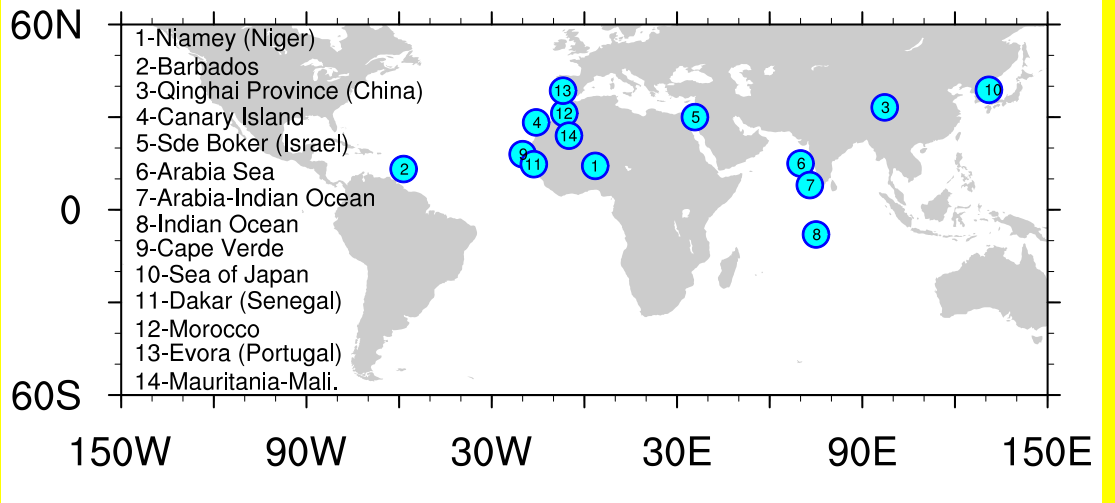

Figure S- 3: Map showing the locations of measurements for evaluation used in this study (Table 2). The measurements in Table 2 that corresponds to the numbers are as follows:
#1 – D'Almeida & Schutz, (1983), Osborne et al., 2008, Chou et al., 2008;
#2 – Li et al., 1996, Jung et al., 2013, Weinzierl et al., 2017;
#3 – Li et al., 2000;
#4 – Maring et al., 2000, Otto et al., 2007; Ryder et al., 2013a
#5 – Andreae et al., 2002;
#6 – Quinn et al., 2002;
#7 – Quinn et al., 2002;
#8 – Quinn et al., 2002;
#9 – Haywood et al., 2003, Kandler et al., 2011, Weinzierl et al., 2017, Ryder et al., 2018;
#10 – Clarke et al. 2004;
#11 – McConnell et al., 2008;
#12 – Weinzierl et al., 2009, Kandler et al., 2009;
#13 – Wagner et al., 2009;
#14 – Ryder et al., 2013b

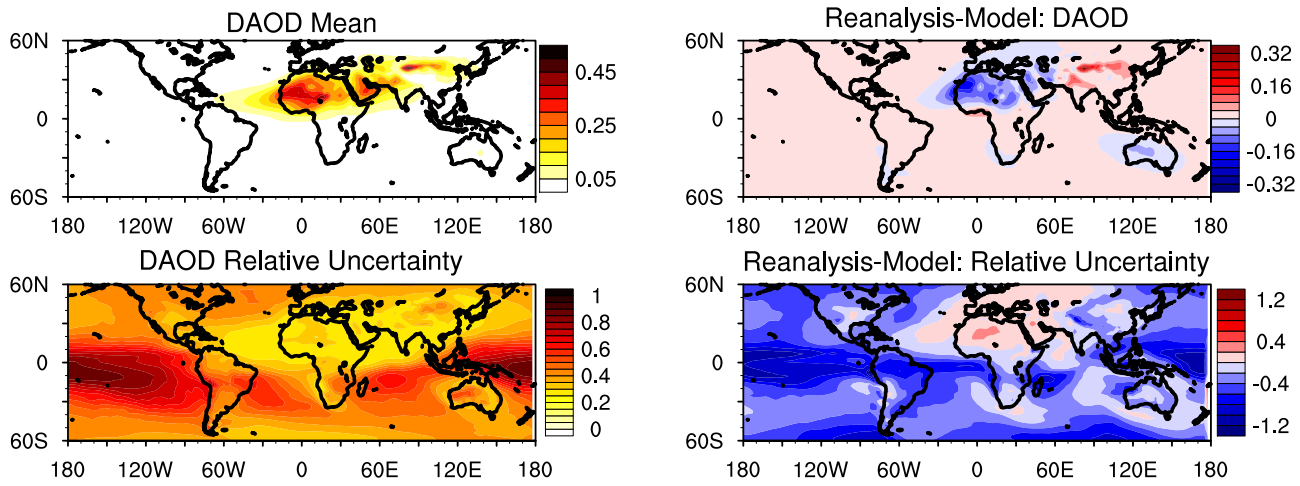

Figure S- 4: Annually-averaged ensemble mean and relative uncertainty of reanalysis dust aerosol optical depth (left panel). See section 3.2 for details Right panel shows the difference between the reanalysis dataset and the model ensemble dust aerosol optical depth.

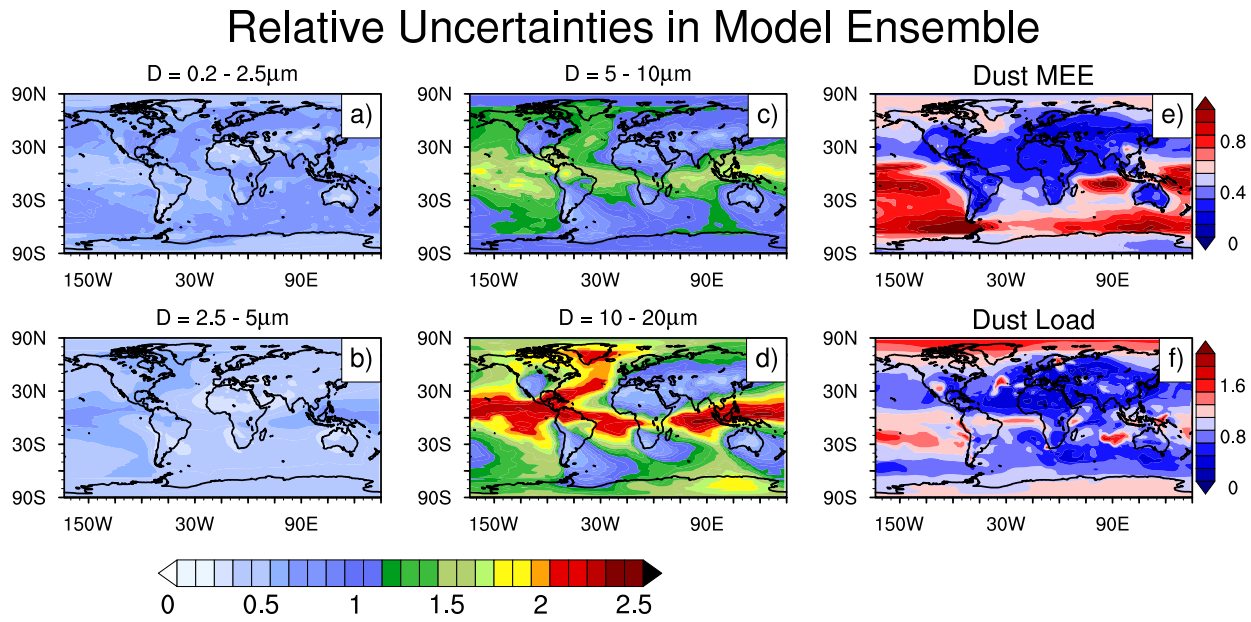

Figure S- 5: Spatial distributions of model ensemble relative uncertainties for (a-d) the dust mass fraction in the diameter range between $0.2-2.5\mu m$, $2.5-5\mu m$, $5-10\mu m$, *and* $10-20\mu m$; *(e) the dust mass extinction efficiency (MEE), and (f) dust load.*

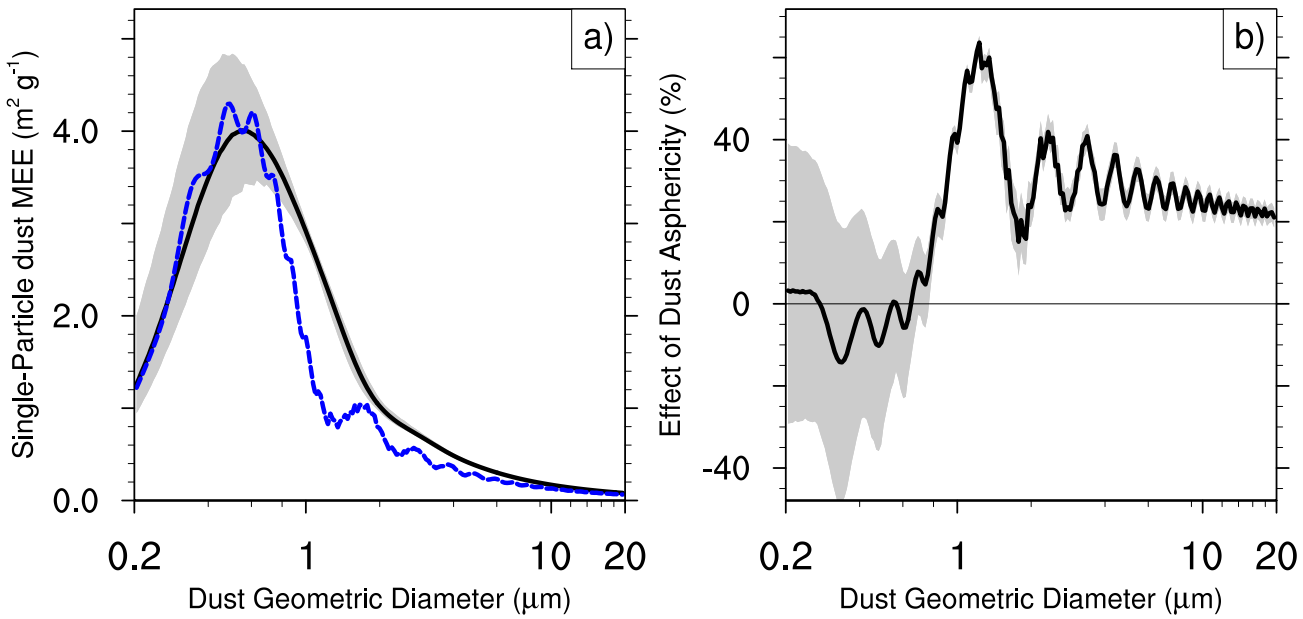

Figure S- 6: (a) Globally-averaged Single-particle DustCOMM dust mass extinction efficiency (MEE; Black line) and one calculated from Mie theory (blue line); (b) the effect of dust asphericity shown as the percentage differences between the dust MEE from DustCOMM and the one from Mie theory. All the black lines present the median of the distribution for each diameter, while the grey shade is the 95% confidence interval. The DustCOMM dust MEE leverages observational constraints on dust shape and dust size distribution (see section 2 in text). In contrast, the blue dashed line denotes the dust MEE calculated from Mie theory, which uses the assumption that dust particles are spherical.

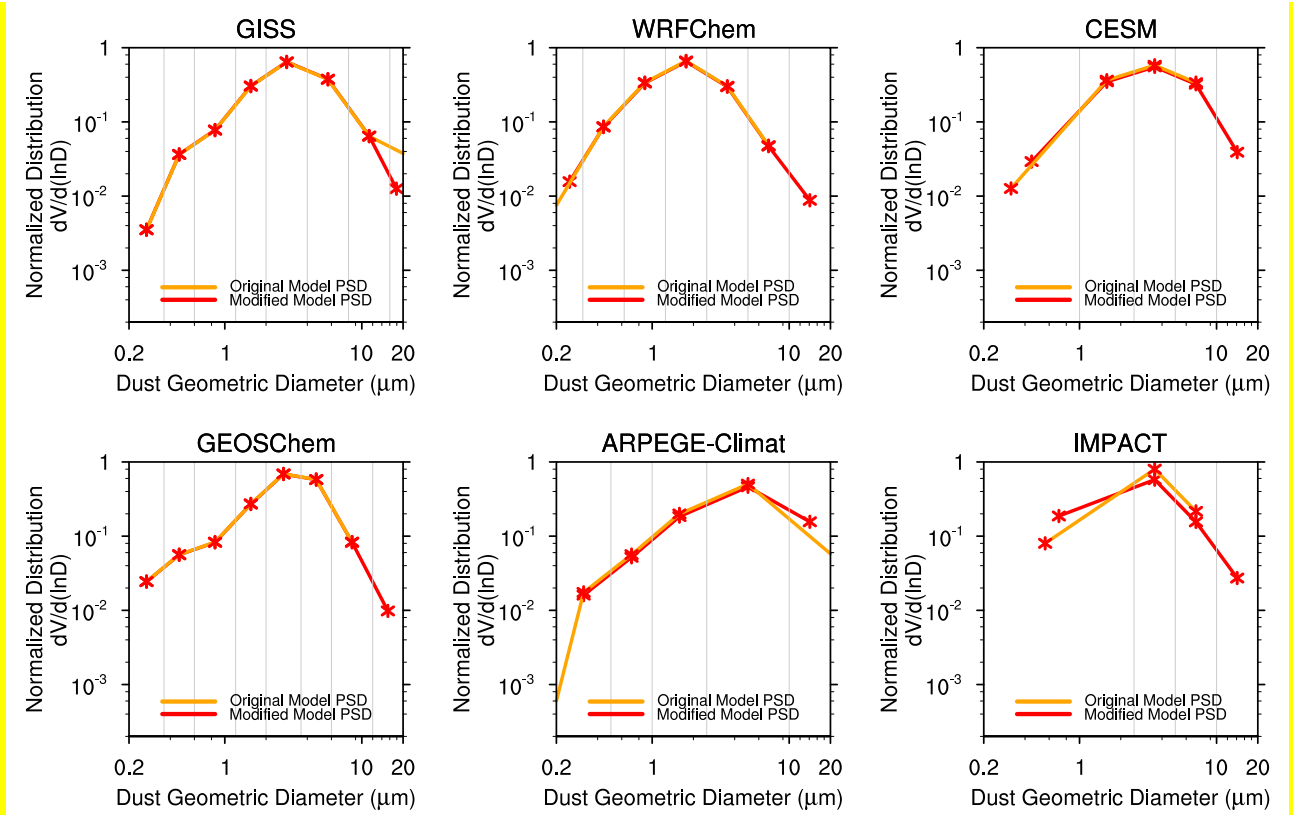

Figure S-7: The original and modified globally-averaged dust size disttribution for each model simulation.

2. Global model simulations

We describe here the model simulations used in this study. The GISS, CESM and GEOS-Chem models are described in detail in Kok et al. (2017) and the references therein (see section 5 of their supplementary document), while the simulations with the WRF-Chem, ARPEGE-Climat and IMPACT models are described below.

2.1.1 WRF-Chem

We use the version of WRF-Chem model (Grell et al., 2005) that is improved by the University of Science and Technology of China (Zhao et al., 2013). This version uses the quasi-global channel configuration with the periodic boundary conditions in the zonal direction and 360 × 145 grid cells (180° W-180° E, 67.5° S-77.5° N) to perform the simulations at 1° horizontal resolution, 35 vertical layers up to 50 hPa, and for the period of 2007-2016. The meteorological initial and lateral meridional boundary conditions are derived from the National Center for Environmental Prediction final analysis (NCEP/FNL) data. In addition, the model simulated winds and atmospheric temperature are nudged towards the NCEP/FNL reanalysis data with a nudging timescale of 6 hr (Stauffer & Seaman, 1990). Furthermore, the simulation uses MOSAIC (Model for Simulation Aerosol Interactions and Chemistry) aerosol module (Zaveri et al., 2008) coupled with the CBM-Z (carbon bond mechanism) photochemical mechanism (Zaveri and Peters, 1999). This aerosol model uses the bin approach with eight discrete size bins to represent aerosol size distributions (Fast et al., 2006). All major aerosol compositions are simulated in the model, including the including sulfate, nitrate, ammonium, black carbon, organic matter, sea-salt, and mineral dust. The MOSAIC aerosol scheme also includes physical and chemical processes of nucleation, condensation, coagulation, aqueous phase chemistry, and water uptake by aerosols. More details, including the model physics scheme used, can be found in Zhao et al. (2013).

Vertical dust emission fluxes are calculated as described in Zhao et al. (2010) based on the GOCART dust emission scheme (Ginoux et al., 2001). The emitted dust particles are distributed into the MOSAIC aerosol size bins following a theoretical expression that is based on the physics of scale-invariant fragmentation of brittle materials derived by Kok (2011). For MOSAIC 8-bin,

dust particles are emitted into eight size bins with mass fractions of 10^{-6} %, 10^{-4} %, 0.02%, 0.2%, 1.5%, 6%, 26%, and 45%, respectively. The dry deposition of aerosol mass and number is simulated following the approach of Binkowski & Shankar (1995), which includes both turbulent diffusion and gravitational settling. Wet removal of aerosols by grid-resolved stratiform clouds and precipitation includes in-cloud removal (rainout) and below-cloud removal (washout) by impaction and interception, following Easter et al. (2004) & Chapman et al. (2009). Cloud-ice-borne aerosols are not explicitly treated in the model, but the removal of aerosols by the droplet freezing process is considered. Convective transport and wet removal of aerosols by cumulus clouds follow Zhao et al. (2010, 2013).

The AOD is computed as a function of wavelength for each model grid box. Aerosols are assumed internally mixed in each bin (i.e., a complex refractive index is calculated by volume averaging for each bin for each chemical constituent of aerosols). The Optical Properties of Aerosols and Clouds (OPAC) data set (Hess et al., 1998) is used for the shortwave and longwave refractive indices of aerosols, except that a constant value of 1.53+0.003i is used for the SW refractive index of dust following Zhao et al. (2010, 2011). A detailed description of the computation of aerosol optical properties in WRF-Chem can be found in Fast et al. (2006) & Barnard et al. (2010).

2.1.2 IMPACT

The global chemical transport model used in this study is a coupled gas-phase (Ito et al., 2007) and aerosol chemistry version (Liu et al., 2005) of the Integrated Massively Parallel Atmospheric Chemical Transport (IMPACT) model (Rotman et al., 2004). A detailed description can be found in Ito & Kok (2017) and references therein. The IMPACT model is driven by assimilated meteorological fields from the Goddard Earth Observation System (GEOS) of the NASA Global Modeling and Assimilation Office (GMAO) with a horizontal resolution of 2.0° × 2.5° and 59 vertical layers up to 0.01 hPa. The model simulates the emissions, chemistry, transport, and deposition of major aerosol species (Liu et al., 2005) and their precursor gases (Ito et al., 2007). IMPACT takes into account emissions of primary aerosols and precursor gases of secondary aerosols such as sulfate, nitrate, ammonium and oxalate. Mineral dust aerosols are distributed among 4 bins in the model. A total dust source is dynamically calculated by a physically-based dust emission scheme (Kok et al., 2014a, 2014b) in conjunction with satellite products of

vegetation cover and soil moisture in the model (Ito & Kok, 2017). The chemical composition of mineral dust aerosols may change dynamically from that in the originally emitted aerosols due to reactions with gaseous species.

Dry deposition of aerosol particles uses a resistance-in-series parameterization (Zhang et al., 2001). Gravitational settling is also taken into account (Rotman et al., 2004; Seinfeld & Pandis, 2016). Aerosols and soluble gases can be incorporated into cloud drops and ice crystals within cloud (rainout), collected by falling rain and snow (washout), and be entrained into wet convective updrafts (Liu et al., 2001; Rotman et al., 2004; Ito et al., 2007; Ito & Kok, 2017). The aging of dust and combustion aerosols from hydrophobic to hydrophilic enhances their dry and wet deposition. Hygroscopic growth of mineral dust and combustion aerosols in gravitational settling uses the Gerber (1991) scheme, including the particle growth due to sulfate, ammonium, and nitrate associated with the particles (Liu et al., 2005; Xu & Penner, 2012). Scavenging efficiencies for mineral dust and combustion aerosols in wet deposition are calculated based on the amount of sulfate, ammonium and nitrate coated on the particles (Liu et al., 2005; Xu & Penner, 2012).

The AOD at 550 nm is calculated online using a look-up table as a function of wavelength and size parameter, following Xu & Penner (2012). Five types of aerosols (i.e., carbonaceous aerosols from anthropogenic combustion, carbonaceous aerosols from open biomass burning, dust, sulfate, and sea salt) were assumed to be externally mixed in each size bin, while sulfate, ammonium, and nitrate coated on each aerosol was internally mixed within each aerosol type and size bin. The refractive index for internally mixed aerosols is calculated based on the volume weighted mixture for each aerosol type and size bin.

2.1.3 ARPEGE-Climat

This study uses the global climate model from CNRM, namely ARPEGE-Climat, in its version 6 used in the CMIP6 exercise, with a horizontal resolution of ~1.4° and 91 vertical levels (Michou et al., 2015). ARPEGE-Climat includes an interactive tropospheric aerosol scheme, named TACTIC (Tropospheric Aerosols for ClimaTe In CNRM), able to represent the main anthropogenic and natural aerosol types in the troposphere. Originally developed in the GEMS/MACC project (Morcrette et al., 2009), this scheme has been adapted to the

ARPEGE/ALADIN-climate code (Michou et al., 2015; Nabat et al., 2015). Aerosols are included through sectional bins, separating desert dust (6 size bins whose limits are 0.1, 0.2, 0.5, 1.0, 2.5, 10.0 and 100 μm), sea-salt (3 bins whose limits are 0.03, 0.5, 5.0 and 20.0 μm), sulfate (1 bin, as well as 1 additional variable for sulfate precursors considered as SO2), organic matter (2 bins: hydrophobic and hydrophilic particles) and black carbon (2 bins: hydrophobic and hydrophilic particles) particles. All these 15 species are prognostic variables in the model, submitted to transport (semi-lagrangian advection, and convective transport), dry deposition, in-cloud and below-cloud scavenging. The interaction with shortwave and longwave radiation, is also taken into account through optical properties (extinction coefficient, single scattering albedo and asymmetry parameter) calculated using the Mie theory. Sulfate, organic matter and sea salt concentrations are used to determine the cloud droplet number concentration following Menon et al. (2002), thus representing the cloud-albedo effect (1st indirect aerosol effect).

Focusing more on dust aerosols, emissions are fully interactive, based on the parameterization of Marticorena & Bergametti (1995) which provides the saltation flux depending on surface wind and soil characteristics. The latter consist in the roughness length and the sand/clay/silt fractions, which are based on the ECOCLIMAP database (Masson et al., 2003). The distribution of the resulting emitted dust vertical flux follows then the study of Kok (2011), assuming an analogy with the fragmentation of brittle materials. The six dust size bins have the following effective diameters: 0.09, 0.18, 0.4, 0.9, 3.7 and 13.2 μm. Dry deposition (for the 6 dust bins) and sedimentation (only applied to the two coarsest size bins) are calculated from fixed vertical speeds (respectively Wisely and Hicks, 2000, and Thompson, 2005). Wet deposition includes below-cloud and in-cloud scavenging. The latter relies on the parameterization of Giorgi & Chameides (1986), assuming a fraction of dust aerosols included in droplets equal to 0.1 for the two finest bins and 0.2 for the 4 other bins.

In the present study, a five-year simulation (2004-2008) has been carried out using the ARPEGE-Climat model and its interactive aerosol scheme.

3. Description of the reanalysis datasets

3.1. MERRA-2 Aerosol Reanalysis

The MERRA-2 is the second version of the MERRA atmospheric reanalysis product from the NASA Global Modeling and Assimilation Office (Gelaro et al., 2017), with updates on the reanalysis system to include addition of more observational platforms and correction of known limitations from previous MERRA version (Mccarty et al., 2016), as well as improvement to the Goddard Earth Observing System -5 (GEOS-5) atmospheric general circulation model, used as the base model for the global assimilation system (Mccarty et al., 2016). For the first time, meteorological and aerosol observations (which include bias-corrected aerosol optical depth from MODIS, AVHRR, MISR – over desserts, and ground-based AERONET instruments) are jointly assimilated into MERRA-2, with the aerosol fields simulated with radiatively-coupled version of Goddard Chemistry, Aerosol, Radiation and Transport model (GOCART) (Colarco et al., 2010). GOCART treats aerosol particles as externally mixed, with dust particles provided in five non-interacting bins (Randles et al., 2017). The dust emission in GOCART is based on Ginoux et al. (2001), which depend on wind speed, following the parameterization of Marticorena & Bergametti (1995). Aerosol loss processes include dry deposition, large-scale wet removal, and convective scavenging. While the dry deposition is mostly model dependent, the precipitation-induced aerosol deposition however, depends largely on the assimilated global precipitation information in MERRA-2 (Reichle et al., 2014, 2017). MERRA-2 aerosol properties are available from 1980 onward, but the number of observations assimilated is more than doubled after the year 2003 (Fig. 3 in Randles et al., 2017). MERRA-2 is available for 3-hourly temporal resolution, and 1.5^{o} X 1.5^{o} horizontal fixed spatial resolution.

We use the monthly averages (calculated from daily means) of MERRA-2 DAOD to construct the seasonal and climatological DAOD values between 2003 and 2012. Aerosol products from MERRA-2 have been validated against independent observation (Buchard et al., 2017; Randles et al., 2017), especially for the aerosol optical depth. It is worth noting here also that only AOD is directly constrained by the assimilation in MERRA-2, while other non-analyzed, non-constrained aerosol properties, like the vertical distribution and aerosol speciation are mostly model-dependent, thereby providing a possible source of uncertainty in the MERRA-2 DOAD reanalysis.

3.2. NAAPS

The Navy Aerosol Analysis and Prediction System (NAAPS) is an offline aerosol transport model (Lynch et al., 2016) driven by the Navy Operational Global Analysis and Prediction System (NOGAPS; Hogan & Rosmond, 1991; Hogan & Brody, 1993). The quality-assured and quality-controlled MODIS and MISR aerosol optical depth are assimilated through the Navy Atmospheric Variational Data Assimilation System (NAVDAS; Zhang et al., 2008), that became operational in 2010. Details on the aerosol model dynamics, emission and sink processes can be found in Lynch et al. (2016). NAAPS contains dust, sea salt, smoke, SO2, and other anthropogenic and biogenic fine particles, all of which are treated as externally mixed. The dust emission in NAAPS is based on Ginoux et al. (2001) erodibility map, with regional source tuning constrained by space-based and ground-based AOT observations (Lynch et al., 2016). While dust removal processes include dry deposition and wet removal, the dry deposition over ocean is adjusted based on assimilated AOT, and the wet deposition is constrained by satellite-based precipitation information retrieved from NOAA Climate Prediction Center MORPHing technique data (CMORPH; Joyce et al., 2004). NAAPS aerosol optical depth are available at 6 h temporal resolution, and 1^{o} X 1^{o} spatial resolution. For consistency with other reanalysis data, seasonal and climatological averages of AOT is also calculated for 2003 to 2012, using monthly averages. Reanalyzed NAAPS coarse and fine-mode AOT have good agreement with ground-based AOT from AERONET stations (Lynch et al., 2016). Similar to MERRA-2 reanalysis, NAAPS does not assimilate aerosol vertical information or speciation, hence the relative dust vertical profiles are uniformly varied, along with other aerosol species, to match the posterior AOT.

3.3. JRAero

The Japanese Reanalysis for Aerosol (JRAero) version 1.0 is produced by the Meteorological Research Institute (MRI) of the Japan Meteorological Agency. The global reanalysis product uses a global aerosol transport model named MASINGAR mk-2 (Model of Aerosol Species IN the Global AtmospheRe; Yukimoto et al., 2012), which consist an updated dust emission scheme (Yumimoto et al., 2017), when compared to the previous version of MASINGAR (Tanaka et al., 2003). MASINGAR mk-2 is coupled to an atmospheric general circulation model, also developed at MRI (Yoshimura and Yukimoto, 2008; Yukimoto et al., 2012), while the aerosol assimilation is done every 6 hours using a two-dimensional variational method (MASINGAR/2D-Var, similar to NAAPS-NAVDAS). Only the level 3 bias-corrected MODIS AOD, developed by the US Naval

Research Laboratory (NRL) and the University of North Dakota (Zhang & Reid, 2006 Hyer, et al., 2011; Shi et al., 2011), is assimilated into MASINGAR mk-2, and this data is largely unavailable over the deserts due to the stringent quality-control procedure (e.g. Yumimoto et al., 2017). Aerosol particles in the model are treated as externally mixed, with mineral dust carried in ten discrete particle bins (Yumimoto et al., 2017). The updated dust emission uses the wind erosion model developed by Shao et al. (1996), with erodibility factors for vegetation cover, snow cover, land-use type, and soil type (Tanaka and Chiba, 2005). Unlike MERRA-2 and NAAPS, both aerosol dry deposition and wet removal processes in MASINGAR mk-2 are model-dependent. Dry deposition in the model depends on the dry deposition velocity, which employs the resistance analog model (Seinfeld and Pandis, 2006), while the wet deposition process follows the parameterization of Giorgi & Chameides (1986) for in-cloud scavenging, and the procedure detailed in Tanaka & Chiba (2005) for below-cloud scavenging. JRAero is available for the period between 2011 and 2015, at 6 hours temporal resolution, and approximately 1.1^{o}x1.1^{o} spatial resolution. We use the monthly averages of JRAero DAOD between 2011—2015 to construct the seasonal and climatological global DAOD values. Though the averaging period of 2011—2015, is different from other reanalysis product used, the spatial distribution of DAOD is largely consistent with other reanalysis products, albeit slightly smaller magnitude.

3.4. CAMSiRA

The Copernicus Atmosphere Monitoring Service (CAMS) interim Reanalysis (CAMSiRA) is a global reanalysis of atmospheric composition (Flemming et al., 2017). It uses a modified version of the European Centre for Medium-Range Weather Forecasts (ECMWF) Integrating Forecasting System for Composition (C-IFS) (Flemming et al., 2015). The aerosol model is based on the LMDZ model of Laboratoire de Météorologie Dynamique aerosol model (Reddy et al., 2005) that uses a bulk–bin scheme simulating desert dust, sea salt, organic carbon, black carbon, and sulfate aerosols (Morcrette et al., 2009). The wet and dry deposition are also modelled with different parameterizations. The wet deposition is based on Jacob et al. (2000) which account for sub-grid scale clouds and precipitation. Dry deposition is based on pre-calculated monthly mean deposition velocities following Wesley (1989). The C-IFS uses a four-dimensional variational (4D-VAR) data assimilation technique to combine satellite observations with chemistry-aerosol modelling. Aerosol optical depth is assimilated mainly from MODIS, with the variational bias correction

scheme developed at ECMWF (Inness et al., 2015). The mass mixing ratios of O3 and CO are also assimilated from various instruments as additional control variables. CAMSiRA is available for the period between 2011 and 2017, at 3 hours temporal resolution, and approximately 1.1°x1.1° spatial resolution. We use the monthly averages of CAMSiRA DAOD to construct the seasonal and climatological global DAOD values.

4. Summary of measurements collected from literature and used for evaluation

4.1. D'Almeida (1987) – Ground Station – PSD only

Aerosol particles are collected on microsorban-98 fiber filter, with size 20cm by 25 cm described in D'Almeida and Schutz (1983). This filter has a low flow resistance, and a high particle retention capacity. The filter is then dissolved in an organic liquid, such as xylene, to convert the dust particles into liquid suspensions. The resulting suspension is counted with scanning electron microscope (See the Fig. 1 in D'Almeida and Schutz (1983)). The procedure avoids charging effects on the sample surface, to guarantee unbiased magnification of the samples up to 30,000 times. The analysis was further corrected for collection efficiency of the filter. We use the average measurements that were taken over three sites between February-March 1979, and January-February 1982. These locations are: Matam (northeast Senegal) Timbuktu (Mali), and Agadez (Niger) and shown in Fig. 3 of D'Almeida (1987). Dust particles were measured for sizes larger than 100µm, but we use size distribution up to 20µm in this study. Since measurements are taken within the boundary layer, we select a representative height level between 0-100 m.

4.2. Li et al., 1996 – Ground Station – MEE only

Measurements are made over Barbados between 4 April to 3 May 1994 (main measurement period in April). Daily aerosol particles are collected using the Whatman-41 filter, and mineral dust components are determined by ashing the filter at 500 °C and weighing the residue. The resulting dust size distribution is mostly for particles of diameter $D \leq 10\ \mu m$. Aerosol scattering is measured by nephelometer at 530 nm, and the resulting mass scattering efficiency is determined by linear regression method over the entire period of measurements.

4.3. Li et al., 2000 – Ground Station – MSE only

Measurements were taken at a station on top of the Waliguan Mountain (3816 m atitude), in the Qinghai Province, China during October-November, 1997 and January 1998. Aerosol sizes up to diameter of $D \leq 18$ μm were measured by a Micro Orifice Uniform Deposit Impactor used with Teflon filter. Measured $CaCO_3$ are assumed as proxy for dust particles, and consequently for dust volume distribution. Mass scattering efficiency is calculated using the Mie theory with density and index of refraction for $CaCO_3$ taken from Williams (1996). Values are reported at 550 nm wavelength (see their table 2).

4.4. Maring et al., 2000 – Ground Station – MSE only

Dust properties are measured during July 1995 at the Global Atmospheric Watch station, located at Izana, Tenerife, Canary Island. Measurements took place at the station 2360 m above sea level, which is above the inversion level that is typically around 1200 m in summer. The dust size distribution is measured using a scanning mobility particle sizer and aerodynamic particle sizer, with diameter mostly up to about 10 μm (see their Fig. 7; it could also sample to 15 μm with stronger wind speed). Aerosol extinction was measured using nephelometer. The mass scattering efficiency is calculated using two methods, as the average for dusty and non-dusty periods: First, by calculating the linear regression between aerosol mass and its scattering (0.52 $m^2\ g^{-1}$), and secondly by using Mie theory (0.48 $m^2\ g^{-1}$). The values are reported for wavelength of 532 nm.

4.5. Andreae et al., 2002 – ARACHNE – MSE only

Over a remote site in the Negev desert (Sde Boker, Israel), measurements of aerosol properties were conducted for a period of 2 years (Dec, 1995 –Oct, 1997) as part of Aerosol Radiation and Chemistry Experiment (ARACHNE) research program. For the entire period, light scattering was measured by nephelometer, but every week a 2-days and a 3-days samples are taken using a "Gent" PM10 stacked filter unit sampler to determine the concentration of the constituent species. The mass scattering efficiency is calculated as a multivariate linear regression of the light scattering coefficients on the coarse-mode, fine-mode, sulphate and dust concentrations. Dust mass scattering efficiency at 550 nm is thereafter obtained. For the value correction for non-Lambertian behavior and truncation errors of the nephelometer has been applied.

4.6. Quinn et al., 2002 – INDOEX – MEE only

As part of Indian Ocean Experiment (INDOEX) Intensive Field Phase (IFP), measurements of aerosol properties were made over the Arabia sea and the Indian Ocean on board the R/V Ronald H. Brown between February and March, 1999. The two-stage multi-jet cascade impactors (Berner et al., 1979) apportioned to differential mobility particle sizer and aerodynamic particle sizer are used for size distributions. From the elemental components (Al, Si, Ca, Fe, and Ti), dust is considered as inorganic oxidized material (IOM), and it is obtained by summing the oxides of the elements, in which each elemental mass concentration is multiplied by a molar correction factor (See their Equation 2). The mass extinction efficiency is calculated using Mie theory, and we use here values for particles with diameter $1.1 \leq D \leq 10$ µm, to avoid possible contamination by other aerosol in the sub-micron range (See their Fig. 10). Campaign-derived index of refraction is used. The values are reported for wavelength of 550 nm.

4.7. Haywood et al., 2003 – SHADE – MEE only

Dust particle measurements were taken during the Saharan Dust Experiment (SHADE) which took place between 19-28 September 2000 close to Sal, Cape Verde, off the coast of North Africa. The size distribution is determined using Passive Cavity Aerosol Spectrometer Probe 100X. The size distributions were not corrected for refractive index because they assumed that the refractive index of latex is approximately similar to that of dust. Due to instrument malfunction during the campaign, calculations of optical properties were largely limited to about 10µm. Mie theory is used to calculate the mass extinction efficiency at wavelength of 550 nm (see their table 2).

4.8. Clarke et al. 2004 – ACE-Asia/TRACE-P – PSD and MSE

Aerosol measurements were taken in the Sea of Japan (between Koran and Japan) in the spring (24 February to 10 April) of 2001, as part of the Asian Pacific Regional Aerosol Characterization Experiment (ACE-Asia) and NASA Transport and Chemical Evolution over the Pacific (TRACE-P). Similar instrumentations as the INDOEX campaign (Quinn et al., 2002) were used during ACE-Asia campaign. ACE-Asia used a laser optical particle counters (OPC) and condensation nuclei (CN) counters for aerosol size distribution. The OPC was operated at150°C and then at 300°C, to drive off low-temperature volatiles. In addition, light scattering of coarse and fine aerosol mode

was measured by two-wavelength TSI 563 nephelometers. Despite some differences in instrumentations in the ACE-Asia and TRACE-P, the authors show that measured aerosol sizing and optical properties agreed within instrument uncertainty at all altitudes. After the size distribution are normalized to emphasize the coarse dust (see their Fig. 5), we select the resulting reference size distribution as the representative size distribution. In addition, based on their Fig. 1, we choose the representative height level between surface and 6km. The mass scattering efficiency is calculated using the Mie theory. The wavelength is at 550 nm.

4.9. Otto et al., 2007 – ACE-2 – PSD only

Aerosol measurements were taken during Aerosol Characterisation Experiment (ACE-2) conducted about 50—200km off the coast of Northern Africa close to Canary Islands on 8th of July, 1997. The aerosol size distributions used data from five instruments, including Condensation Particle Counter (CPC), Differential Mobility Analyser (DMA), Optical Particle Counter (OPC), and Forward Scattering Spectrometer Probe (FSSP). Together, the instruments measured particles up to diameter of ~31μm (see their Table 1). We use reported size distribution, up to 20μm at four specific levels – 2700 m, 4000 m, 5500 m, 7000 m.

4.10. Chou et al., 2008 & Osborne et al. 2008 – AMMA/DABEX – PSD and MEE

Based in Niamey, Niger, aerosol measurements were made between 13 January and 3 February, 2006 over the West Africa Sahel region, as part of the Dust and Biomass-burning Experiment (DABEX), affiliated with the African Monsoon Multidisciplinary Analysis (AMMA). On board the UK BAe-146 research aircraft , aerosol size distribution are measured using the Passive Cavity Aerosol Spectrometer Probe 100-X (PCASP) with additional counter-flow virtual impactor (CVI) inlet to measure particles up to diameter of 10 μm. Because of the aerosol inlet configuration on the aircraft, the measurement of coarse dust were particularly problematic. Both groups of authors reported size distributions measured from 2 flights numbered B160 and B165 out of 14 flights. Dust size distribution is taken from Chou et al, 2008, while the mass extinction efficiency is taken from Osborne et al., 2008. Since most of the flight are below ~1500m above ground level, we select 0-1500m as the representative height level. The mass extinction efficiency is calculated

using Mie theory, at 550 nm wavelength. The mass extinction efficiency is calculated with log-normal fit to the measured dust size distribution, with assumed dust density of 2.65 g cm^{-3} (see Table 4 in Osborne et al, 2008).

4.11. McConnell et al., 2008 – DODO-1/ DODO-2 – PSD and MEE

Based at Dakar, Senegal, measurements of dust properties are conducted as part of the Dust Outflow and Deposition to the Ocean project (DODO) off the coast of North Africa. The project occurred on two phases: One between 7 to 16 February 2006, called DODO-1, and the other between 22 to 28 August, 2006, called DODO-2. During DODO, a combination of wing-mounted Passive Cavity Aerosol Spectrometer Probe (PCASP), Droplet Measurement Technology cloud droplet probe (CDP-100), and bulk filters are used to measure dust size distribution up to diameter of 40 µm. We use the DODO-2 size distribution in this study based on their Fig. 7. Because the height level is given around 1 km altitude for the size distribution (see caption of Fig. 7), we limit our representative height level between 0-1 km. The mass extinction efficiency is calculated with Mie code, using the measured size distribution. Because coarse dust particles are not collected during DODO-1, we use the MEE value reported in Osborne et al., 2008 (see their Table 4) that include coarse dust collected during DABEX.

4.12. Weinzierl et al., 2009 – SAMUM-1 – PSD only

Based in Casablanca, Morocco, in situ dust particle size distribution measurements were taken onboard the German Center for Aviation and Space Flight (DLR) Falcon as part of the Saharan Mineral Dust Experiment (SAMUM-1) in Southern Morocco in May and June 2006. Three dust events were observed during the campaign on 16 to 22 May, 24 to 28 May, and 31 May to 5 June. We use the size distribution measured from a wing-mounted Forward Scattering Spectrometer Probe (FSSP) 300, and the composite size distribution from three Condensation Particle Counters (CPCs) heated with a thermal denuder (TD) at 250°C and a Grimm OPC (Optical Particle Counter). The FSSP-300 measured particles with diameters between 0.3 and 30 µm. The three CPCs measured non-volatile particles in nucleation, Aitken, and accumulation mode, respectively. With the Grimm OPC, non-volatile size distribution was derived for particles smaller than 2.5 µm.

Data are taken from their Fig. 8 which represents the composite size distribution for L02 on flight #060519a and L07 on flight #060604a. For these flights, are respectively 4853m

and 3703m above sea level, and therefore approximated to 3700-4900m in our study.

4.13. Wagner et al., 2009 – DARPO – PSD only

Based in Casablanca, Morocco, in situ measurements were performed in May 2006 over Portugal as part of the Desert Aerosols over Portugal (DAPRO) project affiliated with SAMUM (see section 4.12), using essentially the same instrumentation and derivation as Weinzierl et al. (2009) with an additional high spectral resolution lidar. Measurements were conducted at 2300m and 3245m during a flight onboard Falcon aircraft over Évora on 27 May 2006, and size distribution data between 0.01 and 35 μm were presented (see their Fig. 9). Size distribution at the two different heights were very similar. In this study, we take the representative height range between 2300-5000m.

4.14. Kandler et al., 2009 – SAMUM-1 – PSD only

During the 2006 SAMUM campaign, Kandler et al. conducted size distribution measurements by collecting dust samples at a ground station in Tinfou, Morocco where dust events occur often during summer. However, anthropogenic emissions still exerted a significant impact on particles smaller than 500 nm, despite the remote location of the ground station. Mineral dust dominated particles beyond 500 nm. Employing a combination Differential Mobility Particle Sizer (DMPS), Aerodynamic Particle Sizer (APS) and single-stage impactor (SSI), the authors measured and reported a size distribution under a higher concentration condition, named dust wind condition. The number distribution of particles larger than 500 nm varied by more than one order of magnitude, largely correlated to meteorological conditions. For particles larger than 10 μm, the variation was about three orders of magnitude. Since the station is at an elevation of approximately 684 m above sea level and the inlet of the sampling device ~4 m above ground level, we choose our representative height to be between 0-700m.

4.15. Kandler et al., 2011 – SAMUM-2 – PSD only

A part of the SAMUM-2 campaign which aims to study more aged dust as opposed to fresh dust in SAMUM-1, the effort of Kandler et al. (2011) used the similar instrumentation as SAMUM-1 (Kandler et al., 2009) to measure dust size distribution at a ground station on Praia, Cape Verde in winter 2008. A notably higher concentration of clay minerals was found compared to SAMUM-1, as expected for aged dust. Size distributions from three dust phases were reported. As in SAMUM-1, it was found that wind speed had a significant impact on the distribution between 400 nm and 10 μm, and this strength of this impact increases rapidly beyond 10 μm. The presence of larger particles is highly correlated with mass concentration. Similar to Kandler et al., 2009, because the elevation of the station is approximately 100 m above sea level, we place our representative height levels between 0-110m.

4.16. Ryder et al., 2013a and Ryder et al., 2013b – Fennec 2011 – PSD and MEE

Both Ryder et al studies measured dust properties over and near western side of the North African desert on board the UK's BAe-146-301 Research Aircraft during the Fennec June 2011 campaign. While the Ryder et al., (2013a) study reported dust properties near the Canary Islands, the Ryder et al., (2013b) study reported dust properties farther inland over Mauritania and Mali. Below, we give brief description of the instruments used and measurements taken. For more details, please refer to their studies.

(Ryder et al., 2013b): Although 16 dedicated flights was conducted over Mauritania and Mali during the campaign, only 11 of those with consistent instrumentation were used. A suite of instruments is used to measure dust size distribution (see table 3 in Ryder et al., 2013b), namely wing-mounted Passive Cavity Aerosol Spectrometer Probe 100X (PCASP), Cloud Droplet Probe (CDP), and Cloud Imaging Probe (CIP). The measurement covers significant coarse-mode size range of dust particles, and were corrected for a refractive index appropriate for dust and for instrumental drift during the campaign. Details of the calibration and correction performed on each instrument can be found in (Ryder et al., 2013b). Since most of the measurements taken are below 2-3 km (see their Fig. 2), therefore in this study we use a representative height between 0-3 km. We use data taken from their Fig. 5b, which include the mean size distribution obtained using the PCASP, CDP and CIP.

(Ryder et al., 2013a): Although dust properties are taken near the Canary Islands, in-situ measurements reported in this study uses similar instrumentations as in (Ryder et al., 2013b). Because take-off and landing profiles observations, vertical distribution of the dust size distribution can be made. We obtain these dataset directly from the authors, and present size distribution at four levels – 2500, 4000, 5500, and 6000 m. As reported in the study, we used here the averaged MEE value of 0.31+/-0.08 between the calculate values for aged dust (0.23) and the SAL categories (0.39). Mie scattering code is used to calculate the mass scattering efficiency at wavelength of 550 nm.

4.17. Jung et al., 2013 – BACEX - PSD only

In situ measurements of aged dust size distribution was conducted onboard Center for Interdisciplinary Remotely Piloted Aircraft Studies (CIRPAS) Twin Otter research aircraft under the Barbados Aerosol Cloud Experiment (BACEX) in on 1 and 2 April 2010. Size distribution measured from Passive Cavity Aerosol Spectrometer Probe (PCASP) and the forward scattering section of a Cloud and Aerosol Spectrometer (CASF) covered particle diameters from 0.1 to 54 μm. Data taken while the aircraft was in clouds were excluded because PCASP is known to have low accuracy inside clouds. We use one measurement on 1 April within the Sahara air layer (SAL) at 2726m, and one on 2 April in the intermediate layer at 1289m. For comparison, the representative height is placed between 1250-2700m. The Mass extinction efficiency is calculated using Mie theory, at 550 nm wavelength.

4.18. Weinzierl et al., 2017 – SALTRACE - PSD only

Based in Barbados, Puerto Rico, and Cabo Verde, in situ aerosol size distribution measurements were conducted as part of the Saharan Aerosol Long-Range Transport and Aerosol–Cloud-Interaction Experiment (SALTRACE) in June 2013. The same air mass was first sampled over Cabo Verde at the altitude of 2.6km on 17 June 2013, and again over Barbados at 2.3km on 22 June 2013. Total number distribution below 1 μm was inverted from measurements from three Condensation Particle Counters (CPCs) between 0.005 and 2.5 μm, a Grimm Sky Optical Particle Counter (OPC) between 0.25 and 2.5 μm, and a wing-mounted Ultra-High Sensitivity Aerosol

Spectrometer Airborne (UHSAS-A) between 0.06 and 1 μm. Total number distribution above 1 μm was measured with Cloud and Aerosol Spectrometer with Depolarization (CAS-DPOL). Distribution in the full size range was parametrized with four lognormal distributions. The authors expected 20-μm particles to be removed after 3 days of transport, but 20% of the observed 20-μm particles in Cabo Verde survived in the second measurement above Barbados.

4.19. Ryder et al., 2018 - AER-D - PSD and MEE

In-situ measurements were taken in August, 2015 close to Cape Verde, off the coast of Northern Africa properties during the beginning of trans-Atlantic transport of dust particles. These measurements were part of the AERosol Properties – Dust (AER-D) fieldwork campaign, which ran alongside the Ice in Clouds Experiment – Dust (ICE-D) project, and similarly used the UK's BAe-146-301 Research Aircraft. In addition to the instruments used during Fennec 2011 campaign, the AER-D campaign used cloud imaging probes (CIP15 and 2DS) for size distributions at d>10 microns. They use wing-mounted optical particle counters and shadow probes to measure dust sizes between 0.1 and 100 μm diameter, a nephelometer and an absorption photometer to measure dust optical properties, and an in-cabin filter collection system to collect dust samples. Data for size distribution was obtained directly from the authors. However, reported value of dust mass extinction efficiency, calculated using Mie code at 550 nm wavelength, was obtained from their paper.

References

Andreae, T. W., Andreae, M. O., Ichoku, C., Maenhaut, W., Cafmeyer, J., Karnieli, A. and Orlovsky, L.: Light scattering by dust and anthropogenic aerosol at a remote site in the Negev desert, Israel, J. Geophys. Res., 107(D2), 4008, doi:10.1029/2001JD900252, 2002.

Barnard, J. C., Fast, J. D., Paredes-Miranda, G., Arnott, W. P. and Laskin, A.: Technical Note: Evaluation of the WRF-Chem "Aerosol Chemical to Aerosol Optical Properties" Module using data from the MILAGRO campaign, Atmos. Chem. Phys., 10(15), 7325–7340, doi:10.5194/acp-10-7325-2010, 2010.

Binkowski, F. S. and Shankar, U.: The Regional Particulate Matter Model: 1. Model description and preliminary results, J. Geophys. Res., 100(D12), 26191, doi:10.1029/95JD02093, 1995.

Buchard, V., Randles, C. A., da Silva, A. M., Darmenov, A., Colarco, P. R., Govindaraju, R., Ferrare, R., Hair, J., Beyersdorf, A. J., Ziemba, L. D., Yu, H., Buchard, V., Randles, C. A., Silva, A. M. da, Darmenov, A., Colarco, P. R., Govindaraju, R., Ferrare, R., Hair, J., Beyersdorf, A. J., Ziemba, L. D. and Yu, H.: The MERRA-2 Aerosol Reanalysis, 1980 Onward. Part II: Evaluation and Case Studies, J. Clim., 30(17), 6851–6872, doi:10.1175/JCLI-D-16-0613.1, 2017.

Chapman, E. G., Gustafson, W. I., Easter, R. C., Barnard, J. C., Ghan, S. J., Pekour, M. S. and Fast, J. D.: Coupling aerosol-cloud-radiative processes in the WRF-Chem model: Investigating the radiative impact of elevated point sources, Atmos. Chem. Phys., 9(3), 945–964, doi:10.5194/acp-9-945-2009, 2009.

Chou, C., Formenti, P., Maille, M., Ausset, P., Helas, G., Harrison, M. and Osborne, S.: Size distribution, shape, and composition of mineral dust aerosols collected during the African Monsoon Multidisciplinary Analysis Special Observation Period 0: Dust and Biomass-Burning Experiment field campaign in Niger, January 2006, J. Geophys. Res., 113(D23), D00C10, doi:10.1029/2008JD009897, 2008.

Clarke, A. D., Shinozuka, Y., Kapustin, V. N., Howell, S., Huebert, B., Doherty, S., Anderson, T., Covert, D., Anderson, J., Hua, X., Moore, K. G., McNaughton, C., Carmichael, G. and Weber, R.: Size distributions and mixtures of dust and black carbon aerosol in Asian outflow: Physiochemistry and optical properties, J. Geophys. Res., 109(D15), D15S09, doi:10.1029/2003JD004378, 2004.

Colarco, P., Silva, A., Chin, M. and Diehl, T.: Online simulations of global aerosol distributions in the NASA GEOS - 4 model and comparisons to satellite and ground - based aerosol optical depth, , 115, doi:10.1029/2009JD012820, 2010.

D'Almeida, G. A.: On the variability of desert aerosol radiative characteristics, J. Geophys. Res., 92(D3), 3017, doi:10.1029/JD092iD03p03017, 1987.

D'Almeida, G. A. and Schutz, L.: Number, mass and volume distributions of mineral aerosol and soils of the Sahara., J. Clim. Appl. Meteorol., 22(2), 233–243, doi:10.1175/1520-0450(1983)022<0233:NMAVDO>2.0.CO;2, 1983.

Easter, R. C., Ghan, S. J., Zhang, Y., Saylor, R. D., Chapman, E. G., Laulainen, N. S., Abdul-Razzak, H., Leung, L. R., Bian, X. and Zaveri, R. A.: MIRAGE: Model description and evaluation of aerosols and trace gases, J. Geophys. Res., 109(D20), D20210, doi:10.1029/2004JD004571, 2004.

Fast, J. D., Gustafson, W. I., Easter, R. C., Zaveri, R. A., Barnard, J. C., Chapman, E. G., Grell,

G. A. and Peckham, S. E.: Evolution of ozone, particulates, and aerosol direct radiative forcing in the vicinity of Houston using a fully coupled meteorology-chemistry-aerosol model, J. Geophys. Res., 111(D21), D21305, doi:10.1029/2005JD006721, 2006.
Flemming, J., Huijnen, V., Arteta, J., Bechtold, P., Beljaars, A., Blechschmidt, A.-M., Diamantakis, M., Engelen, R. J., Gaudel, A., Inness, A., Jones, L., Josse, B., Katragkou, E., Marecal, V., Peuch, V.-H., Richter, A., Schultz, M. G., Stein, O. and Tsikerdekis, A.: Tropospheric chemistry in the Integrated Forecasting System of ECMWF, Geosci. Model Dev., 8(4), 975–1003, doi:10.5194/gmd-8-975-2015, 2015.
Flemming, J., Benedetti, A., Inness, A., Engelen, R. J., Jones, L., Huijnen, V., Remy, S., Parrington, M., Suttie, M., Bozzo, A., Peuch, V.-H., Akritidis, D. and Katragkou, E.: The CAMS interim Reanalysis of Carbon Monoxide, Ozone and Aerosol for 2003–2015, Atmos. Chem. Phys., 17(3), 1945–1983, doi:10.5194/acp-17-1945-2017, 2017.
Gelaro, R., McCarty, W., Suárez, M. J., Todling, R., Molod, A., Takacs, L., Randles, C. A., Darmenov, A., Bosilovich, M. G., Reichle, R., Wargan, K., Coy, L., Cullather, R., Draper, C., Akella, S., Buchard, V., Conaty, A., da Silva, A. M., Gu, W., Kim, G.-K., Koster, R., Lucchesi, R., Merkova, D., Nielsen, J. E., Partyka, G., Pawson, S., Putman, W., Rienecker, M., Schubert, S. D., Sienkiewicz, M., Zhao, B., Gelaro, R., McCarty, W., Suárez, M. J., Todling, R., Molod, A., Takacs, L., Randles, C. A., Darmenov, A., Bosilovich, M. G., Reichle, R., Wargan, K., Coy, L., Cullather, R., Draper, C., Akella, S., Buchard, V., Conaty, A., Silva, A. M. da, Gu, W., Kim, G.-K., Koster, R., Lucchesi, R., Merkova, D., Nielsen, J. E., Partyka, G., Pawson, S., Putman, W., Rienecker, M., Schubert, S. D., Sienkiewicz, M. and Zhao, B.: The Modern-Era Retrospective Analysis for Research and Applications, Version 2 (MERRA-2), J. Clim., 30(14), 5419–5454, doi:10.1175/JCLI-D-16-0758.1, 2017.
Gerber, H.: Supersaturation and Droplet Spectral Evolution in Fog, J. Atmos. Sci., 48(24), 2569–2588, doi:10.1175/1520-0469(1991)048<2569:SADSEI>2.0.CO;2, 1991.
Ginoux, P., Chin, M., Tegen, I., Prospero, J. M., Holben, B., Dubovik, O. and Lin, S.-J.: Sources and distributions of dust aerosols simulated with the GOCART model, J. Geophys. Res. Atmos., 106(D17), 20255–20273, doi:10.1029/2000JD000053, 2001.
Giorgi, F. and Chameides, W. L.: Rainout lifetimes of highly soluble aerosols and gases as inferred from simulations with a general circulation model, J. Geophys. Res., 91(D13), 14367, doi:10.1029/JD091iD13p14367, 1986.
Grell, G. A., Peckham, S. E., Schmitz, R., McKeen, S. A., Frost, G., Skamarock, W. C. and Eder,

B.: Fully coupled “online” chemistry within the WRF model, Atmos. Environ., 39(37), 6957–6975, doi:10.1016/J.ATMOSENV.2005.04.027, 2005.
Haywood, J.: Radiative properties and direct radiative effect of Saharan dust measured by the C-130 aircraft during SHADE: 1. Solar spectrum, J. Geophys. Res., 108(D18), 8577, doi:10.1029/2002JD002687, 2003.
Hess, M., Koepke, P., Schult, I., Hess, M., Koepke, P. and Schult, I.: Optical Properties of Aerosols and Clouds: The Software Package OPAC, Bull. Am. Meteorol. Soc., 79(5), 831–844, doi:10.1175/1520-0477(1998)079<0831:OPOAAC>2.0.CO;2, 1998.
Hogan, T. F. and Brody, L. R.: Sensitivity Studies of the Navy’s Global Forecast Model Parameterizations and Evaluation of Improvements to NOGAPS, Mon. Weather Rev., 121(8), 2373–2395, doi:10.1175/1520-0493(1993)121<2373:SSOTNG>2.0.CO;2, 1993.
Hogan, T. F. and Rosmond, T. E.: The Description of the Navy Operational Global Atmospheric Prediction System’s Spectral Forecast Model, Mon. Weather Rev., 119(8), 1786–1815, doi:10.1175/1520-0493(1991)119<1786:TDOTNO>2.0.CO;2, 1991.
Hyer, E. J., Reid, J. S. and Zhang, J.: An over-land aerosol optical depth data set for data assimilation by filtering, correction, and aggregation of MODIS Collection 5 optical depth retrievals, Atmos. Meas. Tech., 4(3), 379–408, doi:10.5194/amt-4-379-2011, 2011.
Inness, A., Blechschmidt, A.-M., Bouarar, I., Chabrillat, S., Crepulja, M., Engelen, R. J., Eskes, H., Flemming, J., Gaudel, A., Hendrick, F., Huijnen, V., Jones, L., Kapsomenakis, J., Katragkou, E., Keppens, A., Langerock, B., de Mazière, M., Melas, D., Parrington, M., Peuch, V. H., Razinger, M., Richter, A., Schultz, M. G., Suttie, M., Thouret, V., Vrekoussis, M., Wagner, A. and Zerefos, C.: Data assimilation of satellite-retrieved ozone, carbon monoxide and nitrogen dioxide with ECMWF’s Composition-IFS, Atmos. Chem. Phys., 15(9), 5275–5303, doi:10.5194/acp-15-5275-2015, 2015.
Ito, A. and Kok, J. F.: Do dust emissions from sparsely vegetated regions dominate atmospheric iron supply to the Southern Ocean?, J. Geophys. Res. Atmos., 122(7), 3987–4002, doi:10.1002/2016JD025939, 2017.
Ito, A., Sillman, S. and Penner, J. E.: Effects of additional nonmethane volatile organic compounds, organic nitrates, and direct emissions of oxygenated organic species on global tropospheric chemistry, J. Geophys. Res., 112(D6), D06309, doi:10.1029/2005JD006556, 2007.
Jacob, D., Liu, H. and Yantosca, R.: Harvard wet deposition scheme for GMI, Harvard Univ. Atmos. Chem. Model. Gr., n/a(n/a), n/a, 2000.

Joyce, R. J., Janowiak, J. E., Arkin, P. A., Xie, P., Joyce, R. J., Janowiak, J. E., Arkin, P. A. and Xie, P.: CMORPH: A Method that Produces Global Precipitation Estimates from Passive Microwave and Infrared Data at High Spatial and Temporal Resolution, J. Hydrometeorol., 5(3), 487–503, doi:10.1175/1525-7541(2004)005<0487:CAMTPG>2.0.CO;2, 2004.

Jung, E., Albrecht, B., Prospero, J. M., Jonsson, H. H. and Kreidenweis, S. M.: Vertical structure of aerosols, temperature, and moisture associated with an intense African dust event observed over the eastern Caribbean, J. Geophys. Res. Atmos., 118(10), 4623–4643, doi:10.1002/jgrd.50352, 2013.

Kandler, K., SchüTZ, L., Deutscher, C., Ebert, M., Hofmann, H., JäCKEL, S., Jaenicke, R., Knippertz, P., Lieke, K., Massling, A., Petzold, A., Schladitz, A., Weinzierl, B., Wiedensohler, A., Zorn, S. and Weinbruch1, S.: Size distribution, mass concentration, chemical and mineralogical composition and derived optical parameters of the boundary layer aerosol at Tinfou, Morocco, during SAMUM 2006, Tellus B Chem. Phys. Meteorol., 61(1), 32–50, doi:10.1111/j.1600-0889.2008.00385.x, 2009.

Kandler, K., Lieke, K., Benker, N., Emmel, C., Küpper, M., Müller-Ebert, D., Ebert, M., Scheuvens, D., Schladitz, A., Schütz, L. and Weinbruch, S.: Electron microscopy of particles collected at Praia, Cape Verde, during the Saharan Mineral Dust Experiment: particle chemistry, shape, mixing state and complex refractive index, Tellus B Chem. Phys. Meteorol., 63(4), 475–496, doi:10.1111/j.1600-0889.2011.00550.x, 2011.

Kok, J. F.: A scaling theory for the size distribution of emitted dust aerosols suggests climate models underestimate the size of the global dust cycle, Proc. Natl. Acad. Sci., 108(3), 1016–1021, doi:10.1073/pnas.1014798108, 2011.

Kok, J. F., Albani, S., Mahowald, N. M. and Ward, D. S.: An improved dust emission model - Part 2: Evaluation in the Community Earth System Model, with implications for the use of dust source functions, Atmos. Chem. Phys., 14(23), 13043–13061, doi:10.5194/acp-14-13043-2014, 2014a.

Kok, J. F., Mahowald, N. M., Fratini, G., Gillies, J. A., Ishizuka, M., Leys, J. F., Mikami, M., Park, M.-S., Park, S.-U., Van Pelt, R. S. and Zobeck, T. M.: An improved dust emission model – Part 1: Model description and comparison against measurements, Atmos. Chem. Phys., 14(23), 13023–13041, doi:10.5194/acp-14-13023-2014-supplement, 2014b.

Li, S.-M., Tang, J., Xue, H. and Toom-Sauntry, D.: Size distribution and estimated optical properties of carbonate, water soluble organic carbon, and sulfate in aerosols at a remote high

altitude site in western China, Geophys. Res. Lett., 27(8), 1107–1110, doi:10.1029/1999GL010929, 2000.
Li, X., Maring, H., Savoie, D., Voss, K. and Prospero, J. M.: Dominance of mineral dust in aerosol light-scattering in the North Atlantic trade winds, Nature, 380(6573), 416–419, doi:10.1038/380416a0, 1996.
Liu, H., Jacob, D. J., Bey, I. and Yantosca, R. M.: Constraints from ^{210}Pb and ^{7}Be on wet deposition and transport in a global three-dimensional chemical tracer model driven by assimilated meteorological fields, J. Geophys. Res. Atmos., 106(D11), 12109–12128, doi:10.1029/2000JD900839, 2001.
Liu, X., Penner, J. E. and Herzog, M.: Global modeling of aerosol dynamics: Model description, evaluation, and interactions between sulfate and nonsulfate aerosols, J. Geophys. Res., 110(D18), D18206, doi:10.1029/2004JD005674, 2005.
Lynch, P., Reid, J. S., Westphal, D. L., Zhang, J., Hogan, T. F., Hyer, E. J., Curtis, C. A., Hegg, D. A., Shi, Y., Campbell, J. R., Rubin, J. I., Sessions, W. R., Turk, F. J. and Walker, A. L.: An 11-year global gridded aerosol optical thickness reanalysis (v1.0) for atmospheric and climate sciences, Geosci. Model Dev., 9(4), 1489–1522, doi:10.5194/gmd-9-1489-2016, 2016.
Maring, H., Savoie, D. L., Izaguirre, M. A., McCormick, C., Arimoto, R., Prospero, J. M. and Pilinis, C.: Aerosol physical and optical properties and their relationship to aerosol composition in the free troposphere at Izaña, Tenerife, Canary Islands, during July 1995, J. Geophys. Res. Atmos., 105(D11), 14677–14700, doi:10.1029/2000JD900106, 2000.
Marticorena, B. and Bergametti, G.: Modeling the atmospheric dust cycle: 1. Design of a soil-derived dust emission scheme, J. Geophys. Res., 100(D8), 16415, doi:10.1029/95JD00690, 1995.
Masson, V., Champeaux, J.-L., Chauvin, F., Meriguet, C., Lacaze, R., Masson, V., Champeaux, J.-L., Chauvin, F., Meriguet, C. and Lacaze, R.: A Global Database of Land Surface Parameters at 1-km Resolution in Meteorological and Climate Models, J. Clim., 16(9), 1261–1282, doi:10.1175/1520-0442-16.9.1261, 2003.
Mccarty, W., Coy, L., Gelaro, R., Huang, A., Merkova, D., Smith, E. B., Sienkiewicz, M., Wargan, K. and Koster, R. D.: MERRA-2 Input Observations: Summary and Assessment. Technical Report Series on Global Modeling and Data Assimilation., 2016.
McConnell, C. L., Highwood, E. J., Coe, H., Formenti, P., Anderson, B., Osborne, S., Nava, S., Desboeufs, K., Chen, G. and Harrison, M. A. J.: Seasonal variations of the physical and optical characteristics of Saharan dust: Results from the Dust Outflow and Deposition to the Ocean

(DODO) experiment, J. Geophys. Res., 113(D14), D14S05, doi:10.1029/2007JD009606, 2008.
Michou, M., Nabat, P. and Saint-Martin, D.: Development and basic evaluation of a prognostic aerosol scheme (v1) in the CNRM Climate Model CNRM-CM6, Geosci. Model Dev., 8(3), 501–531, doi:10.5194/gmd-8-501-2015, 2015.
Morcrette, J.-J., Boucher, O., Jones, L., Salmond, D., Bechtold, P., Beljaars, A., Benedetti, A., Bonet, A., Kaiser, J. W., Razinger, M., Schulz, M., Serrar, S., Simmons, A. J., Sofiev, M., Suttie, M., Tompkins, A. M. and Untch, A.: Aerosol analysis and forecast in the European Centre for Medium-Range Weather Forecasts Integrated Forecast System: Forward modeling, J. Geophys. Res., 114(D6), D06206, doi:10.1029/2008JD011235, 2009.
Nabat, P., Somot, S., Mallet, M., Michou, M., Sevault, F., Driouech, F., Meloni, D., di Sarra, A., Di Biagio, C., Formenti, P., Sicard, M., Léon, J.-F. and Bouin, M.-N.: Dust aerosol radiative effects during summer 2012 simulated with a coupled regional aerosol–atmosphere–ocean model over the Mediterranean, Atmos. Chem. Phys., 15(6), 3303–3326, doi:10.5194/acp-15-3303-2015, 2015.
Osborne, S. R., Johnson, B. T., Haywood, J. M., Baran, A. J., Harrison, M. A. J. and McConnell, C. L.: Physical and optical properties of mineral dust aerosol during the Dust and Biomass-burning Experiment, J. Geophys. Res., 113(D23), D00C03, doi:10.1029/2007JD009551, 2008.
Otto, S., de Reus, M., Trautmann, T., Thomas, A., Wendisch, M. and Borrmann, S.: Atmospheric radiative effects of an in situ measured Saharan dust plume and the role of large particles, Atmos. Chem. Phys., 7(18), 4887–4903, doi:10.5194/acp-7-4887-2007, 2007.
Quinn, P. K., D. J. Coffman, T. S. Bates, T. L. Miller, J. E. Johnson, E. J. Welton, C. Neusüss, M. Miller and Sheridan, P. J.: Aerosol optical properties during INDOEX 1999: Means, variability, and controlling factors, J. Geophys. Res., 107(D19), 8020, doi:10.1029/2000JD000037, 2002.
Randles, C. A., da Silva, A. M., Buchard, V., Colarco, P. R., Darmenov, A., Govindaraju, R., Smirnov, A., Holben, B., Ferrare, R., Hair, J., Shinozuka, Y., Flynn, C. J., Randles, C. A., Silva, A. M. da, Buchard, V., Colarco, P. R., Darmenov, A., Govindaraju, R., Smirnov, A., Holben, B., Ferrare, R., Hair, J., Shinozuka, Y. and Flynn, C. J.: The MERRA-2 Aerosol Reanalysis, 1980 Onward. Part I: System Description and Data Assimilation Evaluation, J. Clim., 30(17), 6823–6850, doi:10.1175/JCLI-D-16-0609.1, 2017.
Reddy, M. S., Boucher, O., Bellouin, N., Schulz, M., Balkanski, Y., Dufresne, J. and Pham, M.: Estimates of global multicomponent aerosol optical depth and direct radiative perturbation in the

Laboratoire de Météorologie Dynamique general circulation model, J. Geophys. Res., 110(D10), D10S16, doi:10.1029/2004JD004757, 2005.
Reichle, R. H., Liu, Q. and Koster, R. D.: Observation-Corrected Precipitation Estimates in GEOS-5. Technical Report Series on Global Modeling and Data Assimilation., 2014.
Reichle, R. H., Liu, Q., Koster, R. D., Draper, C. S., Mahanama, S. P. P., Partyka, G. S., Reichle, R. H., Liu, Q., Koster, R. D., Draper, C. S., Mahanama, S. P. P. and Partyka, G. S.: Land Surface Precipitation in MERRA-2, J. Clim., 30(5), 1643–1664, doi:10.1175/JCLI-D-16-0570.1, 2017.
Rotman, D. A., Atherton, C. S., Bergmann, D. J., Cameron-Smith, P. J., Chuang, C. C., Connell, P. S., Dignon, J. E., Franz, A., Grant, K. E., Kinnison, D. E., Molenkamp, C. R., Proctor, D. D. and Tannahill, J. R.: IMPACT, the LLNL 3-D global atmospheric chemical transport model for the combined troposphere and stratosphere: Model description and analysis of ozone and other trace gases, J. Geophys. Res. Atmos., 109(D4), n/a-n/a, doi:10.1029/2002JD003155, 2004.
Ryder, C. L., Highwood, E. J., Lai, T. M., Sodemann, H. and Marsham, J. H.: Impact of atmospheric transport on the evolution of microphysical and optical properties of Saharan dust, Geophys. Res. Lett., 40(10), 2433–2438, doi:10.1002/grl.50482, 2013a.
Ryder, C. L., Highwood, E. J., Rosenberg, P. D., Trembath, J., Brooke, J. K., Bart, M., Dean, A., Crosier, J., Dorsey, J., Brindley, H., Banks, J., Marsham, J. H., McQuaid, J. B., Sodemann, H. and Washington, R.: Optical properties of Saharan dust aerosol and contribution from the coarse mode as measured during the Fennec 2011 aircraft campaign, Atmos. Chem. Phys., 13(1), 303–325, doi:10.5194/acp-13-303-2013, 2013b.
Ryder, C. L., Marenco, F., Brooke, J. K., Estelles, V., Cotton, R., Formenti, P., McQuaid, J. B., Price, H. C., Liu, D., Ausset, P., Rosenberg, P., Taylor, J. W., Choularton, T., Bower, K., Coe, H., Gallagher, M., Crosier, J., Lloyd, G., Highwood, E. J. and Murray, B. J.: Coarse mode mineral dust size distributions, composition and optical properties from AER-D aircraft measurements over the Tropical Eastern Atlantic, Atmos. Chem. Phys. Discuss., 1–49, doi:10.5194/acp-2018-739, 2018.
Seinfeld, J. and Pandis, S.: Atmospheric Chemistry and Physics: From Air Pollution to Climate Change., 2006.
Shao, Y., Raupach, M. and Leys, J.: A model for predicting aeolian sand drift and dust entrainment on scales from paddock to region, Aust. J. Soil Res., 34(3), 309, doi:10.1071/SR9960309, 1996.
Shi, Y., Zhang, J., Reid, J. S., Holben, B., Hyer, E. J. and Curtis, C.: An analysis of the collection

5 MODIS over-ocean aerosol optical depth product for its implication in aerosol assimilation, Atmos. Chem. Phys., 11(2), 557–565, doi:10.5194/acp-11-557-2011, 2011.
Stauffer, D. R. and Seaman, N. L.: Use of Four-Dimensional Data Assimilation in a Limited-Area Mesoscale Model. Part I: Experiments with Synoptic-Scale Data, Mon. Weather Rev., 118(6), 1250–1277, doi:10.1175/1520-0493(1990)118<1250:UOFDDA>2.0.CO;2, 1990.
Tanaka, T. Y. and Chiba, M.: Global Simulation of Dust Aerosol with a Chemical Transport Model, MASINGAR, J. Meteorol. Soc. Japan. Ser. II, 83A(0), 255–278, doi:10.2151/jmsj.83A.255, 2005.
Tanaka, T. Y., Orito, K., Sekiyama, T. T., Shibata, K., Chiba, M. and Tanaka, H.: MASINGAR, a global tropospheric aerosol chemical transport model coupled with MRI/JMA98 GCM: Model description, Pap. Meteorol. Geophys., 53(4), 119–138, doi:10.2467/mripapers.53.119, 2003.
Wagner, F., Bortoli, D., Pereira, S., Costa, M. Jo., Maria Silva, A., Weinzierl, B., Esselborn, M., Petzold, A., Rasp, K., Heinold, B. and Tegen, I.: Properties of dust aerosol particles transported to Portugal from the Sahara desert, Tellus B Chem. Phys. Meteorol., 61(1), 297–306, doi:10.1111/j.1600-0889.2008.00393.x, 2009.
Weinzierl, B., Petzold, A., Esselborn, M., Wirth, M., Rasp, K., Kandler, K., SchüTZ, L., Koepke, P. and Fiebig, M.: Airborne measurements of dust layer properties, particle size distribution and mixing state of Saharan dust during SAMUM 2006, Tellus B Chem. Phys. Meteorol., 61(1), 96–117, doi:10.1111/j.1600-0889.2008.00392.x, 2009.
Weinzierl, B., Ansmann, A., Prospero, J. M., Althausen, D., Benker, N., Chouza, F., Dollner, M., Farrell, D., Fomba, W. K., Freudenthaler, V., Gasteiger, J., Groß, S., Haarig, M., Heinold, B., Kandler, K., Kristensen, T. B., Mayol-Bracero, O. L., Müller, T., Reitebuch, O., Sauer, D., Schäfler, A., Schepanski, K., Spanu, A., Tegen, I., Toledano, C., Walser, A., Weinzierl, B., Ansmann, A., Prospero, J. M., Althausen, D., Benker, N., Chouza, F., Dollner, M., Farrell, D., Fomba, W. K., Freudenthaler, V., Gasteiger, J., Groß, S., Haarig, M., Heinold, B., Kandler, K., Kristensen, T. B., Mayol-Bracero, O. L., Müller, T., Reitebuch, O., Sauer, D., Schäfler, A., Schepanski, K., Spanu, A., Tegen, I., Toledano, C. and Walser, A.: The Saharan Aerosol Long-Range Transport and Aerosol–Cloud-Interaction Experiment: Overview and Selected Highlights, Bull. Am. Meteorol. Soc., 98(7), 1427–1451, doi:10.1175/BAMS-D-15-00142.1, 2017.
Williams, M. L.: CRC Handbook of Chemistry and Physics, 76th edition, Occup. Environ. Med., 53(7), 504, 1996.
Xu, L. and Penner, J. E.: Global simulations of nitrate and ammonium aerosols and their

radiative effects, Atmos. Chem. Phys., 12(20), 9479–9504, doi:10.5194/acp-12-9479-2012, 2012.
Yoshimura, H. and Yukimoto, S.: Development of a Simple Coupler (Scup) for Earth System Modeling, Pap. Meteorol. Geophys., 59, 19–29, doi:10.2467/mripapers.59.19, 2008.
Yukimoto, S., ADACHI, Y., HOSAKA, M., SAKAMI, T., YOSHIMURA, H., HIRABARA, M., TANAKA, T. Y., SHINDO, E., TSUJINO, H., DEUSHI, M., MIZUTA, R., YABU, S., OBATA, A., NAKANO, H., KOSHIRO, T., OSE, T. and KITOH, A.: A New Global Climate Model of the Meteorological Research Institute: MRI-CGCM3 ^|^mdash;Model Description and Basic Performance^|^mdash;, J. Meteorol. Soc. Japan, 90A(0), 23–64, doi:10.2151/jmsj.2012-A02, 2012.
Yumimoto, K., Tanaka, T. Y., Oshima, N. and Maki, T.: JRAero: the Japanese Reanalysis for Aerosol v1.0, Geosci. Model Dev., 10(9), 3225–3253, doi:10.5194/gmd-10-3225-2017, 2017.
Zaveri, R. A. and Peters, L. K.: A new lumped structure photochemical mechanism for large-scale applications, J. Geophys. Res. Atmos., 104(D23), 30387–30415, doi:10.1029/1999JD900876, 1999.
Zaveri, R. A., Easter, R. C., Fast, J. D. and Peters, L. K.: Model for Simulating Aerosol Interactions and Chemistry (MOSAIC), J. Geophys. Res., 113(D13), D13204, doi:10.1029/2007JD008782, 2008.
Zhang, J. and Reid, J. S.: MODIS aerosol product analysis for data assimilation: Assessment of over-ocean level 2 aerosol optical thickness retrievals, J. Geophys. Res., 111(D22), D22207, doi:10.1029/2005JD006898, 2006.
Zhang, J., Reid, J. S., Westphal, D. L., Baker, N. L. and Hyer, E. J.: A system for operational aerosol optical depth data assimilation over global oceans, J. Geophys. Res., 113(D10), D10208, doi:10.1029/2007JD009065, 2008.
Zhang, L., Gong, S., Padro, J. and Barrie, L.: A size-segregated particle dry deposition scheme for an atmospheric aerosol module, Atmos. Environ., 35(3), 549–560, doi:10.1016/S1352-2310(00)00326-5, 2001.
Zhao, C., Wang, Y., Yang, Q., Fu, R., Cunnold, D. and Choi, Y.: Impact of East Asian summer monsoon on the air quality over China: View from space, J. Geophys. Res., 115(D9), D09301, doi:10.1029/2009JD012745, 2010a.
Zhao, C., Liu, X., Leung, L. R., Johnson, B., McFarlane, S. A., Gustafson, W. I., Fast, J. D. and Easter, R.: The spatial distribution of mineral dust and its shortwave radiative forcing over North

Africa: modeling sensitivities to dust emissions and aerosol size treatments, Atmos. Chem. Phys., 10(18), 8821–8838, doi:10.5194/acp-10-8821-2010, 2010b.
Zhao, C., Liu, X., Ruby Leung, L. and Hagos, S.: Radiative impact of mineral dust on monsoon precipitation variability over West Africa, Atmos. Chem. Phys., 11(5), 1879–1893, doi:10.5194/acp-11-1879-2011, 2011.
Zhao, C., Chen, S., Leung, L. R., Qian, Y., Kok, J. F., Zaveri, R. A. and Huang, J.: Uncertainty in modeling dust mass balance and radiative forcing from size parameterization, , 13(21), 10733–10753, doi:10.5194/acp-13-10733-2013, 2013.